Chem Soc Rev

Environmental Applications of Graphene-Based Nanomaterials

Journal:	*Chemical Society Reviews*
Manuscript ID:	CS-REV-01-2015-000021.R1
Article Type:	Review Article
Date Submitted by the Author:	25-Feb-2015
Complete List of Authors:	Perreault, Francois; Yale University, Chemical and Environmental Engineering Fonseca de Faria, Andreia; Yale University, Chemical and Environmental Engineering Elimelech, Menachem; Yale University, Department of Chemical and Environmental Engineering

INVITED REVIEW ARTICLE
Special Issue on
Sustainable Nanotechnology

Environmental Applications of Graphene-Based Nanomaterials

Chemical Society Reviews

Revised: February 25, 2015

François Perreault[1]*, Andreia Fonseca de Faria[1]*, and Menachem Elimelech[1]

**Equal contributions*

[1]*Department of Chemical and Environmental Engineering, Yale University, New Haven, Connecticut 06520-8286, United States*

* Corresponding author: Menachem Elimelech, Email: menachem.elimelech@yale.edu, Phone: (203) 432-2789

Abstract

Graphene-based materials are gaining heightened attention as novel materials for environmental applications. The unique physicochemical properties of graphene, notably its exceptionally high surface area, electron mobility, thermal conductivity, and mechanical strength, can lead to novel or improved technologies to address the pressing global environmental challenges. This critical review assesses the recent developments in the use of graphene-based materials as sorbent or photocatalytic materials for environmental decontamination, as building blocks for next generation water treatment and desalination membranes, and as electrode materials for contaminant monitoring or removal. The most promising areas of research are highlighted, with a discussion of the main challenges that we need to overcome in order to fully realize the exceptional properties of graphene in environmental applications.

Textual and Graphical Abstract

A critical assessment of recent developments in environmental applications of graphene and graphene-based materials

1. Introduction

The 21st century has been termed the Century of the Environment.[1] With growing world population; intensification of agricultural and industrial activities; contamination of air, soils and aquatic ecosystems; and global climate change; environmental issues are becoming a major focus of political and scientific attention.[1] There is currently a global effort to understand the influence of human activities on the environment and to develop new technologies to mitigate associated health and environmental implications. Among the different strategies to address these pressing environmental challenges, recent developments in the field of nanotechnology have triggered increased interest in using the unique properties of nanomaterials for environmental applications.

Nanomaterials possess unique properties, owing to their nanoscale dimensions, that can be used to design novel technologies or improve the performance of existing processes. Nanomaterials have found multiple applications in water treatment, energy production, and contaminant sensing, and a growing amount of literature describes how novel nanomaterials may be used to address major environmental challenges.[2–6] The latest material to capture the attention of researchers is graphene, a two-dimensional layer of carbon atoms arranged in a hexagonal crystalline structure.[7] The interest in graphene originates from its unique physicochemical properties, notably the exceptionally high surface area, electron and thermal mobility, and mechanical strength.

These exceptional properties have triggered extensive efforts to use graphene in all fields of technology, from electronic systems to biomedical devices.[8,9] In the environmental field, graphene and graphene-based materials have been used to develop novel sorbent or photocatalytic materials for environmental decontamination, as building blocks for next generation water treatment membranes, and as electrode materials for contaminant monitoring or removal. These different environmental applications of graphene-based materials are the focus of this review.

We first discuss the main properties of graphene nanomaterials relevant to environmental applications in order to assess the possibilities offered by this novel carbon nanomaterial. We then critically review the recent developments in applications of graphene-based materials for environmental decontamination, water treatment, and contaminant detection, emphasizing how

using graphene-based materials may lead to technological improvements in each area. Finally, we will highlight the main challenges to overcome in order to realize the full potential of graphene-based materials in environmental systems.

2. Graphene materials: Concepts and properties

Graphene, in its pristine form, is composed of a single layer of carbon atoms arranged in a sp^2-bonded aromatic structure (Figure 1). It is naturally found as the building block of graphite, where π-stacking of graphene sheets holds the lamellar graphite structure strongly in place, with an interlayer spacing 3.34 Å between the sheets.[10] Graphite can be exfoliated to generate single layers of graphene. This was initially demonstrated by micromechanical exfoliation, the sequential cleavage of graphite to graphene using adhesive tape.[11] Micromechanical exfoliation generates very high quality graphene, ideal for research purposes. This simple approach to produce pristine single-layer graphene sheets was used by Geim and Novoselov in their pivotal work on the electronic properties of graphene, leading to the Nobel Prize in Physics in 2010.[7,9]

FIGURE 1

Micromechanical exfoliation, however, is labor-intensive and not scalable for large-scale use of graphene. Graphene can be exfoliated from graphite by ultrasonication of graphite in organic solvents; however, this approach was found to generate relatively low yields.[11,12] To produce high quality graphene on an industrial scale, the most common approach is to directly synthesize graphene sheets by thermal decomposition of SiC[13] or epitaxial growth of graphene on transition metals (Ni, Pd, Ru, Ir, Cu) via chemical vapor deposition (CVD) of hydrocarbons or alcohols.[14–19] CVD has been highlighted as the most promising, inexpensive, and scalable strategy to produce high quality graphene.[14,15]

Graphene possesses several properties that make it attractive for environmental applications. The most studied aspect of graphene is probably its electronic properties.[7,20] Electrons were found to have high mobility in graphene, reaching 10,000 to 50,000 $cm^2\ V^{-1}\ s^{-1}$ at room temperature, with an intrinsic mobility limit of >200,000 $cm^2\ V^{-1}\ s^{-1}$.[21,22] Graphene can sustain current densities up to six orders of magnitude higher than copper.[7] These remarkable

electronic properties of graphene, however, were obtained under ideal conditions, with mechanically exfoliated graphene under vacuum.[21] Several factors were found to hinder the electronic properties of graphene, such as the number of layers, the presence of defects, impurities, functional groups, the size and flatness of the sheet, and the nature of the substrate.[5,22] Nonetheless, the promising electronic properties of graphene have triggered research and development for of its use in novel electronic devices,[9] photocatalytic materials,[23] environmental sensors,[5,24] and energy production and storage.[25]

Despite being one atom in thickness, graphene is also a very strong material. It is in fact the strongest material measured, with a Young's modulus of E = 1.0 TPa and intrinsic strength of 130 GPa in its pristine, atomically perfect form.[26] These exceptional mechanical properties have triggered interest in the use graphene as a filler to strengthen the mechanical properties of softer materials.[27] Compared to carbon nanotubes (CNTs), which have also been extensively investigated as nanofillers for polymer matrixes,[28] graphene can offer even superior improvement of the mechanical properties of polymers, due to better interactions between the sheets and the polymer matrix resulting from the high surface area of the planar graphene sheets.[29]

Graphene, like all nanoscale materials, also possesses a high specific surface area. In fact, graphene represents the most extreme case of high-surface materials, since every atom of a single-layer graphene sheet is exposed from both sides to its environment.[30] Graphene has the highest specific surface area of all materials, with a theoretical value of 2,630 m^2 g^{-1}. The high surface area of graphene makes it an ideal candidate for processes involving adsorption or surface reactions. In addition, graphene represents an excellent support to anchor chemical functionalities or nanomaterials and, thus, graphene-based nanocomposites have been an active area of research for novel materials.[31]

One of the most popular approaches to graphene-based nanomaterials is to use graphene oxide (GO), due to its lower production costs. GO is an oxidized form of graphene, showing a high density of oxygen functional groups (carboxyl, hydroxyl, carbonyl, and epoxy) in the carbon lattice (Figure 1). GO can be produced at low cost by chemical oxidation of graphite to graphite oxide and subsequent exfoliation by ultrasonication.[32] Oxidation of the graphite structure increases the interlayer distance from 0.34 to 0.65 nm, thus decreasing the energy

required to separate the graphene layers.[10] The hydrophilic nature of oxidized graphite will also allow water to adsorb into the lamellar structure, further increasing the interlayer distance to 1.15 nm.[33] The most common approach to produce GO from graphite was first developed by Hummer and Offeman in 1958 and involves $KMnO_4$ as an oxidizing agent in concentrated sulfuric acid.[34] Since then, different reactions were proposed to increase the yield and reduce the emission of toxic gases,[35,36] but $KMnO_4$ remains the most frequently used oxidant for GO production.

Although a much more affordable approach to obtain exfoliated graphene sheets, the oxidation of graphene to GO results in significantly altered physicochemical properties (Figure 1). The high defect density introduced in the carbon structure significantly lowers the electronic and mechanical properties of graphene.[22,37] On the other hand, these oxygen functionalities make GO a hydrophilic material that can form stable suspensions in aqueous media. This hydrophilic nature, combined with its high surface area and functional group density, allows for a wide variety of chemical functionalizations to be performed on GO sheets. GO is therefore widely considered as a building block for novel graphene-based materials.[31,32]

Due to its low production costs, GO could be a very affordable intermediate to graphene production if the original carbon lattice could be restored. The reduction of GO can be achieved using chemical reducing agents, thermal annealing, photoreduction, or microwave-assisted reduction.[38,39] Even though reduction of GO can remove a large fraction of its oxygen content, with the C:O ratio increasing from 2:1 to up to 246:1 (Figure 1), complete reduction of GO is challenging.[39] More importantly, reduction of GO results in an altered chemical structure, with carbon vacancies, residual oxygen content, and clustered pentagons and heptagons carbon structures.[40,41] Because of these defects, reduction of GO only shows a partial restoration of its mechanical and electronic properties compared to pristine graphene (Figure 1). This altered chemical structure must be differentiated from graphene and is termed as chemically converted graphene, reduced graphene, or reduced GO (rGO). Understanding the reduction process of GO, and the successful synthesis of rGO having structural properties close to graphene, will represent significant steps in the development of graphene-based materials.[38,39,42]

Restoring the physicochemical properties of graphene is also vital for the production of graphene-based composite materials. In combination with other types of functional materials, graphene-based composites were found to improve the performance of photocatalytic, biocidal,

electroactive, and adsorbent materials.[23,25,31,43] However, the improved performance of graphene-based composites often relies on synergetic interactions between the properties of graphene, in its reduced form, and of the materials attached to the graphene sheets. The quality of the graphene materials will therefore have an important impact on the performance of the final nanocomposite. A careful optimization of the fabrication process is necessary for optimal performance of graphene-based nanocomposites.[44,45]

3. Graphene materials for contaminant adsorption

Rapid population growth and intensification of agricultural and industrial activities have resulted in a dramatic increase in the number of contaminants released into the environment. These contaminants, which are very diverse in nature, represent a major environmental and public health concern.[1] As a consequence, a global effort exists to develop robust technologies to effectively remove contaminants from both air and water. Among these technologies, adsorption is a fast, inexpensive, and effective method for removal of contaminants from aquatic environments.[46,47] Adsorption is a process where the pollutant (adsorbate) is captured by the nanomaterial (adsorbent) *via* physicochemical interactions.[47] Herein, we describe the application of graphene-based materials as adsorbents for the removal of inorganic and organic contaminants. In addition, we delineate key adsorption mechanisms and advantages/disadvantages of applying graphene materials as adsorbents for decontamination.

3.1 Metal ion adsorption

Metals are common pollutants that can undesirably enter aquatic environments and drinking water supplies from anthropogenic activities, such as mining and industrial wastes, or from the corrosion of pipes, soldered joints, and plumbing materials.[48] Hence, there is a growing interest in controlling the concentration of toxic metals in water. For example, according to the United States Environmental Protection Agency (EPA), the allowed concentrations of copper (Cu) and lead (Pb) in drinking water are, respectively, 1.3 ppm and 15 ppb.

Conventionally, activated carbon has been used as adsorbent due to its excellent adsorption capacity for a wide range of contaminants.[49] However, the wide use of activated carbon has been restricted because of its high production cost and the difficulty in regenerating it.[46,50] Carbonaceous adsorbents based on CNTs and graphene materials have been developed as an alternative to conventional adsorbents.[51,52] Carbon nanomaterials have been chosen as a platform to build new adsorbents, mostly because of their high surface area, non-corrosive property, presence of oxygen-containing functional groups, tunable surface chemistry, and scalable production.[53,54]

For CNTs, the sorption capacity is mainly determined by the chemical nature of CNTs, the surface area, and the number of oxygen functional groups.[53,55] The mechanism of metal ion sorption on CNT surface has been related to electrostatic interactions and sorption-precipitation between metal ions and the oxygen-containing groups.[56] These oxygenated groups provide a negative residual charge to the surface of CNTs. Thus, depending on the solution pH, the oxygen atoms hold a lone electron pair that is responsible for ion-exchange and electrostatic interaction with metal ions.[55,56]

Compared to CNTs, the utilization of graphene-based materials as adsorbents may offer several advantages. First, single-layered graphene materials possess two basal planes available for pollutant adsorption.[54,57] In contrast, the inner walls in CNTs are not accessible by the adsorbates.[54] Second, GO and rGO can be easily synthesized through chemical exfoliation of graphite, without using complex apparatus or metallic catalysts.[54] The resulting graphene material is free of catalyst residues, and no further purification steps are needed. In the specific case of GO, the as-prepared material already possesses a large number of oxygen-containing functional groups and no additional acid treatments are required to impart a hydrophilic character and reactivity to GO.[52] This is a significant advantage, since those functional groups are likely responsible for the adsorption of metal ions by GO sheets.

A variety of studies have described the application of graphene-based materials as adsorbents for the removal of inorganic species from aqueous solutions.[52,58] Most of these studies have employed GO as a model adsorbent for remediation of metal ions in water.[52,58–60] GO is preferable to pristine graphene for metal ion adsorption due to GO's high content of oxygen groups available to interact with metal ions. The importance of these oxygen-containing

functional groups was demonstrated by comparing the Pb(II) adsorption performance of pristine and oxidized graphene sheets.[61] Pristine graphene was first prepared through a vacuum-promoted low-temperature exfoliation and submitted to heat treatments at 500 and 700°C (GNS500 and GNS700) to introduce oxygen functional groups. GNS500 and GNS700 revealed a higher adsorption capacity for Pb(II) compared to pristine graphene, which underscores the importance of carboxyl groups in the adsorption mechanism of Pb(II).[61]

Numerous factors, such as ionic strength, pH, number of layers of GO, and presence of natural organic matter were found to influence the adsorption capacity of GO.[52,59,60,62] For instance, the influence of ionic strength on the adsorption capacity may be due to competition between electrolytes (NaCl, KCl, and $NaClO_4$) and the metal ions for the GO surface.[62] In fact, the introduction of electrolytes may affect the electrical double layer of hydrated particles, thus changing the way metal ions bind to the GO sheets.[57,62] Wang *et al.* demonstrated that the adsorption ability towards Zn(II) was decreased after addition of $NaNO_3$, NaCl, and KCl to GO suspension.[62] Conversely, the sorption capacity of GO for Cd(II) and Co(II) was weakly dependent on $NaClO_4$ concentration, while the adsorption of Pb(II) was not affected by changes in ionic strength.[52,60]

The adsorption of metal ions on GO is also greatly affected by pH, with the adsorption capacity decreasing at lower pH.[52,59,60,62] The behavior of GO in aqueous solution is governed by its pH_{pzc} (pzc: point of zero charge). When solution pH is higher than pH_{pzc} ($pH > pH_{pzc}$), the GO surface is negatively charged because of the deprotonation of carboxyl and hydroxyl groups. When the GO surface is negatively charged, the electrostatic interaction with metal ions (positively charged) is favorable, leading to improvement in adsorption capacity.[52,59,62] In contrast, when $pH < pH_{pzc}$, GO becomes positively charged and electrostatic interactions are weakened due to charge repulsion.[52,59]

In a similar way, pH also influences the charged nature of the adsorbates.[57] Depending on the pH, metallic ions can form hydroxide species: $Me(OH)^+$, $Me(OH)_2$, and $Me(OH)_3^-$.[52,59] The practical implications of these hydroxides are: (*i*) due to a lower residual charge, $Me(OH)^+$ species have less affinity to the GO surface compared to its counterpart M^{+2}; and (*ii*) at higher solution pH, precipitation of $Me(OH)_2$ or electrostatic repulsion of negative species by the

negatively charged surface of GO can prevent the adsorption of metals on the graphene surface.[52,59,60,62]

In practical terms, the ideal procedure is to establish a pH condition where the metal maintains its Me^{+2} form, while the GO surface is negatively charged. This optimal pH range might be different according to each metal species and graphene sample. Sitko *et al,* for example, demonstrated the removal of Cu(II), Zn(II), Cd(II), and Pb(II) ions at pH 5.0,[59] while Zhao *et al.* showed that Co(II) and Cd(II) were effectively adsorbed by GO sheets at pH 6.0.[52]

Even though electrostatic interaction between oxygenated groups and metal ions has been considered the major adsorption mechanism, a second type of interaction may occur. Huang *et al.* suggested that the delocalized π-electrons in the sp^2 network of graphene can act as Lewis bases donating electrons to metal ions.[61] In this context, π-electrons on the graphene aromatic plane can be classified as the base (electron donors), while the metal species is the acid (electron acceptors). The same mechanism was previously proposed to explain the adsorption of Pb(II) ions on graphene.[49]

Due to its large surface area and chemical stability, graphene has also become a versatile candidate for building adsorbent nanocomposites with inorganic nanomaterials.[63] Of particular interest is the conjugation of graphene with magnetic nanoparticles (e.g., iron or iron oxide), which has been the most common approach to prepare graphene-based composites for the removal of metal ions.[63–69] Although the high adsorption capacity and magnetic property of iron oxide nanoparticles have stimulated their use as adsorbents, their application in continuous flow systems is difficult because of their small size and susceptibility to oxidation/dissolution.[65,70] To overcome this drawback, graphene sheets can be used as a physical support to stabilize magnetic nanoparticles, facilitating their recycling and reuse.[65,67] In addition, immobilizing magnetic nanoparticles on graphene sheets also prevents their aggregation, thus reducing the associated losses in surface area and adsorption capabilities.[67] Also, the graphene-magnetic nanoparticle composites can be rapidly and efficiently separated from aqueous solutions using a simple magnet.[68]

Graphene-magnetic nanoparticle composites were highlighted as having improved adsorption performance.[65,67] The high sorption capacity of magnetite-graphene composites may

be attributed to a combined effect of metal complexation on the nanoparticles and on the adsorption sites on graphene aromatic layer.[65] Beyond that, the decoration of graphene sheets with magnetic nanoparticles increases the surface area of the material, improving the number of binding sites for metal ions.[65,69] The adsorption capacity of magnetic-graphene materials, like GO, is affected by changes in pH conditions and adsorbent dosage,[65,66,68] time of contact,[64,66–68] temperature,[67,69] and presence of natural organic matter such as fulvic acid.[66]

New adsorbents have also been prepared by modifying graphene materials with organic molecules that possess a natural ability to capture metal ions. As the intrinsic functional groups located on GO sheets are limited, the number of adsorption sites can be improved by grafting compounds such as ethylenediamine triacetic acid (EDTA)[71] and chitosan.[72] Most of these functionalization procedures have been performed taking advantage of the oxygenated functional groups on GO or rGO. For example, carboxyl groups were used to graft poly(acrylamine) (PAM) chains on the surface of rGO sheets.[73] The dispersibility and adsorption capacity of rGO for Pb(II) was remarkably improved after grafting with PAM, increasing from 500 to 1000 mg g^{-1}. In another study, chelating groups were also introduced to the GO surface through reaction of EDTA-silane with C-OH groups of graphene.[71] After modification, the adsorption capability towards Pb(II) was enhanced due to the intrinsic complexation property of EDTA. The anchoring of EDTA molecules also resulted in improvement of surface area and number of functional groups on the original GO sheets.[71]

In addition to increasing the adsorption capacity, functionalization of graphene materials with organic molecules can also be used to enhance the material recovery process. Thermo-responsive properties were imparted to graphene-based adsorbent materials using a non-covalent assembly of graphene-based adsorbent material with poly(N-isopropylacrylamide).[74] The low critical solution temperature of poly(N-isopropylacrylamide) (32 °C) results in a nanocomposite material that undergoes rapid aggregation and sedimentation at temperatures higher than 36 °C. This aggregation is reversible and the nanocomposites can be resuspended upon decreasing the temperature below 34 °C.[74] Compared to magnetic graphene-based composites, thermo-responsive materials allow for an increased material recovery without the requirement of a strong magnetic field.

Even though most studies report on the adsorption of cationic metal ions, graphene-based materials have also been explored for the removal of anionic pollutants from aqueous solutions, such as phosphate (PO_4^-), perchlorate (ClO_4^-), and fluoride (F^-).[75–77] Unlike the immobilization of cationic metal species, the mechanism of anion (e.g., F^-, Cl^-, and Br^-) adsorption was previously attributed to anion-π interactions.[77] This anion-π association is based on the interaction between the negatively charged anion (or lone electron pair) with an electron-deficient aromatic ring on graphene layer.[77]

Table 1 depicts the most common adsorption mechanisms as well as advantages and disadvantage of using graphene materials and their derivatives as adsorbents for remediation and sequestration of metal ions from aqueous solutions. In addition, Figure 2 illustrates the different methods of applying graphene-related materials as adsorbents for removal of metallic contaminants from aqueous solutions. Table 2 summarizes the maximum adsorption capacity (Qe in mg g^{-1}) of multiple carbon-based materials, including the pristine forms (activated carbon, CNTs, GO, rGO, and graphene), magnetic composites, and eventually nanocomposites prepared through the functionalization of graphene sheets with organic molecules.

TABLE 1

FIGURE 2

TABLE 2

3.2 Organic compound adsorption

Graphene materials have also been applied as absorbents for the removal of organic pollutants, such as dyes, antibiotics, hydrocarbons, crude oil, pesticides, and natural organic matter.[78–83] The mechanism of interaction between nanomaterials and organic compounds is dependent on their structural properties (e.g., molecular conformation, dipole moment, presence of functional groups).[57,84] Hence, the adsorption capacity of the same molecule might be different whether the

absorbent materials are composed of GO, rGO, or pristine graphene sheets. Similarly, the presence or absence of functional groups (-NH_2, -OH, -COOH) in the adsorbate structure will determine the mechanism and efficiency of the adsorption process.[84]

Previously, the mechanisms involved in the adsorption of organic compounds on the surface of CNTs were well-documented by Yang and Xing.[84] Briefly, the adsorption of organic compounds by CNTs was associated with five different molecular interactions, which include electrostatic interaction, hydrophobic effect, π-π bonding, hydrogen bonding, and covalent bonding. The same mechanisms described for CNTs eventually have been applied to understand the adsorption of organic compounds by graphene-based materials.[57]

Electrostatic interaction is prevalent when the adsorbate has charged functional groups while the adsorbents preserve their charged surface.[84] For instance, the adsorption of cationic dyes such as methylene blue and methyl violet by GO over a wide pH range (6-10) is mediated through electrostatic interactions between exfoliated GO and the dye molecules.[85] Conversely, the adsorption of anionic dyes (rhodamine B and orange G) by GO was not favorable at the same pH range. As the carboxyl groups in both materials were negatively charged, a subsequent electrostatic repulsion was possibly created between GO sheets and the anionic dyes molecules.[85] Other studies have also shown the efficient sequestration of cationic dyes by GO sheets, and electrostatic interactions have been recognized as an important adsorption mechanism.[86–88]

Few studies, however, consider that the adsorption of cationic dyes on GO is also governed by π-π interactions.[87,89] In addition, it has been suggested that under conditions where the pH was not adjusted, the formation of hydrogen bonds could be an important component in the molecular interaction between a cationic acridine orange dye (which contains –NH_2 groups) and GO monolayers.[90] In another study, the uptake of cationic methylene blue by GO exfoliated layers was extensively improved when samples with higher oxidation degree were used.[78] With increasing oxidation degree, the mechanism of sorption was presumed to change from parallel π-π stacking to vertical electrostatic interactions.

Interestingly, the use of rGO-based adsorbents did not benefit the adsorption of cationic dyes, but increased the adsorption of anionic dyes.[85] Besides the existence of possible electrostatic interactions, the major mechanism of adsorption was attributed to van der Waals

interactions between aromatic rings of both adsorbate and adsorbent.[85] Recently, a sample of rGO was activated using $CO_2/ZnCl_2$ in order to increase its oxygen content.[91] In this specific case, because of the abundant presence of negatively charged groups, electrostatic interactions were believed to dominate the adsorption mechanism of methylene blue.[91]

Hydrogen bonding interaction plays an important role when the elements involved in the adsorption contain functional groups (e.g., amine, hydroxyl, and carboxyl groups). Thus, hydrogen bonding has been reported to participate in the adsorption of polar hydrocarbons by GO-based materials, including anthracenemethanol, naphthol, and 1-naphthylamine.[80,92–94] The formation of hydrogen bonds was used to explain the adsorption of bisphenol A on graphene sheets obtained by the chemical reduction of GO. In this case, the adsorption was related to hydrogen bonding interactions between hydroxyl groups on bisphenol A molecules and the remaining oxygenated groups on the graphene sheets. Because bisphenol A also contains an aromatic nature, the hydrogen bonding likely coexists with π-π stacking interaction during the adsorption process.[95]

While hydrogen bonding is related to the adsorption of polar hydrocarbons on GO, hydrophobic effects can be used to interpret the adsorption of hydrophobic organic compounds (HOCs) by graphene.[57,84] Among these HOCs, the adsorption of naphthalene, phenanthrene, pyrene, and polychlorinated biphenyls compounds on graphene-based materials has been explored.[92,94,96–98] Hydrophobic interactions were assumed to be involved in the adsorption mechanism of non-polar hydrocarbons on rGO or pristine graphene sheets,[93,97,99] likely because their surfaces are substantially more hydrophobic than GO. Previous studies have demonstrated that pristine graphene sheets exhibited an enhanced adsorption performance compared to GO for polycyclic aromatic hydrocarbons, such as naphthalene, phenanthrene, pyrene, and biphenyl.[97,99] In addition to the improved π-π interactions, the high affinity between graphene sheets and the hydrocarbons was also attributed to a sieving effect created by the grooved regions present on graphene surface.[99]

Beless *et al.* compared the adsorption capacity of carbonaceous materials (activated carbon, CNTs, GO, and graphene) against 11 homologues of polychlorinated biphenyls (PCBs).[98] According to Langmuir, Freundlich, and Polanyi-Manes isotherms, activated carbon

exhibited the highest adsorption capacity for PCBs among the adsorbents investigated. In general, even though pristine graphene presented slightly higher adsorption capacities than both GO and CNTs, the adsorption performances for the three nanomaterials were found to be comparable.[98] This result differs from those reported in a prior study cited above,[97] which reports a significantly higher maximum adsorption capacity towards biphenyl for graphene compared to GO.

These controversial findings suggest that further research is still needed to understand the real contribution of graphene materials in the adsorption of organic contaminants. It is also worth mentioning that a fair comparison between the studies in the literature is a challenge, since graphene samples are frequently prepared using different methodologies. Small changes in the synthesis procedure, such as concentration and type of oxidizing agents, might lead to materials with markedly different physicochemical characteristics.[35]

Overall, extensive efforts have been made to develop graphene-based materials for application as environmental adsorbents. Several obstacles, however, must be overcome. First, although graphene nanomaterials have demonstrated effective adsorption performance, their likely superior adsorption capacity compared to conventional technologies remains inconclusive. In addition, even though graphene nanomaterials can be easily produced by chemical exfoliation, the cost and manufacturing of large amounts of graphene nanomaterials for contaminant adsorption are not yet established. A comparison between the adsorption performance of activated carbon, CNTs, and graphene-related materials to organic compounds is shown in Table 3.

TABLE 3

3.3 Gaseous adsorption

Among gaseous contaminants, carbon dioxide (CO_2) has attracted great attention because of its implications for global warming.[100] Conventionally, aqueous solutions containing amines or ionic liquids have been used for CO_2 capture.[101,102] However, these technologies are expensive and energy-consuming.[103] Nanostructured materials were found to be promising alternatives to mitigate the environmental impacts related to the excessive emission of CO_2.[104] The

development of materials with gas adsorption and storage capacity is also a subject of interest for various industrial activities, including advanced oil recovery and shale gas extraction.[105,106] Due to its high surface area, layered structure, and tunability of functional groups, graphene-based materials were found to have great applicability as adsorbents to capture gaseous pollutants.[107,108]

Mathematical simulations, such as *ab initio* density functional theory (DFT), have been used to obtain adsorption isotherms and understand the underlying factors involved in the adsorption/desorption energies of CO_2 on graphene nanomaterials.[107,109,110] For example, Ghosh *et al.* demonstrated the uptake of CO_2 and H_2 by graphene derivative materials prepared by the exfoliation of graphitic oxide and transformation of nanodiamonds.[107] Using generalized gradient approximations to explore how CO_2 molecules interact with graphene sheets, they found that the maximum CO_2 uptake on a single-layer graphene sheet is 37.93 wt%, considering that CO_2 molecules have a parallel orientation on graphene layer.[107] DFT calculations were also performed to study the CO_2 adsorption to defective graphene sheets.[110] The results indicated that CO_2 exothermically adsorbs on the vacancy defects of graphene sheets. Similarly, the CO_2 adsorption capacity was shown to be four times higher in defective graphene with monovacancies than in defect-free graphene.[106] It was also found that CO_2 molecules could react with the reactive carbon atoms on the vacancy, leading to the formation of C-O bonds.[106]

The influence of oxygen functionalities on the adsorption of CO_2/CH_4, CO_2/N_2, and CO_2/H_2O gaseous mixtures by porous carbon surfaces was also investigated.[105] Grand canonical Monte Carlo simulations showed that CO_2 is preferentially adsorbed on the oxygen functionalities of the surface compared to methane (CH_4) and nitrogen (N_2). This improved adsorption was facilitated by the higher dipole moment of CO_2 over CH_4 and N_2. For CO_2/H_2O mixture, however, the water vapor was preferentially adsorbed on the oxygen-containing functional groups in comparison to CO_2. These results suggest that the chemistry of graphitic surfaces can be potentially tuned to generate selective gas separation properties.

In this regard, graphene sheets were modified with amine functionalities, layered double hydroxides (LDHs), and metal species to improve their gas adsorption capacity.[111–117] For example, the combination of GO sheets with two-dimensional LDHs resulted in a 62% increase in the absolute CO_2 adsorption capacity of pure LDHs.[115] Additionally, graphene sheets decorated with polyaniline showed a higher CO_2 adsorption performance in comparison to

pristine graphene,[111] an effect attributed to chemical interactions between CO_2 molecules and amine functional groups.[111,114] Indeed, the chemical modification of graphene with amine groups increases the basicity of the surface, making the adsorption of the acidic CO_2 favorable through carbamate formation ($R\text{-}NHCOO^-$).[113]

The removal of other greenhouse gases such as nitrogen dioxide (NO_2), sulfur dioxide (SO_2), carbon monoxide (CO), and hydrogen sulfide (H_2S) by graphene-based adsorbents was also investigated.[118–120] Zirconium hydroxide/graphene composites were applied as adsorbents for SO_2 removal.[119] The interaction between $Zr(OH)_4$ and the acid groups of GO precursor generated basic sites and porosity which were associated with the strong SO_2 adsorption capacity of the composite. Further, the adsorption of nitrogen oxides (NO_x) on graphene was investigated using DTF simulations.[121] The presence of oxygen functional groups is responsible for the stronger adsorption of NO_x on GO compared to graphene. The adsorption process of NO_2 on GO was attributed to the formation of hydrogen bonding and weak covalent bonds (e.g., C--N and C--O). Depending on the GO configuration, NO_2 could also sequester hydrogen atoms from the hydroxyl groups and form a sort of nitrous acid-like structures (H-ONO), leading to single C-O bonds that potentially can be converted to more stable bonding configuration (C=O).[121] Some experimental and theoretical studies have also demonstrated the potential of graphene-based materials to remove ammonia (NH_3).[122–126] Seredych and Bandosz demonstrated that the presence of adsorbed water on graphite oxide surface was responsible for the enhancement in NH_3 adsorption,[127] whereas water vapor in the gas phase (moist condition) decreased gas adsorption due to the competition between NH_3 and water molecules for the active sites. In general, the adsorption of NH_3 on graphite oxide is done through reaction with hydroxyl and carboxyl groups, hydrogen bonding, and physical trapping into the interlayer space or pores.[127] A similar trend was later reported for the reactive adsorption of NH_3 by layered graphite oxide.[122] The presence of water in the interlayer space was found to enhance NH_3 adsorption by a dissolution mechanism. On the other hand, excess water probably led to the formation of a film around the oxygenated groups, thus preventing them from reacting with NH_3 molecules.[122]

Surface chemistry was also found to affect NH_3 adsorption capacity of graphite oxide.[125] Gas adsorption by graphite oxide was likely caused by the binding of NH_3 to carboxyl, sulfonic,

and epoxy groups. The increase in porosity owing to the reduction of GO with hydrazine did not play an important role in the adsorption mechanism. However, the reduction of graphite oxide led to a lower NH_3 adsorption because of the decrease in oxygen content on the material's surface. These experimental observations were in accordance with a theoretical study performed by Tang and Cao.[124] Using DFT calculations, the theoretical adsorption of NH_3 by either GO or graphene was also compared. Due to the large number of defects and oxygenated functional groups, GO presented a stronger NH_3 adsorption in comparison to graphene. NH_3 molecules were found to interact with hydroxyl and carboxyl groups of GO through hydrogen bonds. Moreover, charge transfer from NH_3 to oxygen groups and subsequent formation of NH_2 and NH groups was also considered a feasible mechanism of adsorption.[124]

The adsorption capacity of graphene-based materials can be further increased by their integration in hybrid metal-organic frameworks (MOFs).[123,126] MOFs-graphene composites are usually prepared through the coordination of oxygen groups of GO with the metallic structures of MOFs (ZnO, copper, or iron). Specifically, for Cu-based MOF-graphene composite, an enhanced NH_3 adsorption in comparison to their pristine precursors (GO and MOFs) was observed.[123] This improved capacity was associated with an increase in porosity and the binding of NH_3 to copper sites on the surface of the nanocomposite.

4. Graphene-based photocatalytic materials for water decontamination

Even though adsorption can remove contaminants from water, this technique does not degrade the compounds, which require further disposal.[128] Complete mineralization or destruction of contaminants potentially can be achieved using photocatalytic treatment.[128,129] In this endeavor, photocatalysis has arisen as an attractive strategy for water remediation and wastewater treatment, since it is low in cost and effective.[128] In this section, we describe the different strategies to prepare graphene-based photocatalysts and their role in the degradation of organic and biological contaminants.

4.1 Preparation of graphene-based photocatalysts

Heterogeneous photocatalysis is based on the production of highly oxidative species or free radicals (such as -OH•, O_2^-•, and H_2O_2) by semiconductor catalysts upon presence of light energy.[129] Conceptually, these semiconductor materials are characterized by having an electronic structure comprising a filled valence band and an empty conduction band.[23] When a photon of energy ($\lambda\nu$) that exceeds the band gap energy (E_g) reaches the semiconductor catalyst, a lone pair of electrons on the valence band is excited to the conductance band, thus leaving behind a hole.[23,129,130] The photoactivated electron-hole (e^-/h) pair, which concentrates on the semiconductor surface, is then responsible for the oxidative reactions involved in the degradation of organic molecules or energy production *via* solar cells.[23,129] One of the greatest hurdles regarding semiconductor catalysts is that the excited electron can rapidly recombine with the empty hole on the valence band. When the photoactivated electron recombines with the valence band, part of the energy is dissipated, thus decreasing the photocatalytic activity and limiting the commercial applicability of semiconductors.[130]

Since the demonstration of the electrochemical decomposition of water by TiO_2 under visible light irradiation by Fujishima and Honda in 1972,[131] the number of studies focusing on the development of photocatalysts with improved efficiency has grown exponentially.[132] However, TiO_2 is limited by its absorption in the near ultraviolet (UV).[133] Advances in nanotechnology allowed researchers to address this issue by the development of novel nanosized photocatalysts with different photocatalytic properties.[134–136] The conjugation of TiO_2 nanoparticles with carbonaceous materials, including activated carbon, CNTs, and graphene, has also been explored as an approach to improve the photocatalytic properties of TiO_2.[132]

One of the most important characteristics of graphene for photocatalysis is its ability to tune the band gap energy of semiconductors. In addition, the presence of graphene, due to its high electron mobility, contributes to the suppression of rapid recombination of electron-hole pairs, thus leading to an enhancement in photocatalytic activity.[137–139] The formation of composites between semiconductor particles and graphene sheets can therefore contribute to extending the photocatalytic activity of conventional photocatalysts, such as TiO_2, by decreasing the frequency of electron-hole pair recombination.

Graphene-based photocatalysts are prepared by anchoring photoactive nanostructures on graphene. Prior reviews on this subject described in detail the methods used to prepare graphene nanocomposites for photocatalysis purposes.[23,130] Even though the focus of our review is on environmental applications, we provide a brief review of the different methods to prepare graphene-based hybrid photocatalysts.

Graphene-based photocatalytic nanocomposites are synthesized using three main strategies.[23,130] The first methodology involves the formation of nanoparticles directly on GO surface using the oxygen-containing groups of GO as nucleation sites for the nanoparticle growth. For example, TiO_2-GO nanocomposites were prepared via hydrolysis of TiF_4 in aqueous solution of GO at 60°C for 24 h.[140] A similar protocol was developed by Liang et al.,[141] who coated GO sheets with TiO_2 particles by hydrolyzing $Ti(BuO)_4$ at 80°C in the presence of H_2SO_4 and a mixture of ethanol/H_2O. Ag/AgX/GO nanocomposites were obtained by reacting GO and silver nitrate ($AgNO_3$) in the presence of cetyltrimethylammonium bromide or chloride.[142]

One of the greatest advantages of the *in-situ* growth of nanoparticles on GO is that it provides an intimate chemical interaction between the semiconductor and the graphene sheet.[138,141,143] To increase the capacity for electron transfer, some of these *in-situ* procedures also reduce GO to rGO. For instance, ZnO/graphene composites were prepared by first exposing a GO dispersion to the salt precursor (($Zn(AcO)\cdot 3H_2O$).[135] The resulting powder was then reacted with $NaBH_4$ at 120°C to obtain rGO sheets decorated with crystalline ZnO nanoparticles.[135] In another study, a graphene photocatalytic composite was prepared *via* a one-step direct redox reaction.[144] This reaction allowed the simultaneous reduction of GO and subsequent oxidation of $TiCl_3$ and $SnCl_2$ precursors to SnO_2 and TiO_2, respectively, on the rGO sheet. Interestingly, during this reaction, the precursor compounds ($TiCl_3$ and $SnCl_2$) acted as reducing agents, reducing the oxygen groups of GO and simultaneously oxidizing themselves to metal oxide nanoparticles.

The second method of producing graphene-based photocatalysts is by the direct contact of pre-synthesized photoactive nanoparticles with graphene sheets. The adhesion of the photocatalysts on graphene can be facilitated through sonication or stirring. For example, a TiO_2-graphene nanocomposite was prepared by mixing a suspension of TiO_2 nanoparticles with GO in ethanol, followed by UV-irradiation to reduce GO sheets.[145] Wang, et al. also reported the

synthesis of $BiVO_4$-rGO composite through electrostatic interactions between positively charged $BiVO_4$ and the negatively charged GO, followed by reduction of GO and nanoparticle crystallization *via* hydrothermal treatment.[136]

The third and certainly the most frequently used method to produce graphene photocatalysts is the hydrothermal treatment.[134,146–150] The hydrothermal synthesis has been extensively applied to produce crystals of inorganic salts under high temperature and pressure. The crystallization of metal precursors by the hydrothermal method depends on numerous parameters, including the source of metal, temperature, pH, solvent, and time.[151] Although many of those variables must be optimized to achieve a reproducible methodology, the hydrothermal synthesis provides the crystallization of semiconductor metal in a single-step procedure. All the reactants can be mixed together, placed in an autoclave, and readily treated to produce the nanostructures of interest.

Hydrothermal methods offer the additional advantage of partially or completely reducing GO to rGO during the crystallization process. TiO_2-graphene nanocomposites were synthesized using the one-step hydrothermal synthesis.[150] In this case, a commercial sample of TiO_2 (P25) was used as a precursor. During the hydrothermal reaction, the reduction of GO and the deposition of P25 on graphene surface were simultaneously achieved. A homologue procedure was also described for graphene-TiO_2 nanotube composites, in which commercial TiO_2 nanoparticles (P90) were reacted with GO in an alkaline hydrothermal process.[147] In this case, high temperature treatment simultaneously converted the TiO_2 nanoparticles to narrow nanotubes and reduced GO to rGO. The few oxygen functional groups on rGO were assumed to provide nucleation sites for growth of nanotubes from TiO_2 nanoparticles.[147]

As each of these methodologies has pros and cons, the choice of which method is more appropriate will depend on the properties the users wish to achieve, the availability of instrumentation, and the specific applications intended for the photocatalysts.

4.2 Graphene photocatalysts for degradation of organic compounds, reduction of heavy metals, and water disinfection

Due to its low cost and strong oxidizing activity, TiO_2 is the most commonly used semiconductor for forming graphene-based photocatalytic nanocomposites for the photodegradation of organic and biological contaminants. The popularity of TiO_2 is also explained by its commercial availability: TiO_2 products P25 or P90 serve as both reference material and reagents for the synthesis of graphene-based TiO_2 photocatalysts.[137,141] For example, P25-graphene nanocomposites, prepared *via* hydrothermal reaction, showed higher capacity to degrade methylene blue over pure P25 nanoparticles under UV and visible light.[150] The presence of graphene increases the capacity to adsorb pollutants, extends the light absorption range, and improves the charge transport/separation properties of P25-graphene composite.[150]

P90 TiO_2 nanoparticles were also conjugated with GO and, through an alkaline hydrothermal process, converted to rGO decorated with TiO_2 nanotubes (rGO-TNT).[147] The rGO-TNT composites were prepared using various concentrations of rGO and the photodegradation of malachite green (dye) was found to be influenced by the rGO/TNT ratio. rGO-TNT containing 10% rGO showed the highest photodegradation activity against malachite green, a performance three times higher compared to neat TiO_2 nanotubes. Rather than spherical-like nanoparticles, the formation of inorganic nanotubes was preferred because TiO_2 nanotubes have improved surface area and larger number of active sites.[147]

The enhancement in photocatalytic activity for P25-graphene and rGO-TNT nanocomposites goes beyond the improved electron transfer provided by the presence of graphene sheets. Actually, the mechanism by which graphene-TiO_2 composites display such an enhanced photocatalytic performance for degradation of organic dyes has three sequential steps, as illustrated in Figure 3.[147,150] Overall, these three mechanistic components contribute to the increased efficiency of photocatalytic degradation of pollutants by graphene-based photocatalysts.

FIGURE 3

The first step is the adsorption of the dye molecule on the surface of graphene sheets. As dyes are aromatic molecules, their adsorption on graphene is promoted by π-π stacking interactions between the sp^2 domains from both systems.[150] Therefore, the adsorption capacity of graphene-TiO_2 composites for organic dyes can be higher than bare TiO_2 nanomaterials. Upon

interaction with graphene sheets, the oxidative species surrounding the catalyst can readily access the adsorbed dye, making the photodegradation process more effective.[147]

The second step in the photocatalytic mechanism concerns light absorption. The range of light absorption may be shifted when the photocatalyst is attached on graphene. For example, a red shift of approximately 30-40 nm was observed for graphene-P25 nanocomposites compared to pristine P25 particles.[150] This behavior suggests that the band gap of P25 nanoparticles is narrowed after its attachment on graphene surface, leading to lower electron-hole recombination rates and better utilization of the light energy.[150] A similar red shift in light absorption, from 325 to 400 nm, was also observed for TiO_2 nanorods combined with GO sheets.[137]

The third step is related to the charge carrier separation and transport.[140,144,150] It is well-established that the electron-hole recombination rates in semiconductors are quite high.[128] However, it is also believed that the electron-hole recombination and electron transfer rate can be improved when the photoactive nanoparticles are anchored on graphene sheets. In presence of graphene, the excited electrons are quickly transferred through the sp^2-hybridized network of graphene sheets.[150] If the electron-hole pairs are prevented from recombining, the excited electrons on the valence band will be available to reach the reaction points and generate oxidative species, thus enhancing the performance of photocatalytic processes. In this way, graphene sheets work as electron acceptors and provide a conductive platform to transport electrons participating in the oxidation-reduction reactions during the photodegradation of organic molecules.[147,150]

In addition to these studies using commercial TiO_2 nanoparticles, several reports have been devoted to the preparation of graphene modified with TiO_2 nanostructures for the photodegradation of organic dyes.[137,141,152] For example, graphene/TiO_2 composite produced by direct growth of TiO_2 nanocrystals on GO sheets showed a strong photocatalytic activity for the degradation of rhodamine B under UV irradiation.[141] Graphene-TiO_2 nanocomposite exhibited a photocatalytic performance three and four-times higher than P25 and bare TiO_2 nanoparticles, respectively. Interestingly, this nanocomposite prepared by *in-situ* growth of TiO_2 nanoparticles was found to be twice as effective for the photodegradation of rhodamine B than graphene-P25 composite synthesized by hydrothermal treatment.[141] The extended photocatalytic activity of graphene-TiO_2 was attributed to the stronger interaction between TiO_2 and GO which could

facilitate the charge transfer from TiO_2 to graphene and hinder electron-hole pair recombination.[141] A similar trend was described by Liu *et al.*, who demonstrated that, forlong-term exposure, self-assembled TiO_2 nanorods on GO exhibited faster degradation rates of methylene blue than graphene-P25 nanocomposite.[137]

Additional studies have also concluded that graphene-TiO_2 photocatalysts were more efficient in the degradation of organic dyes in comparison to bare TiO_2 or P25 nanoparticles.[153,154] The increased adsorption of the organic dyes on graphene and the excellent ability to transfer electrons were correlated with the exceptional photocatalytic performance of graphene-related photocatalysts.[137,141,153] Another important factor that may be associated with the improvement in photocatalytic activity for graphene-based photocatalysts is their increased surface area.[141,153] In any case, the photocatalytic activity of graphene-based photocatalysts is dependent on the relative concentration of graphene on the photocatalyst, and the morphology, content, and size of TiO_2 nanoparticles on the graphene nanocomposites.[137,152,154]

Three-dimensional materials have the capacity to improve the performance of photocatalytic materials by providing open channels and improved surface area. Hierarchically ordered macro-mesoporous TiO_2-graphene composite films were produced by a self-assembly method using polystyrene spheres as templates.[155] GO has been incorporated in the macro-mesoporous structures and then reduced to graphene by hydrazine vapor. The hierarchically ordered macro-mesoporous TiO_2-graphene composite films showed higher capacity for adsorption and photodegradation of methylene blue compared to ordinary 2D hexagonal TiO_2 mesoporous films.

Semiconductor photocatalysts such as silver orthophosphate (Ag_3PO_4), bismuth vanadate (BiVO4), cadmium sulfide (CdS), and Ag/AgX (X=Br, Cl) nanoparticles were also conjugated with graphene sheets to create hybrid photocatalysts for the photodegradation of organic dyes.[134,136,142,156] These graphene-based photocatalysts all showed an enhanced photocatalytic activity compared to their respective pristine nanostructures.

Generally, the photodegradation of dyes occurs due to the photoexcitation of semiconductor materials upon light irradiation. However, Xiong *et al.* emphasized that the photodegradation of rhodamine B was achieved by excitation of the dye molecule itself under

visible light (dye*).[157] The ejected electron from the excited dye could be transferred to GO surface and then conducted to the semiconductor nanoparticles.

A similar observation was also reported for rGO-SnO_2 nanocomposites, where the degradation of rhodamine B was mostly associated with the photosensitization of the dye molecules instead of the rGO-SnO_2 composite.[144] The photogenerated electrons from the excited dye molecules could move to the conductance band of SnO_2, with the graphene sheets acting as bridges between these electrons and the SnO_2 nanostructures.[144] A similar mechanism was also reported for the photodegradation of rhodamine B by ZnO-graphene nanocomposites under visible light irradiation.[135]

In addition to dye degradation, graphene-based photocatalysts have also shown increased efficiency for the degradation of hydrocarbon derivatives. As an example, graphene-CdS nanocomposites, prepared by self-assembling positively charged CdS nanostructures with negatively charged GO sheets, were applied as photocatalysts for selective reduction of nitro aromatic compounds.[158,159] Additional studies also demonstrated the enhanced degradation of pesticides, methanol, and endocrine disruptors (phenol, bisphenol, and atrazine) by graphene-hybrid photocatalysts.[160–162] All these studies consistently reported that graphene sheets played a crucial role in the enhancement of the photocatalytic ability of pristine semiconductor particles (e.g., TiO_2, Ag nanoparticles, and CdS).[63,160,162]

Even though the mechanism of degradation has been associated with the electron-accepting capacity of graphene and its ability to prevent hole-pair recombination, Zhang, et al. have proposed an alternative mechanism to explain the role of graphene in the selective oxidation of alcohols and alkenes by graphene-ZnS nanocomposites.[139] To prove their proposed mechanism, experiments were conducted under visible light irradiation, where ZnS is not able to be photoexcited. Rather than providing an electron conductive platform as proposed by most studies in the literature, graphene sheets were found to act as a macromolecular “photosensitizer.” In other words, upon visible light irradiation, photo-induced electrons from the graphene itself could be shuttled into the conductance band of ZnS nanoparticles. As a main consequence, the presence of graphene imparts to ZnS particles photocatalytic activity under visible light.

Graphene-based hybrid photocatalysts have also been utilized for the reduction of heavy metals. Specifically, the reduction of Cr(IV) to Cr(III) by graphene-based phtocatalysts was demonstrated.[143,163,164] For example, the photocatalytic reduction of Cr(VI) was significantly improved from 58 to 98% after integration of ZnO nanoparticles with graphene sheets.[143] The enhancement in photoreduction performance was attributed to an increase in light absorption intensity and alteration of the ZnO band gap due to the presence of graphene materials. Thus, Cr(VI) can be reduced by the photoexcited electrons transported from the valence band of ZnO particles through graphene sheets.[143]

Graphene-based photocatalysts were also shown to be able to inactivate pathogens such as viruses, nematodes, and bacteria in contaminated waters.[165–168] Graphene-tungsten oxide composites, for example, showed a strong photoinactivation of bacteriophage MS2 virus under visible light irradiation.[165] Graphene-TiO_2 has also demonstrated a high toxic effect against the nematode *Caenorhabditis elegans* and *Escherichia coli* bacteria under solar light irradiation. The intensive chemical interaction between TiO_2 and graphene surface was related to the increased charge carrier separation and the efficient generation of ROS, which were likely able to inactivate both model organisms through oxidative stress mechanism.[166]

The promising physicochemical properties of graphene, such as high surface area, transparency, and high electron mobility, have stimulated the production of graphene-based photocatalysts to increase the photocatalytic performance of conventional semiconductors. However, some studies have questioned whether the combination of TiO_2 with graphene really provides a substantial improvement in photocatalytic activity in comparison to other carbonaceous materials (e.g., CNTs, fullerenes, and activated carbon).[138,148,169] Essentially, Zhang et al. claimed that graphene plays a role similar to that of CNTs in enhancing the photocatalytic activity of TiO_2.[148] In addition, they emphasized that graphene/TiO_2 and CNT/TiO_2 composition ratios should be investigated for meaningful comparison. A thoughtful and comprehensive comparison between graphene and CNTs is therefore needed to better understand the contribution of each individual carbon nanomaterial to the enhanced photocatalytic performance of semiconductors.[138]

5. Graphene in membrane and desalination technologies

5.1 Graphene-based membranes

Graphene, despite being only one atom in thickness, is an impermeable material in its pristine form. The delocalized electron clouds of the π orbitals obstruct the gap that would be found in the aromatic rings in graphene, effectively blocking the passage of even the smallest molecular species.[170] The impermeable nature of graphene has allowed its application as a barrier for gas and liquid permeation,[171] or to protect metallic surfaces against corrosion.[172] In the area of water treatment, this unique property of graphene has triggered extensive efforts to use graphene for the design of ultrathin graphene-based water-separation membranes. Two strategies have been explored to use graphene nanomaterials in membrane processes: nanoporous graphene sheets and stacked GO barriers (Figure 4).

FIGURE 4

The interest in nanoporous graphene arises from the already demonstrated potential of aligned CNT membranes to achieve very high permeability due to the unique behavior of water in confined graphenic structures.[173,174] Graphene offers a smooth, frictionless surface for the fast flow of water. In addition, phase transition and molecular alignment of water in confined environments increase the water flux to values much higher than what would be expected from fluid flow theories.[173,174] Nanoporous graphene differs from aligned CNT membranes in two aspects — thickness and mechanical strength. Due to its one-atom thickness, nanoporous graphene represents an ideal membrane barrier. While a similar thickness may also be possible with CNT membranes, the softer polymer-nanotube composite matrix would be very weak and impractical at such low thickness. The high in-plane stiffness of graphene (~1 TPa), on the other hand, makes single-layer graphene sheets a possible approach for single-atom thick membranes.[175]

The promise of nanoporous membranes in water treatment is potentially significant. Modeling results suggest that nanoporous graphene membranes can achieve water permeability of 400−4000 L m^2 h^{-1} bar^{-1} while still rejecting salts, a performance 2 to 3 orders of magnitude higher than current reverse osmosis membranes.[176] High permeability membranes can reduce the membrane area needed for desalination and the energy consumption for brackish water

desalination.[177] A recent modeling study indicates that energy savings from using high permeability membranes, such as nanoporous graphene, can be as high as 46% for brackish water desalination.[178] However, for other processes involving higher feed salinities like seawater desalination, the impact of high permeability membrane on energy consumption will be very small as the process is controlled by the feed solution osmotic pressure rather than membrane permeability.[177] Using state-of-the-art thin-film composite membranes, seawater reverse osmosis desalination is already operating very close to the practical thermodynamic limit of seawater desalination.[177]

Initial demonstration of the potential of graphene as a water separation membrane was realized by molecular dynamics simulations showing the selective passage of ions through nanoporous graphene.[179] Rejection of ions was found to involve steric effects, hydrodynamic interactions, and electrostatic repulsion between charged species and the pores.[179,180] Ion rejection can thus be tuned by functionalization of the pores. Hydrophilic pores provide more water flux but less salt rejection than hydrophobic pores.[176] Gai *et al*. investigated the performance of pores with fluorine (GF), nitrogen (GN), oxygen (GO), and hydrogen (GH) containing functional groups. They found that for the largest pore, providing complete salt rejection, water flux increases in the order GO>GF>GH>GN, while pore size increases in the order GN>GF>GH>GO.[181,182] Although charged groups seem to provide the best permeability and rejection, high ionic strength, as in seawater, suppresses the electrostatic interactions between the pores and the ions by screening the pore charges. When comparing carboxylated, aminated, and hydroxylated pores, Konatham *et al*. concluded that hydroxylated pores may be optimal for nanoporous graphene separation since they offer strong free-energy barriers for ions passage at both low and moderate ionic strength (0.025 and 0.25 M); at the same time, the selectivity of charged functionalized pores decreases significantly as ionic strength increases.[180] For practical purposes, designing the most permeable membrane may not be relevant in order to improve the performance of membrane-based separations. Indeed, high-permeability membranes are limited by increased concentration polarization, scaling and fouling effects, and the inherent thermodynamic limit of the separation process.[177,183] Therefore, focus should be on controlling the selectivity of the pores to ensure good membrane performance.

One of the major technical challenges in the design of nanoporous graphene membranes, especially for salt rejection, is the precise control of pore sizes. Simulations have indicated that 1 nm pore size demarcates the pore diameters that allow for water flow (7 to 9 Å) from the pore diameters that allow for salt permeation (10 to 13 Å).[180–182] Considering the current methods of generating nanopores in graphene (Table 4), fine control of pore sizes in the subnanometer range on a large surface area will be challenging. Nanopores of controlled pore size can be formed in graphene using focused electron beam irradiation above the carbon knockout potential (80 kV).[184–188] However, this approach is not scalable for generating large areas of high pore density. Chemical or oxidative etching, which relies on the enlargement of defects found in graphene, may be more favorable as these methods can be easily performed on larger surfaces.[189–191] Control of the pore size distribution may remain a challenge due to the heterogeneous nature of defects found in graphene.[192]

TABLE 4

Recently, O'Hern *et al*. combined low energy ion irradiation and chemical oxidation etching to generate a single-layer graphene sheet with high-density nanoscale pores having a size distribution of less than 0.2 nm.[193] By changing the etching time, different pore sizes can be obtained. The macroscale nanoporous graphene membrane obtained by this method demonstrated either rejection of anions (short oxidation time) or organic dyes (longer oxidation time). This represents a first step towards the production of a nanoporous graphene membrane, since this approach is scalable and yields well-defined pore size distribution.[193] Yet, the performance of this nanoporous membrane was severely limited by the presence of intrinsic tears and defects in the pristine graphene sheet.[193] Producing a large area, defect-free single-layer graphene on a porous support represents the next important challenge in the development of nanoporous graphene membranes. The economic implications of these membranes must also be considered, as large-area defect-free graphene remains a very expensive material.[194]

Until these economic and technical limitations are overcome, one alternative to graphene-based water separation is based on stacked GO membranes (Figure 4B). In stacked GO membranes, water flows between the GO layers via the narrow hydrophobic channels formed by

792 the unoxidized regions on GO.[195] Like other graphenic surfaces, the frictionless surface of these
793 unoxidized regions allows for a very fast water transport in GO stacks. Membranes formed of
794 stacked GO sheets were shown to reject both salts and organic molecules, indicating that they
795 may be an alternative to using the unique properties of graphene nanomaterials for membrane
796 development.[195–198] In comparison to nanoporous graphene, producing membranes from GO
797 sheets is cheaper and more easily achievable on a large scale.

798 The primary rejection mechanism of ions and molecules by stacked GO membranes is size
799 exclusion. The nanochannels between stacked reduced graphene sheets have a width of 0.4 nm,
800 allowing only water vapor to go through.[195] When the sheets are oxidized, electrostatic repulsion
801 between GO sheets and hydration of the sheets increase the interlayer distance to ~0.9 nm, thus
802 allowing water to flow through the space between the sheets.[195,197] For stacked rGO and GO
803 membranes, water permeabilities values of 21.8 and 71 L m^{-2} h^{-1} bar^{-1} were reported.[196,199]
804 However, over time, in the presence of water, hydration of the sheets will further increase the
805 interlayer distance, thus increasing the water flux but decreasing the selectivity of the
806 membrane.[197,200] Moreover, since the distance between GO sheets is determined by electrostatic
807 interactions between the charged oxygen functionalities of GO, increasing ionic strength or
808 changes in pH have a marked influence on the interlayer distance by altering GO surface
809 charges.[196] For example, water permeabilities for GO membranes were found to be 12.2, 71.0,
810 and 18.9 L m^{-2} h^{-1} bar^{-1} at pH 3, 6, and 12, respectively.[196] High hydraulic pressure can also
811 compress the GO sheets, thereby reducing water permeation through the GO stack.[196]

812 The instability of the nanochannels formed by stacking GO sheets represents a major
813 challenge for using GO as a selective separation barrier, since the selectivity of the membrane
814 will fluctuate over time. Stabilizing the GO sheets is thus necessary to make stacked GO sheets
815 practical for membrane separation. Reducing GO sheets may increase the stability of the stacked
816 sheets by increasing the π-π interactions between the sheets; however, this also decreases the
817 water permeation due to the smaller channel width.[195] Using charged spacers, like charged
818 polymers or nanowires, between GO sheets can stabilize the GO by electrostatic
819 interactions.[201,202] GO sheets can also be cross-linked using chemical groups, offering a stable,
820 covalently bound GO layer with well-defined pore size.[198] GO-composite can be produced by
821 mixing GO sheets and linking agents together and depositing the suspension on a support

layer,[201] or by using a layer-by-layer assembly approach.[198,202] Compared to the former approach, layer-by-layer assembly provides more control on the GO layer thickness and channel width.[203] Since water flux decreases as the number of GO layers increases,[196,199] having control of the membrane thickness will be important in controlling the membrane transport properties.

The other mechanism by which stacked GO membranes prevent the passage of ions and molecules involves the adsorption of ions on GO sheets by cation-π interactions, π-π interactions, or coordination of metal species.[200] Over time, ion adsorption in the GO layers results in a build-up of salts in the membrane. The accumulation of salts in the GO layers was found to contribute to the high flux of stacked GO membranes by providing a strong capillary force and internal osmotic pressure for the permeation of water and small ions.[197] However, this also implies an eventual saturation of stacked GO membranes, an effect that has not been investigated up to now.

Stacked GO membranes represent an attractive alternative to nanoporous graphene, as their production is scalable and relatively inexpensive. Such membranes possess similar attractive properties as nanoporous graphene: inorganic separation layer, high water permeability, and thin structure. Stacked GO membranes are more brittle than single-layer graphene, but a highly porous support layer can be used to strengthen the stacked GO membranes.[196,199,201] To date, however, the selectivity of stacked GO membranes has been mostly limited to relatively large organic molecules and hydrated ions, rendering such membranes comparable to ultrafiltration or nanofiltration membranes. Controlling the channel width in the subnanometer range to obtain high salt rejection remains highly challenging.

5.2 Membrane modification with graphene-based materials

Until the technical and economical limitations of graphene-based membranes can be overcome, polymeric membranes will remain the state-of-the-art for membrane-based separations. While the energy consumption of several pressure-driven membrane processes is high, their permeability, selectivity, and affordability remain unchallenged by pure graphene-based membranes. However, by integrating graphene nanomaterials in the design of polymeric

membranes, it is possible to improve the performance of polymeric membranes by increasing their mechanical properties or reducing their organic and biological fouling propensity.

The excellent mechanical properties of graphene nanomaterials can be used to improve the mechanical strength of polymeric membranes. Strong membrane materials are desirable to avoid membrane failure and to reduce the impact of membrane compaction under pressure, especially for membrane processes subject to high hydraulic pressures like pressure-retarded osmosis.[204,205] Integrating GO sheets at around 1 wt. % directly into the polymer solution can increase the Young's modulus of polysulfone membranes from ~150 MPa to up to 218 MPa.[206,207] Further increase in the GO concentration, however, weakens the membrane due to the poor compatibility of GO with organic solvents; the result is an incomplete dispersion and uneven distribution of GO in the polymer matrix.[27,206]

Previous research on the use of CNT to improve the mechanical properties of polymers has highlighted the importance of optimizing the solubility, dispersion, and stress transfer between the polymer and the nanomaterials.[28] This can be achieved by functionalization of the nanomaterials to increase their affinity to the polymer. Using HPEI-functionalized GO sheets, the loading of PVDF membranes could be increased to 3%, with a concomitant increase in membrane mechanical properties.[208] Further developments in the use of graphene nanomaterials should therefore aim at optimizing graphene surface functionalization in order to better integrate the nanomaterials into the polymer matrix.

Due to the hydrophilic nature of GO and the atomically smooth surface of graphene sheets, incorporation of graphene into membranes results in a smoother and more hydrophilic membrane surface.[208–213] These improved surface properties were found to reduce the adhesion of proteins on GO composite membranes compared to pristine membranes.[210,212,214] For fouling resistant membranes, most studies have focused on blending GO in the polymer solution during membrane synthesis. However, to reduce the adhesion of foulants, only the outer layer truly contributes to the antifouling effect, with the rest being buried in the polymer matrix. Solution blending further uses more nanomaterials than necessary to impart antifouling properties to the membrane. Considering the environmental cost of producing nanomaterials,[215] reducing the amount of nanomaterials used is important when integrating nanomaterials into membrane design.

Surface functionalization of membranes represents a material-efficient approach to enhance antifouling properties, by concentrating the desired material only where it is contributing to fouling resistance. Surface functionalization of membranes has been realized by direct binding of GO sheets to the native functional groups of the membrane or by using an intermediate coating compound to provide reactive sites (Figure 5, A and B). Membrane functionalization can also be obtained by electrostatic deposition of graphene nanomaterials (Figure 5, C and D). These surface functionalization strategies can be used to provide a single layer of graphene nanomaterials, or used sequentially to obtain a layer-by-layer deposition of graphene nanomaterials on the membrane surface (Figure 5, B-D).

FIGURE 5

Layer-by-layer assembly offers a controlled approach to optimize the GO loading on the membrane surface. For example, by using a layer-by-layer approach based on GO and amine-terminated GO sheets, surface functionalization of polyamide thin-film composite membranes was found to impart antifouling properties and chlorine resistance to the membrane.[216] The increased chlorine resistance was attributed to the limited diffusion of active chlorine species towards the polyamide layer in the layered GO structure, and was shown to increase as the number of layers increases.[216] GO sheets on a membrane support can also serve as a selective barrier for salt,[198] as recently demonstrated with hollow fiber membranes.[217] Under those conditions, a layer-by-layer approach can allow for optimal membrane functionalization. On the other hand, for applications where only the top layer is active, such as antifouling or antimicrobial properties, a surface functionalization providing only a monolayer of graphene is sufficient.[218]

Biological fouling can also be reduced by membrane functionalization with graphene nanomaterials. Graphene nanomaterials have intrinsic antimicrobial properties, which induce inactivation of bacterial cells upon direct contact by physical and oxidative damage to cell membranes.[30] By blending graphene nanomaterials into the polymer matrix,[207,208] or functionalizing the membrane surface with graphene nanomaterials,[218,219] microbial development on the membrane surface can be reduced. This approach is an alternative to biocide-releasing membranes, which are limited by the eventual depletion of biocides from the membrane. The antimicrobial properties of graphene-based materials and their different environmental

applications are discussed in more detail in the next section. Graphene nanomaterials have the potential to significantly improve membrane-based water treatment. Although several technical challenges remain in order to design graphene-based membranes for large scale applications, significant advances have been made towards achieving high selectivity from either nanoporous or stacked GO membranes. The main limitations may remain economic. Compared to the well-established polymeric membranes technology, graphene-based membrane production will probably remain expensive and limited to small-scale devices, such as microfluidic systems, where the high performance of graphene-based membranes may be needed.

5.3 Capacitive Deionization

Capacitive deionization (CDI) is an emerging water treatment process that uses pairs of porous electrodes to remove charged species from water. Upon application of an electric potential (1–2 V), the polarized electrodes form a strong electrical double layer that holds oppositely charged ions adsorbed on the electrode surface.[220,221] These ions can be desorbed by removing the electric potential, regenerating the electrodes for a new cycle. This electrosorption technology was highlighted as being a low-cost, energy efficient, and cleaner approach to water treatment, as CDI does not generate secondary pollution.[220,221] The potential of CDI is particularly important for low salinity water, where the energy requirement can be lower than for reverse osmosis technology.[221,222]

Since CDI relies on the electrosorption of ions at the surface of the electrode, the nature and design of the electrode material is a key component of the performance of CDI. The ideal electrode for CDI should have a high specific surface area with a pore structure offering high ion mobility, have a high conductivity, be chemically and electrochemically stable over a wide range of pH and water chemistry, possess good wettability, have low fouling propensity, and be made of a cheap, scalable, and easily processable material.[220,221] Carbon materials meet most of these criteria and the development of CDI electrodes has been mostly focused on carbon materials like carbon aerogel, activated carbon, ordered mesoporous carbon, and carbon nanotubes.[221] Graphene, due to its high electron mobility and specific surface area, may be an excellent material for the development of high performance CDI electrodes; many efforts were made in the last five years to integrate graphene-based materials into electrode design.

The initial attempt to use rGO for CDI resulted in relatively low Na^+ electrosorption capacity (1.85 mg g^{-1}), due to the tendency of rGO to aggregate, which resulted in relatively low surface area (14.2 m^2 g^{-1}).[223] Still, rGO electrodes, despite a lower surface area than activated carbon electrodes, demonstrated higher electrosorption capacity due to the interlayer structure of graphene that is more accessible to ions than the small micropores of activated carbon.[223] These results highlighted the potential of graphene for CDI applications, with the condition that the surface area of the graphene-based electrode can be increased.

Functionalization of rGO sheets can reduce aggregation by increasing the electrostatic repulsion between the sheets. For example, partial sulfonation of rGO sheets was found to reduce sheet aggregation, which increased the specific surface area to 464 m^2 g^{-1} and the electrosorption capacity to 8.6 mg g^{-1}.[224] Alternatively, spacing materials can be placed between sheets to prevent aggregation. Carbon-based materials, such as activated carbon, mesoporous carbon, and CNTs, due to their conductive nature and high surface area, are the most commonly used type of material to produce graphene composite electrodes.[225–228] CNTs, in particular, were found to produce composite electrodes with high electrosorption capacity, reaching up to 26.42 mg g^{-1} for an rGO-SWNT composite electrode reduced by hydrazine treatment.[228] The high performance of this composite electrode was attributed to the increased specific surface area (391 m^2 g^{-1}) and specific capacitance (220 F g^1) compared to both rGO and SWNT electrodes.[228]

High surface area and porous electrodes can also be achieved by using three-dimensional structures based on graphene and polymers, nanoparticles, or nanofibers.[229–233] Hierarchically three-dimensional porous graphene electrodes with good electrosorption capacity (6.18 mg g^{-1}) were obtained using SiO_2 spheres as a hard template and the triblock copolymer Pluronic F127 as a soft template.[230] This three-dimensional electrode possessed a bimodal pore size distribution, with both macropores and mesopores, resulting in enhanced electrosorption capacity.[230] TiO_2 nanoparticles were also used to generate a three-dimensional graphene composite electrode with very high maximum electrosorption capacity (25 mg g^{-1}).[229] The higher performance of graphene-TiO_2 was attributed to the open porous structure of the composite and the high capacitance (119.7 F g^{-1}) of the material resulting from the electronic properties of TiO_2.[229]

From these different composite materials, it appears that the architecture of graphene-based electrodes can be optimized to take full advantage of the unique physicochemical properties of graphene. Even the highest specific surface area reported for graphene-based electrodes (685.2 m^2 g^{-1} for a graphene/mesoporous carbon composite)[226] remains lower than electrodes produced from other carbon-based materials.[221] Thus, room for improvement exists in controlling the aggregation state of graphene for electrode design. Pore structure and material conductance can also be tuned to improve the performance of the electrode for CDI applications. Research shows that very small pores, even though they increase the overall surface area, may limit the electrosorption capacity due to the limited diffusion of ions in very small pores.[221] On the other hand, improving the material conductance can reduce the energy consumption for CDI operations, as higher conductivity allows for a lower applied voltage to achieve deionization.

The optimal electrode material for CDI should therefore have high surface area, porosity, and conductivity. Considerable progress has been made in increasing the surface area and capacitance of graphene-based electrodes, leading to increased electrosorption performance compared to the initial demonstration of rGO in CDI.[223] However, when comparing the performance of the different graphene-based electrodes produced, the importance of the material properties is not evident due to the high influence of the experimental conditions when measuring the electrosorption capacity. When measured at high salt concentrations, materials show a higher electrosorption capacity, regardless of the actual material properties (Figure 6). From these results, it is difficult to identify the future avenues to explore for graphene-based electrode development. This phenomenon was previously highlighted by Porada *et al*, who proposed a set of experimental conditions to be met in order to compare the performance of CDI electrodes.[221] A standardized methodology will help identify the best strategies for using graphene for CDI applications.

FIGURE 6

6. Antimicrobial applications of graphene-based materials

The control of bacterial growth is a challenging task in most environmental applications, where surfaces are exposed for a prolonged period to complex media rich in microorganisms and

nutrients. Biofouling, the adhesion of microorganisms to a surface and their growth into a biofilm, is a major hindrance for efficient operation of, for example, both membrane-based water treatment technologies and heat exchangers in industrial settings.[177,234] In marine systems, biofouling of a ship's hull increases drag and leads to an increase in fuel consumption[235] In other situations, microbiologically influenced corrosion accelerates the degradation of biofouled metallic surfaces.[236] Traditional anti-biofouling coatings usually involve the release of metals, biocides, or antibiotics to control bacterial growth. However, the release of these highly toxic compounds is of concern because of their potential environmental impacts.[237] Therefore, there is a critical need to design efficient, long-lasting, and environmentally friendly antimicrobial coatings.

Graphene-based materials are promising for the design of antimicrobial surfaces. The interest in graphene for antimicrobial coatings lies in its contact-mediated mode of action,[30] which allows for an antimicrobial material that does not deplete over time or release biocides into the environment. Although the exact mechanism of bacterial inactivation by graphene is still a matter of investigation, several effects of graphene nanomaterials on bacterial cells were identified as possible pathways of antimicrobial activity (Figure 7).[30,238,239] These graphene-bacteria interactions range from sheet adsorption on the cell membrane surface, membrane puncturing and penetration through the lipid bilayer, lipid extraction by the graphene sheet, and oxidative stress. The different mechanisms involved in the interactions between graphene nanomaterials and bacterial cells will be presented in the following section, together with a discussion on the properties of graphene nanomaterials known to influence their antimicrobial activity.

FIGURE 7

6.1 Antimicrobial activity of graphene nanomaterials

Membrane disruption appears to play a major role in the antimicrobial effect of graphene nanomaterials. The efflux of RNA in bacterial cells exposed to graphene nanomaterials was used to indicate that cell integrity is compromised by graphene.[219,240] The perturbation of the cell membrane by GO was also demonstrated by the decrease in trans-membrane potential and the

leakage of intracellular electrolytes in bacterial and fungal pathogens exposed to GO.[241] Electron microscopy further confirmed these results by revealing a compromised cell morphology and damaged cell membranes in cells exposed to graphene nanomaterials.[218,241–243] Due to its stronger mechanical properties, rGO may induce more membrane damage compared to GO.[240] However, this explanation only considers that cell membrane damage is the result of a physical effect, while there are several other mechanisms by which graphene sheets may interact with cell membranes.

Molecular dynamics (MD) simulations highlighted different possible interactions between graphene and lipid bilayers.[243–245] According to their size and oxidation level, graphene sheets can adsorb on the membrane surface, penetrate across or be integrated into the lipid bilayer, or taken up in vesicular structures.[244] Larger and more oxidized graphene sheets were found to penetrate more easily into the lipid bilayer due to the lower energy state existing when an oxidized graphene sheet lies across the membrane.[244] In another MD study, the penetration of graphene into lipid bilayers was found to be mediated by the edges of graphene sheets.[245] The initial piercing of the membrane, made possible by the sharp and rough edges of graphene, lowers the energy barrier for graphene penetration.[245] MD simulations further revealed that graphene sheets can also extract phospholipids directly from the lipid bilayer, aided by van der Waals forces between graphene planes and hydrophobic lipid tails. Once lipids are extracted from the membrane, hydrophobic interactions will promote a dewetting of the graphene plane as phospholipids spread on the sheet to maximize contact.[243]

MD simulation is a useful technique to identify the molecular mechanism by which graphene sheets may interact and possibly alter cell membrane integrity. We note, however, that while some experimental evidence exists supporting these theoretical studies, this mechanism needs to be demonstrated using bacterial cells. For example, experiments using artificial lipid bilayer revealed the ability of GO to adsorb to and detach lipid molecules from a lipid bilayer.[246] However, bacterial cells show a completely different cellular architecture and the intrinsic complexity of the bacterial outer layer[247] may change the interactions proposed by MD simulations.

A growing amount of evidence also indicates that oxidative stress is involved in the antimicrobial activity of graphene nanomaterials. Oxidative stress in bacteria exposed to GO and rGO was demonstrated using dichlorofluorescein[248] and nitro blue tetrazolium[249] assays, indicators of free radicals and superoxide anions, respectively. Oxidative stress is usually found to be higher in cells exposed to GO compared to rGO.[219,249,250] This effect can be due to the colloidal stability of GO, as aggregation can significantly affect the toxicity of carbon nanomaterials.[251,252] However, the high defect density in GO may also directly contribute to the induction of oxidative stress. Indeed, the generation of reactive oxygen species by graphenic surfaces was found to be mediated by the adsorption of O_2 on the defect sites and edges of the graphenic structure and its subsequent reduction by cellular reducing enzymes (i.e. glutathione).[253] The high defect density of GO may thus allow this material to induce higher oxidative stress in bacterial cells.

Under biological conditions, oxidative stress may be caused by multiple stress pathways. The mitochondria in particular are a major source of reactive oxygen species and any disruption of the cell metabolism that affects its energetic balance may result in the induction of oxidative stress by electron transfer from the respiratory electron transfer chain to oxygen.[254] In cells exposed to graphene nanomaterials, uncoupling the different pathways of reactive oxygen species formation may be challenging, as it is very likely that they participate together in the overall upset of cellular oxidative balance. Nevertheless, the contribution of oxidative pathways induced by graphene exposure is undoubtedly an important aspect of graphene-induced bacterial inactivation.

In suspension assays, adsorption of graphene sheet on the cell membrane was shown to contribute to the antimicrobial effect of graphene nanomaterials. When visualized by atomic-force microscopy, bacterial cells exposed to GO appear to be completely wrapped in GO sheet.[255] Cell wrapping may limit bacterial growth by isolating cells from the medium, preventing nutrient absorption, or blocking active sites on the cell surface. Bacteria wrapped in graphene can remain viable for at least 24 hours and be reactivated if separated from the graphene aggregates.[256] In agreement with the cell-wrapping effect, sheet size was found to correlate with antimicrobial activity, as larger sheets can wrap around cells more easily.[255] However, even though cell wrapping may be important in suspension, this mechanism probably

1084 does not contribute significantly to bacterial inactivation in graphene-based surface coatings,
1085 where the sheets are bound to the surface and do not have the freedom to completely wrap
1086 around the cell.

1087

1088 ## 6.2 Graphene-based antimicrobial nanocomposites

1089 In addition to their intrinsic antimicrobial properties, graphene nanomaterials have been used as a
1090 platform for the design of antimicrobial nanocomposites with improved antimicrobial activity.
1091 The high specific surface area of graphene makes it an ideal scaffold material to anchor different
1092 types of nanoparticles or macromolecules. Compounds as diverse as quaternary phosphonium
1093 salts,[257] enzymes,[258] and metal nanoparticles[259] have been attached to graphene to increase its
1094 antimicrobial properties (Figure 8). Silver, due to its excellent antimicrobial properties,[260] is by
1095 far the most extensively studied material for the design of graphene-based antimicrobial
1096 nanocomposites. The focus of this section will therefore be on the progress in the development of
1097 graphene-silver antimicrobial nanocomposites.

1098 FIGURE 8

1099 Graphene-silver nanocomposites have been produced using a variety of synthesis methods,
1100 generating different sizes, shapes, and silver loading. Silver nanoparticles can be synthesized
1101 from silver ions by nucleating the nanoparticles directly on the functional groups of GO using
1102 reducing agents like $NaBH_4$ [261–263] and hydroquinone,[264] or by heating in the presence of citrate
1103 as a capping agent.[265,266] Green syntheses have also been developed based on leaf extract,[267]
1104 fungi,[268] glucose,[269] and supercritical CO_2[270] as reducing agents. Alternatively, the synthesis of
1105 silver nanoparticles can be mediated by the presence of polyelectrolytes adsorbed on the
1106 graphene sheets. The use of polyelectrolytes allows the full reduction of GO sheets to rGO, while
1107 maintaining the aqueous stability of the nanocomposite. Graphene-silver nanocomposites were
1108 synthesized with this approach using polyethyleneimine,[271] polyacrylic acid,[272] poly (N-vinyl-2-
1109 pyrrolidone),[269] poly (diallyldimethylammonium chloride),[273] or natural biopolymers.[274]

1110 The main advantage of using silver as a graphene-silver nanocomposite compared to
1111 silver nanoparticles alone, is the increased antimicrobial activity of the nanocomposite.[267,271,273–

[275] Due to the cell membrane disrupting properties of graphene, the penetration of silver ions, leached from the nanoparticles, into the cell is facilitated in graphene-silver nanocomposites.[271] This mechanism was first proposed as an explanation for the synergetic effect of graphene and silver when present together as a nanocomposite,[271,274] and later supported by proteomic analysis of the effect of graphene-silver nanocomposites compared to silver nanoparticles alone.[262]

The propensity of graphene sheets to adhere to bacterial cells can also increase the antimicrobial properties of graphene-silver nanocomposites. The release of silver ions in proximity to the cell will result in a higher local concentration of silver ions and increased bacterial inactivation.[267,271,275,276] This effect was also observed for graphene-zinc oxide nanocomposites.[259] However, similar to the cell-wrapping effect of graphene nanomaterials, this effect is probably more important for suspension assays than for surface coatings based on graphene-silver nanocomposites.

In the design of graphene-based nanocomposites, careful control of the material properties can lead to optimal antimicrobial activity. Zhu *et al*. showed that graphene-silver nanocomposites with small nanoparticles have a higher antimicrobial activity than nanocomposites with large nanoparticles,[273] an effect that can be explained by the higher silver release rate when nanoparticle size is decreased.[277,278] Additionally, Tang *et al*. observed that the ratio between silver and graphene used during the synthesis can be tuned to obtain higher antimicrobial activity. When comparing nanocomposites made with a silver:GO ratio of 0.65:1, 1:1, and 2:1, the ratio yielding the highest antimicrobial activity was 1:1.[269] Changing the amount of silver used during the synthesis will change the nanoparticles size,[261] or the total silver loading on the sheet. Silver loading in graphene-silver nanocomposites can range from 4% to 85.4%, depending on the conditions used in synthesis.[266,268,272,273,275] These studies suggest that optimal conditions for antimicrobial activity are nanocomposites with high silver loading of small nanoparticles.

Graphene-based nanocomposites can also be designed in order to combine the antimicrobial properties of graphene with additional functionalities (Figure 8). Grafting photocatalytic nanoparticles like TiO_2 and quantum dots to graphene results in contaminant degradation and bacterial inactivation using both the antimicrobial effect of graphene and the photocatalytic activity of the nanoparticles.[279,280] The combination of quantum dots with GO was

also found to increase its peroxidase-like activity and was used to convert H_2O_2 to the more reactive $OH^{\bullet}$ for antimicrobial activity.[281] Metal oxide nanoparticles and chelatants attached to graphene nanomaterials can impart high contaminant adsorption capacity and increased antimicrobial activity.[282,283] These graphene-based nanocomposites may be of interest if the performance of both components is improved. For example, graphene-TiO_2 materials display both increased antimicrobial activity and improved photocatalytic properties.[279,284] In this case, the added complexity of material synthesis is balanced by the improved properties of the nanocomposite.

Graphene-based composite materials have also been designed to facilitate the use of graphene as an antimicrobial surface coating. By blending GO sheets in a conductive polymer (polyvinyl-N-carbazole, PVK), high bacterial inactivation was obtained using only 3% of the amount of graphene required for the same antimicrobial effect.[285–287] The conductive properties of PVK also permit surface coating by a simple electrodeposition procedure. PVK-graphene composite surface coating was shown to inactivate bacterial cells attached to the surface and to reduce biofilm growth on the surface.[287] This approach is promising since it significantly reduces the amount of nanomaterials needed for antimicrobial activity, therefore reducing the material and environmental costs associated with the use of nanomaterials.

7. Graphene-based electrodes for environmental sensing

Among carbon nanomaterials, CNTs and fullerenes have been explored as electrochemical materials mainly because of their outstanding electronic properties associated with the graphene layer component.[288] CNT samples obtained by CVD are usually contaminated with metallic residues, which could significantly alter their intrinsic transport properties. Therefore, the use of bidimensional graphene materials for sensing purposes may offer all the benefits related to the sp^2 hybridized structure of graphene, without the presence of metallic impurities.[288] Since the first demonstration of the electrochemical capacity of pristine graphene by Schedin *et al.*,[289] many additional efforts have been made in order to improve the electrochemical capacity and selectivity of graphene materials. These efforts include the conjugation of graphene with metallic

nanostructures and functionalization with organic molecules.[290–293] In this section, we will provide an overview of the application of graphene-based materials for the electrochemical detection of environmental pollutants and other relevant biomolecules, including hormonal disruptors and microbial metabolites.

7.1 Graphene properties relevant to electrochemical sensing

Owing to graphene's large theoretical surface area (2,630 cm^2 g^{-1}) and unique electronic properties, graphene-based sensors have been developed for detection of environmental pollutants, such as toxic gases and heavy metals, as well as biomolecules, including nucleic acids, hormones, and microbial toxins.[289,294–298] Pristine graphene, having remarkable intrinsic charge carrier mobility, high charge concentration, extremely high optical transmittance, and almost zero band gap energy, has emerged as an attractive two-dimensional nanomaterial for constructing electrodes for chemical and biological sensing.[7,18,299,300] Notably, the electron transport property of graphene is only weakly dependent on temperature,[299,301] which makes graphene-related materials even more promising for environmental sensing applications.

Both pristine graphene and rGO sheets can be effectively applied in the construction of sensors for contaminant monitoring and detection. As mentioned in Section 2, single-layer graphene is typically prepared by mechanical exfoliation of highly oriented pyrolytic graphite (HOPG),[11] CVD of hydrocarbons on metallic surfaces,[14,15] and thermal decomposition of silicon carbide (SiC) under high temperatures.[13] In addition, conductive rGO can also obtained from the chemical reduction of GO.[39] In comparison to the other methodologies, chemical reduction of GO represents the most feasible, reproducible, and scalable method to produce graphene-based materials for electrochemical applications.[295]

Although electron transport might be affected by the insertion of defects and oxygen functional groups on the graphene structure, previous studies have been successful in demonstrating the electronic properties of rGO samples, which motivate their application in the development of sensors and other electronic devices.[296,302,303] For example, rGO monolayers exhibited electron conductivity from 0.05 to 2 S cm^{-1} and charge carrier mobility of 2-200 cm^2 V^{-1} s^{-1}, which were two to three orders of magnitude lower than graphene.[303] Irreparable

structural defects and vacancies on the graphitic structure are considered the main causes for the decreased conductivity and carrier mobility of rGO.[303] Despite the decreased electronic conductivity, the oxygenated groups that remain from the oxidative treatment may offer great opportunities to tune the electrochemical properties of rGO sheets through the attachment of metallic nanoparticles or organic compounds.[295]

7.2 Pristine graphene-based sensors for gas sensing

Although the vast majority of the literature is focused on the electrochemical performance of rGO and its nanocomposites,[304–308] several studies explored, the sensing capacities of pristine graphene.[289,309,310] The first attempt to apply graphene as sensors for gas detection was reported by Schedin *et al*.[289] They used pristine graphene sheets obtained from the mechanical cleavage of graphite and supported on Si wafers to prepare a sensor device by lithography. The graphene-based sensor showed high sensitivity for the detection of individual NO_2 molecules, which was attributed to the large surface area combined with the superior charge carrier mobility and low intrinsic electronic noise of graphene.[289] Undoubtedly, this study was an inspiration and continues to be a reference work for further investigations regarding the electrochemical potential of graphene materials.

Considering that the electronic properties of graphene are very sensitive to the adsorption of gas molecules, the sensing capacity is evaluated through the changes in electrical conductivity throughout the graphene film during a gas exposure.[289,311] Hence, by measuring the electrical resistance, it is possible to evaluate the sensitivity and limit of detection of graphene sensors during adsorption of different gas molecules.[289] In general, these changes in resistance (increase or decrease) will be dependent on the properties of the adsorbed gas molecule (donor or acceptor).[291] For example, nitrogen dioxide (NO_2) (*p*-type) has been categorized as an electron acceptor capable of lowering the resistance of graphene-based sensors.[289,310] In contrast, ammonia (NH_3) was found to act as electron donor (*n*-type) and increases electrical resistance upon adsorption on graphene surface.[311,312] Overall, the sensing response will be based on the charge transfer between graphene and the adsorbed gas molecules.[310,312] For instance, in the study conducted by Schedin *et al*., changes in the electrical resistance and conductivity were associated with individual events of NO_2 adsorption and desorption on graphene surface.[289]

Additional experimental studies have investigated the capacity of pristine graphene to detect toxic gases and to understand how the selectivity and limit of detection can be affected by changes in the chemical nature of the gas molecules, physicochemical characteristics of graphene, and experimental conditions. For example, graphene films prepared by CVD and supported on SiO_2/Si substrates, exhibited high sensitivity for NH_3, CH_4, and H_2.[311] In presence of a gas mixture (NH_3 and CH_4), the graphene sensor was able to show a very clear response for NH_3 regardless of the excess of CH_4 in the mixture. This result suggests that NH_3 possesses greater ability to change the conductivity of graphene compared to CH_4, which made the sensor more selective and sensitive to the presence of NH_3.[311] Besides the influence of the gaseous phase composition, the sensitivity of the graphene sensor was also affected by other parameters such as temperature and gas concentration.[311]

Recognizing the influence of electrical noise on the selectivity and sensitivity of sensor devices, Rumyantsev *et al*. demonstrated that vapors of different chemicals (e.g., ethanol, tetrahydrofuran, and acetonitrile) led to specific changes in the low-frequency noise spectra of graphene-like transistors.[309] These graphene sensors displayed distinct parameters of frequency and relative resistance for different types of chemical vapors, which could be used as signal fingerprints to detect these organic vapors selectively in real sensing conditions. In another study, the detection of CO, O_2, and NO_2 by graphene films and ribbons grown on Si substrate was investigated.[310] The increase in the deposition time from five to ten minutes led to the creation of ribbon structures rather than planar graphene films. In general, graphene-like films showed better sensing response than their ribbon counterparts. Nonetheless, graphene sensors constructed through mechanical cleavage of highly oriented pyrolytic graphite and further support on Si substrates showed high performance for CO_2 sensing at room temperature.[313]

Functionalization with organic molecules and doping with metallic elements has been carried out to modulate the selectivity or sensitivity of pristine graphene sensors to the adsorbed molecules.[292,293,314,315] Using DFT calculations, the sensitivity of pristine graphene for CO, NO, NO_2, and NH_3 gases was shown to increase after inclusion of single defects or doping with boron and nitrogen elements.[314] Both boron and nitrogen-doped graphene presented improved sensing performance in comparison to non-defected graphene. In another study, in addition to preventing agglomeration, the functionalization of graphene sheets with platinum nanoparticles resulted in

larger surface area and improved electrical conductivity compared to non-modified graphene; this feature supports the application of this hybrid material as an electrode for supercapacitors and fuel cells.[293]

It is worthwhile to emphasize that the surface chemistry of graphene can be manipulated to provide an improved sensing performance.[315] However, the electrochemical response is also dependent on the physicochemical properties of the gas molecules and their ability to interact with the surface of graphene. A theoretical investigation demonstrated that NO_2 may adsorb on pristine graphene sheets through different configurations.[314] The results also indicated a possible charge transfer from graphene to NO_2 molecules, which confirms NO_2 as an electron acceptor. In contrast, the interaction of CO with either pristine or B-N-doped graphene was associated with physiosorption, where chemical bonding does not play any role. However, when single-defects were incorporated in the graphene aromatic structure, CO was found to interact with the binding sites on the vacancies through chemisorption. These observations provide strong evidence that the sensitivity and selectivity of graphene-like sensors are governed by the intrinsic physicochemical characteristics of both graphene materials (presence of defects or functional groups) and the gaseous molecules (acceptor or donors).[311–313,316]

Although the earlier studies described above have shown very promising electrochemical activity for graphene materials, Dan *et al*. demonstrated that an electron beam nanolithography technique leaves a layer of residue on the graphene surface.[317] Such contamination was attributed to residues of polymethylmethacrylate (PMMA), the electron beam resist used during the sensor device fabrication. This contamination was found to alter the transport properties and sensing response of sensor devices. In fact, the electrochemical response to the presence of vapors was significantly lowered after the graphene surface was subjected to a cleaning process. The residue seemed to act as an adsorbent-like layer, contributing to gas adsorption and improving the sensitivity of graphene sensors. This observation suggests that sensing performance can be affected by the presence of impurities and thorough cleaning is needed before initiating graphene surface functionalization.[317]

7.3 Reduced graphene oxide (rGO)-based sensors for gas sensing

In addition to pristine graphene, rGO has also been extensively applied for gas sensor development.[304,306,307,318] Previous studies have reported the preparation of rGO-based sensors for gas monitoring from the chemical reduction of GO by hydrazine (vapor or solutions).[305,319,320] Consequently, GO (an insulating material) is converted to rGO, which possesses a higher charge carrier transport capacity. For instance, rGO sensors obtained from the chemical conversion of GO with liquid hydrazine were applied for NH_3 and NO_2 detection.[305] Fowler *et al*. claimed that rather than hydrazine vapor, liquid hydrazine produces an rGO with smaller number of structural defects.[305] The sensors were also sensitive to the presence of DNT (2,4-dinitrotoluene), with a detection limit of 28 ppb.

Recognizing the importance of the content of oxygen functional groups on the performance of rGO sensors, Robinson *et al*. described the fabrication of rGO sensors by spin coating GO sheets on Si substrates and subsequently reducing the GO film with hydrazine vapor at different exposure times.[319] The results indicated that longer hydrazine treatments led to rGO samples with decreased low-frequency noise and higher conductivity due to the increase of sp^2 bonds.[319]

Interestingly, the response curve for acetone vapors was shown to be composed of two different parts: a fast response step that corresponds to the adsorption of acetone on low energy sites (sp^2 layer of graphene), and a slow response that is associated with the adsorption of gas molecules to high energy sites, such as structural defects and oxygen functional groups that remain on the rGO surface.[319] Therefore, longer exposure times to hydrazine provided rGO sensors with faster response times. The same response curve pattern was observed during the detection of NO_2 molecules by sensors fabricated from GO chemically reduced by hydrazine.[320] One of the most important implications of the slow response step for rGO-based sensors is their prolonged recovery time due to the intimate chemical interactions between the graphene layer and adsorbed gas molecules.[319,320]

Following the same approach, but using a different chemical reducing agent, the influence of different $NaBH_4$ exposure times on the sensitivity and response time of rGO sensors was evaluated.[306] rGO sensors prepared from short reduction time (30 minutes) displayed higher response for NH_3 than those reduced for a longer period of time (180 minutes). For a more oxidized sample (30-minute exposure), the sensing response was likely increased due to the

chemisorption of NH_3 on the high energy oxygen functional groups of rGO. On the other hand, the adsorption of NH_3 on a less oxidized rGO sample (180 minutes) appears to be possible through physisorption (weak interaction), which leads to low response.[306] The optimal exposure time to $NaBH_4$ was found to be 90 minutes.[306] Henceforth, the main challenge is to find an oxidation level that combines good sensitivity with a satisfactory response and recovery time.

A similar trend was described for rGO-based gas sensors prepared by reducing GO through an annealing process.[308] The reduction of GO was found to be affected by the annealing temperature. For example, rGO samples generated after 300°C treatment were more effectively reduced compared to those prepared at 100 and 200°C annealing. Thus, rGO sensors fabricated at 300°C showed improved sensitivity and faster response time for NO_2 detection than samples annealed at 200°C. The rapid response time was due to the increase in sp^2 network, which provides low-energy binding sites and a faster adsorption of NO_2 molecules.[308] Furthermore, rGO sensors prepared through *in-situ* reduction of GO with ascorbic acid and subsequent layer-by-layer intercalation of ionic liquids have shown great selectivity and sensitivity for detection of NH_3/Cl_2/NO_2 and hydrocarbon vapors, respectively.[304,307]

As discussed with regard to pristine graphene, rGO sheets have also been functionalized with nanoparticles and organic compounds to achieve higher electrochemical performance. Modification of rGO sheets with tin oxide (SnO_2) nanocrystals and palladium (Pd) nanoparticles, or conjugation with conducting polymeric structures such as polyaniline (PANI), has been reported.[290,291,321] For example, the attachment of PANI nanoparticles on rGO led to a synergetic effect on NH_3 sensing, since the combination of both materials led to a 3.4 and 10.4 times increase in the sensor response compared to PANI and bare rGO, respectively. Besides the improvements in surface area, the excellent electrochemical response of rGO-PANI hybrid composites was related to the intrinsic acid-base doping capacity of PANI.[292,321] In addition, due to the likely intimate π-π interactions between PANI and rGO, electron transfer might occur between PANI and rGO sheets, which could explain the enhanced sensing capacities of rGO-PANI nanocomposites.[321] Nevertheless, enhancements in the detection response of NO_2 and H_2 have been achieved through modification of rGO with SnO_2 nanostructures.[291,322] While the mechanism by which rGO-SnO_2 composite exhibits such an enhanced sensitivity is not complete understood, it was suggested that such sensitivity may be due to the formation of a *p*-*n* junction

at the interface of SnO_2 (*n*-type) and rGO sheet (*p*-type).[291] The formation of this *p*-*n* junction may facilitate the electron transfer process from rGO to NO_2 molecules.[291]

7.4 Graphene-based sensors for chemical and biological sensing

Although we emphasized in this section the use of graphene-based sensors for gas detection, graphene materials have also been applied for sensing chemical contaminants and biometabolites of environmental importance. Among the chemical compounds, the detection of hydrogen peroxide (H_2O_2), heavy metals, hazardous hydrocarbons, and some pharmaceutical contaminants has been made possible through graphene-based sensors.[323] The schematic diagram displayed in Figure 9 illustrates the potential application of graphene and graphene-based nanocomposites for sensing of gases, organic compounds, and biological pollutants.

FIGURE 9

Electrochemical sensors fabricated *via* self-assembly of cationic modified gold nanoparticles and graphene nanosheets showed good sensitivity for detection of H_2O_2 with a detection limit of 0.44 μM.[324] Similarly, Liu *et al*. showed that nanocomposites, prepared from reduction of GO by hydrazine in the presence of cationic polyelectrolytes and further decoration with silver nanoparticles (GN-Ag), displayed a high electrocatalytic activity for reduction of H_2O_2, which could eventually support their application as sensors with a very low limit of detection (about 28 μM).[323] Complementing these electrochemical sensors, graphene-enzyme electrodes have also been fabricated for detection of H_2O_2.[325,326] Nanocomposites prepared by the self-assembly of dodecyl benzene sulfonate (SDBS) functionalized graphene sheets and horseradish peroxidase (HRP) revealed a fast and sensitive response to H_2O_2.[326] The graphene-HRP composite exhibited higher sensing performance than glassy carbon electrodes modified with bare graphene sheets. Despite the excellent electronic properties of graphene, this higher sensing activity was associated with a better diffusion of H_2O_2 through the 3D structure of the nanocomposite and the synergetic effect provided by the conjugation of graphene with HRP enzymes.[326]

Another class of chemical compounds that received great attention is heavy metals. Several studies have developed graphene sensors with high sensitivity and rapid response time to

detect toxic metals like mercury (Hg) and lead (Pb).[327–330] For instance, field-effect transistor (FET) based on rGO sheets decorated with thioglycolic acid (TGA) functionalized gold nanoparticles (AuNP) exhibited a sensitive response to the presence of Hg(II) in aqueous suspension.[327] While control transistors prepared by bare rGO, rGO-Au (without TGA), and rGO-TGA (without AuNP) did not show any response to Hg(II), rGO-AuTGA hybrid composites were able to detect Hg^{+2} ions even at low concentration (2.5×10^{-8} M). This indicates how important is the functionalization of AuNP with TGA in providing sensing activity to rGO-AuNP-TGA nanocomposites. The remarkable sensing performance of rGO-AuNP-TGA composites was attributed to the interaction of Hg^{+2} ions with carboxyl groups of TGA on the AuNP surface and the subsequent changes in the charge carrier concentration on rGO layers.[327] In another study, FET transistors based on AuNP-DNAzyme functionalized graphene sheets were used for the detection of Pb^{+2} ions.[328] DNAzymes are enzyme-like molecules comprising an enzymatic and a substrate component at the same molecule. The great sensitivity of the rGO-AuNP-DNAzyme sensors (detection limit of 20 pM) was due to a cleavage reaction provided by the enzyme portion of DNAzyme. Upon Pb^{2+}contact, the DNAzyme molecule suffers a self-cleavage, thus leading to intimate changes in the electronic coupling between the AuNP and graphene.[328]

Graphene-based sensors have also been developed for the detection of persistent hydrocarbons, insecticides, hormone disruptors, and pharmaceutical contaminants.[331–334] Graphene sheets decorated with carbon quantum dots were used as electroluminescent sensors for detection of chlorinated phenols, at concentrations as low as 1×10^{-12} M.[331] In addition, bisphenol A, an endocrine disruptor, was selectively detected by nitrogen-doped graphene sheets, which demonstrated a detection limit of 5×10^{-9} M.[333]

The detection of microbial cells and biomolecules has also been shown through graphene derivative sensors. Probes composed of GO sheets functionalized with fluorescent conjugated oligomers were used for selective and sensitive detection of *Escherichia coli* and lectin concanavalin A (Con A).[335] Because GO has the ability to quench the fluorescent background of conjugated oligomers, an increase in specificity of the sensor under interaction with ConA was observed. This sensor showed a detection limit of ConA around 0.5 nM. In another study, the

biosensing of *E. coli* cells was also possible by immobilizing specific anti-*E. coli* antibodies on graphene sheets. The biosensor showed great sensitivity, being able to detect cells at *E. coli* concentration of 10 CFU/mL.[336]

Multi-layer graphene sheets were also employed as electrochemical sensors for detection of urea, with detection limit of 39 mg L^{-1}.[337] In addition, glassy carbon electrodes functionalized with rGO sheets showed high electrochemical activity for the sensing of bases of DNA (guanine, adenine, tyamine, and cytosine), which can allow future detection of polymorphisms in human and microbial oligonucleotide fragments.[296] Moreover, the biosensing of important neurotransmitters, such as dopamine and serotonin, was also demonstrated through graphene-modified electrodes.[338] Ultimately, the conjugation of GO with DNA and toxin-specific aptamers, provided a sensitive detection of microcystin (a toxin produced by cyanobacteria) and ochratoxin A (produced by *Penicillium verrucosumm*).[298,339] Additional information on applications of graphene-based sensors for detection of gases, chemical, microorganisms, and biomolecules is summarized in Table 5. For comparison, a few studies involving the application of CNTs as sensing materials were also included in Table 5.

TABLE 5

Graphene-based materials have provided a good platform for the development of sensor devices with extraordinary sensitivity and selectivity. However, strategies must be developed to provide a scalable amount of single-layer graphene with optimal electronic properties. Another challenge is the sensor's recovery efficiency. For rGO sensors, the recovery can be performed through exposure to high temperature and UV-irradiation.[289,304,321] In addition to the possible damage to the rGO film structure, irradiation and heating treatments are time- and energy-consuming, which contributes to increased associated costs.[306] Questions on the performance of graphene compared to CNT-based sensors have also been raised in a previous publication.[5] According to Yang *et al*., one of the major drawbacks for both CNTs and graphene samples is the control of their inherent structural and physicochemical characteristics (such as purity, size of the sheet or length of the tubes, number of layers for graphene, and propensity to agglomeration).[5] So far, it appears that the advantages of using graphene over CNTs for sensing applications will depend on future scientific advances in production of metal catalyst-free CNTs or development of reproducible methods to control the number of layers and oxidation level of

graphene samples.[5] We have provided here just a summary of the potential applications of graphene-based sensors; the subject has also been extensively discussed in other previous reviews.[288,295,340,341]

9. Outlook

During the past decade, significant progress has been made in understanding how graphene and graphene-based materials can be used to address environmental challenges. The unique properties of graphene have opened new possibilities to improve the performance of numerous environmental processes. However, in other cases, the improvement brought by the use of graphene was merely similar to what was achieved with other carbon-based nanomaterials, or even with traditional carbonaceous materials like activated carbon.

The limited performance in some applications can be, in part, attributed to synthesis challenges in the design of graphene-based composites. The tendency of graphene nanomaterials to aggregate and the presence of intrinsic defects in the carbon structure of graphene nanomaterials obtained via GO modification can lead to sub-optimal performance compared to what could be expected from the predicted properties of graphene. In this case, a better understanding of the underlying mechanisms involved in the production and functionalization of graphene nanomaterials is crucial to overcome this limitation.

Due to similarities between the chemical structure of graphene, CNTs, and fullerenes, it may be that these different materials will demonstrate a similar performance when used in certain environmental applications. Hence, the choice of whether to use graphene as a carbon-based nanocomposite will be determined by the cost, processability, and environmental implications of each material. In this regard, environmental applications based on GO offer more realistic possibilities compared to pristine graphene due to GO's lower production costs. At this writing, prices of low-grade GO are comparable to multiwalled carbon nanotubes, more expensive than activated carbon, but lower than single-walled carbon nanotubes or single-layer CVD graphene. However, as the production capacities increase and the supply-chain is optimized, the costs of graphene-based materials will decrease significantly over time.[342,343] At

the lab scale, the costs of graphene materials already decreased to a quarter of their price per gram between 2012 and 2014.[342]

In addition to economic considerations, environmental implications of graphene-based materials will represent an important factor in the development of graphene-based technologies. The fate, transformation, and toxicological impacts of graphene materials in the environment have been extensively reviewed in previous publications[30,57,239,344–346] and therefore were not discussed in this review. However, the importance of carefully evaluating the environmental implications of graphene-based materials must be emphasized. Detailed ecotoxicological assessments and life-cycle analyses still need to be performed, in order to identify the forms of graphene-based nanomaterials that will allow us to utilize the properties of graphene, while minimizing the associated health and environmental impacts.

Until these economic and environmental considerations are known and better understood, it would be hard to determine the most promising areas of research for graphene-based materials. In some applications, graphene was found to offer distinct advantages over other carbon nanomaterials due to its two-dimensional structure. For example, graphene-based sensor devices were found to be more amenable to controlled microfabrication techniques compared to CNTs.[5] In membrane processes, the flat morphology of graphene may offer an easier control on the assembly of graphene layers for separation purposes.[203] On the other hand, for applications that rely on the high surface area of graphene, its tendency to aggregate and restack was found to reduce its performance to levels comparable to other carbon nanomaterials. In these applications, the choice of using graphene over CNTs or activated carbon will be mainly economical.

Since several aspects of the expected high performance of graphene nanomaterials rely on theoretical values of pristine graphene, an important factor in enabling graphene for environmental applications will be low cost and scalable production methods. One of the most important challenges will be to reduce GO successfully to a pristine graphene material in order to restore its exceptional electronic and mechanical properties. Reduction of GO for the production of graphene certainly appears a most promising approach to produce low cost graphene on a large scale.

Graphene remains a unique material with properties that could lead potentially to significant development in numerous environmental applications. From atomically thin membranes to ultra-high surface area materials, this two-dimensional material thought to be impossible 80 years ago, is now providing new solutions to the global environmental challenges that humanity must address.

Acknowledgements

F.P. acknowledges the financial support of the Natural Sciences and Engineering Research Council of Canada. A.F.F acknowledges the financial support of the Science without Borders program, through the Brazilian Council of Science and Technology (CNPq Grant 246407/2012-3), and the Lemann Institute for Brazilians Studies.

References

1 J. Lubchenco, *Science*, 1998, **279**, 491–497.

2 X. Qu, P. J. J. Alvarez and Q. Li, *Water Res.*, 2013, **47**, 3931–46.

3 P. Xu, G. M. Zeng, D. L. Huang, C. L. Feng, S. Hu, M. H. Zhao, C. Lai, Z. Wei, C. Huang, G. X. Xie and Z. F. Liu, *Sci. Total Environ.*, 2012, **424**, 1–10.

4 Q. Zhang, E. Uchaker, S. L. Candelaria and G. Cao, *Chem. Soc. Rev.*, 2013, **42**, 3127–71.

5 W. Yang, K. R. Ratinac, S. P. Ringer, P. Thordarson, J. J. Gooding and F. Braet, *Angew. Chem. Int. Ed. Engl.*, 2010, **49**, 2114–38.

6 M. S. Mauter and M. Elimelech, *Environ. Sci. Technol.*, 2008, **42**, 5843–5859.

7 A. K. Geim, *Science*, 2009, **324**, 1530–1535.

8 Y. Zhang, T. R. Nayak, H. Hong and W. Cai, *Nanoscale*, 2012, **4**, 3833–42.

9 A. K. Geim and K. S. Novoselov, *Nat. Mater.*, 2007, **6**, 183–91.

10 C. Hontoria-Lucas, a. J. López-Peinado, J. d. D. López-González, M. L. Rojas-Cervantes and R. M. Martín-Aranda, *Carbon*, 1995, **33**, 1585–1592.

11 Y. Zhu, S. Murali, W. Cai, X. Li, J. W. Suk, J. R. Potts and R. S. Ruoff, *Adv. Mater.*, 2010, **22**, 3906–24.

12 Y. Hernandez, V. Nicolosi, M. Lotya, F. M. Blighe, Z. Sun, S. De, I. T. McGovern, B. Holland, M. Byrne, Y. K. Gun'Ko, J. J. Boland, P. Niraj, G. Duesberg, S. Krishnamurthy, R. Goodhue, J. Hutchison, V. Scardaci, A. C. Ferrari and J. N. Coleman, *Nat. Nanotechnol.*, 2008, **3**, 563–8.

13 W. a. de Heer, C. Berger, X. Wu, P. N. First, E. H. Conrad, X. Li, T. Li, M. Sprinkle, J. Hass, M. L. Sadowski, M. Potemski and G. Martinez, *Solid State Commun.*, 2007, **143**, 92–100.

14 X. Li, W. Cai, J. An, S. Kim, J. Nah, D. Yang, L. Colombo and R. S. Ruoff, *Science*, 2009, **3893**, 1312–1315.

15 S. Bae, H. Kim, Y. Lee, X. Xu, J.-S. Park, Y. Zheng, J. Balakrishnan, T. Lei, H. R. Kim, Y. Il Song, Y.-J. Kim, K. S. Kim, B. Ozyilmaz, J.-H. Ahn, B. H. Hong and S. Iijima, *Nat. Nanotechnol.*, 2010, **5**, 574–8.

16 S.-Y. Kwon, C. V Ciobanu, V. Petrova, V. B. Shenoy, J. Bareño, V. Gambin, I. Petrov and S. Kodambaka, *Nano Lett.*, 2009, **9**, 3985–90.

17 A. T. N'Diaye, J. Coraux, T. N. Plasa, C. Busse and T. Michely, *New J. Phys.*, 2008, **10**, 043033.

18 K. S. Kim, Y. Zhao, H. Jang, S. Y. Lee, J. M. Kim, K. S. Kim, J.-H. Ahn, P. Kim, J.-Y. Choi and B. H. Hong, *Nature*, 2009, **457**, 706–10.

19 A. Guermoune, T. Chari, F. Popescu, S. S. Sabri, J. Guillemette, H. S. Skulason, T. Szkopek and M. Siaj, *Carbon*, 2011, **49**, 4204–4210.

20 A. H. Castro Neto, N. M. R. Peres, K. S. Novoselov and A. K. Geim, *Rev. Mod. Phys.*, 2009, **81**, 109–162.

21 K. I. Bolotin, K. J. Sikes, Z. Jiang, M. Klima, G. Fudenberg, J. Hone, P. Kim and H. L. Stormer, *Solid State Commun.*, 2008, **146**, 351–355.

22 T. S. Sreeprasad and V. Berry, *Small*, 2013, **9**, 341–50.

23 Q. Xiang, J. Yu and M. Jaroniec, *Chem. Soc. Rev.*, 2012, **41**, 782–796.

24 G. Zhao, T. Wen, C. Chen and X. Wang, *RSC Adv.*, 2012, **2**, 9286.

25 Y. Sun, Q. Wu and G. Shi, *Energy Environ. Sci.*, 2011, **4**, 1113.

26 C. Lee, X. Wei, J. W. Kysar and J. Hone, *Science*, 2008, **321**, 385–388.

27 J. R. Potts, D. R. Dreyer, C. W. Bielawski and R. S. Ruoff, *Polymer*, 2011, **52**, 5–25.

28 J. N. Coleman, U. Khan, W. J. Blau and Y. K. Gun'ko, *Carbon*, 2006, **44**, 1624–1652.

29 M. A. Rafiee, J. Rafiee, Z. Wang, H. Song, Z. Yu and N. Koratkar, *ACS Nano*, 2009, **3**, 3884–3890.

30 V. C. Sanchez, A. Jachak, R. H. Hurt and A. B. Kane, *Chem. Res. Toxicol.*, 2012, **25**, 15–34.

31 O. C. Compton and S. T. Nguyen, *Small*, 2010, **6**, 711–23.

32 D. R. Dreyer, S. Park, C. W. Bielawski and R. S. Ruoff, *Chem. Soc. Rev.*, 2010, **39**, 228–40.

33 A. Lerf, A. Buchsteiner, J. Pieper, S. Schöttl, I. Dekany, T. Szabo and H. P. Boehm, *J. Phys. Chem. Solids*, 2006, **67**, 1106–1110.

34 W. S. Hummers and R. E. Offeman, *J. Am. Chem. Soc.*, 1958, **80**, 1339.

35 D. C. Marcano, D. V Kosynkin, J. M. Berlin, A. Sinitskii, Z. Sun, A. Slesarev, L. B. Alemany, W. Lu and J. M. Tour, *ACS Nano*, 2010, **4**, 4806–14.

36 V. C. Tung, M. J. Allen, Y. Yang and R. B. Kaner, *Nat. Nanotechnol.*, 2009, **4**, 25–29.

37 J. W. Suk, R. D. Piner, J. An and R. S. Ruoff, *ACS Nano*, 2010, **4**, 6557–64.

38 C. K. Chua and M. Pumera, *Chem. Soc. Rev.*, 2014, **43**, 291–312.

39 S. Pei and H.-M. Cheng, *Carbon*, 2012, **50**, 3210–3228.

40 C. Gómez-Navarro, J. C. Meyer, R. S. Sundaram, A. Chuvilin, S. Kurasch, M. Burghard, K. Kern and U. Kaiser, *Nano Lett.*, 2010, **10**, 1144–8.

41 A. Bagri, C. Mattevi, M. Acik, Y. J. Chabal, M. Chhowalla and V. B. Shenoy, *Nat. Chem.*, 2010, **2**, 581–7.

42 S. Park and R. S. Ruoff, *Nat. Nanotechnol.*, 2009, **4**, 217–24.

43 K. C. Kemp, H. Seema, M. Saleh, N. H. Le, K. Mahesh, V. Chandra and K. S. Kim, *Nanoscale*, 2013, **5**, 3149–71.

44 H.-P. Cong, J.-F. Chen and S.-H. Yu, *Chem. Soc. Rev.*, 2014, **43**, 7295–325.

45 H. Bai, C. Li and G. Shi, *Adv. Mater.*, 2011, **23**, 1089–1115.

46 I. Ali and V. K. Gupta, *Nat. Protoc.*, 2007, **1**, 2661–2667.

47 A. Dąbrowski, *Adv. Colloid Interface Sci.*, 2001, **93**, 135–224.

48 US EPA, *Drinking Water and Groundwater Quality Standards*, 2014.

49 M. Machida, T. Mochimaru and H. Tatsumoto, *Carbon*, 2006, **44**, 2681–2688.

50 G. Crini, *Bioresour. Technol.*, 2006, **97**, 1061–1085.

51 Y.-H. Li, S. Wang, Z. Luan, J. Ding, C. Xu and D. Wu, *Carbon*, 2003, **41**, 1057–1062.

52 G. Zhao, J. Li, X. Ren, C. Chen and X. Wang, *Environ. Sci. Technol.*, 2011, **45**, 10454–10462.

53 X. Ren, C. Chen, M. Nagatsu and X. Wang, *Chem. Eng. J.*, 2011, **170**, 395–410.

54 R. Sitko, B. Zawisza and E. Malicka, *TrAC Trends Anal. Chem.*, 2013, **51**, 33–43.

55 A. Stafiej and K. Pyrzynska, *Sep. Purif. Technol.*, 2007, **58**, 49–52.

56 G. P. Rao, C. Lu and F. Su, *Sep. Purif. Technol.*, 2007, **58**, 224–231.

57 J. Zhao, Z. Wang, J. C. White and B. Xing, *Environ. Sci. Technol.*, 2014, **48**, 9995–10009.

58 W. Wu, Y. Yang, H. Zhou, T. Ye, Z. Huang, R. Liu and Y. Kuang, *Water, Air, Soil Pollut.*, 2012, **224**, 1–8.

59 R. Sitko, E. Turek, B. Zawisza, E. Malicka, E. Talik, J. Heimann, A. Gagor, B. Feist and R. Wrzalik, *Dalt. Trans.*, 2013, **42**, 5682–5689.

60 G. Zhao, X. Ren, X. Gao, X. Tan, J. Li, C. Chen, Y. Huang and X. Wang, *Dalt. Trans.*, 2011, **40**, 10945–10952.

61 Z.-H. Huang, X. Zheng, W. Lv, M. Wang, Q.-H. Yang and F. Kang, *Langmuir*, 2011, **27**, 7558–7562.

62 H. Wang, X. Yuan, Y. Wu, H. Huang, G. Zeng, Y. Liu, X. Wang, N. Lin and Y. Qi, *Appl. Surf. Sci.*, 2013, **279**, 432–440.

63 Y. Yao, Z. Yang, D. Zhang, W. Peng, H. Sun and S. Wang, *Ind. Eng. Chem. Res.*, 2012, **51**, 6044–6051.

64 G. Gollavelli, C.-C. Chang and Y.-C. Ling, *ACS Sustain. Chem. Eng.*, 2013, **1**, 462–472.

65 J. Zhu, S. Wei, H. Gu, S. B. Rapole, Q. Wang, Z. Luo, N. Haldolaarachchige, D. P. Young and Z. Guo, *Environ. Sci. Technol.*, 2011, **46**, 977–985.

66 J. Li, S. Zhang, C. Chen, G. Zhao, X. Yang, J. Li and X. Wang, *ACS Appl. Mater. Interfaces*, 2012, **4**, 4991–5000.

67 V. Chandra, J. Park, Y. Chun, J. W. Lee, I.-C. Hwang and K. S. Kim, *ACS Nano*, 2010, **4**, 3979–3986.

68 M. Liu, C. Chen, J. Hu, X. Wu and X. Wang, *J. Phys. Chem. C*, 2011, **115**, 25234–25240.

69 H. Jabeen, V. Chandra, S. Jung, J. W. Lee, K. S. Kim and S. Bin Kim, *Nanoscale*, 2011, **3**, 3583–3585.

70 A.-H. H. Lu, E. L. L. Salabas and F. Schüth, *Angew. Chemie Int. Ed.*, 2007, **46**, 1222–1244.

71 C. J. Madadrang, H. Y. Kim, G. Gao, N. Wang, J. Zhu, H. Feng, M. Gorring, M. L. Kasner and S. Hou, *ACS Appl. Mater. Interfaces*, 2012, **4**, 1186–1193.

72 L. Liu, C. Li, C. Bao, Q. Jia, P. Xiao, X. Liu and Q. Zhang, *Talanta*, 2012, **93**, 350–357.

73 Y. Yang, Y. Xie, L. Pang, M. Li, X. Song, J. Wen and H. Zhao, *Langmuir*, 2013, **29**, 10727–10736.

74 L. Wang, L. Jiang, D. Su, C. Sun, M. Chen, K. Goh and Y. Chen, *J. Colloid Interface Sci.*, 2014, **430**, 121–128.

75 S. Vasudevan and J. Lakshmi, *RSC Adv.*, 2012, **2**, 5234–5242.

76 S. Zhang, Y. Shao, J. Liu, I. A. Aksay and Y. Lin, *ACS Appl. Mater. Interfaces*, 2011, **3**, 3633–3637.

77 G. Shi, Y. Ding and H. Fang, *J. Comput. Chem.*, 2012, **33**, 1328–1337.

78 H. Yan, X. Tao, Z. Yang, K. Li, H. Yang, A. Li and R. Cheng, *J. Hazard. Mater.*, 2014, **268**, 191–198.

79 Y. Gao, Y. Li, L. Zhang, H. Huang, J. Hu, S. M. Shah and X. Su, *J. Colloid Interface Sci.*, 2012, **368**, 540–546.

80 C. Zhang, L. Wu, D. Cai, C. Zhang, N. Wang, J. Zhang and Z. Wu, *ACS Appl. Mater. Interfaces*, 2013, **5**, 4783–4790.

81 J. Li, F. Wang and C. Liu, *J. Colloid Interface Sci.*, 2012, **382**, 13–16.

82 X. Liu, H. Zhang, Y. Ma, X. Wu, L. Meng, Y. Guo, G. Yu and Y. Liu, *J. Mater. Chem. A*, 2013, **1**, 1875–1884.

83 I. Chowdhury, M. C. Duch, N. D. Mansukhani, M. C. Hersam and D. Bouchard, *Environ. Sci. Technol.*, 2014, **48**, 9382–9390.

84 K. Yang and B. Xing, *Chem. Rev.*, 2010, **110**, 5989–6008.

85 G. K. Ramesha, A. Vijaya Kumara, H. B. Muralidhara and S. Sampath, *J. Colloid Interface Sci.*, 2011, **361**, 270–277.

86 S.-T. Yang, S. Chen, Y. Chang, A. Cao, Y. Liu and H. Wang, *J. Colloid Interface Sci.*, 2011, **359**, 24–29.

87 F. Liu, S. Chung, G. Oh and T. S. Seo, *ACS Appl. Mater. Interfaces*, 2011, **4**, 922–927.

88 Z. Yang, H. Yan, H. Yang, H. Li, A. Li and R. Cheng, *Water Res.*, 2013, **47**, 3037–3046.

89 M. Sinoforoglu, B. Gur, M. Ark, Y. Onganer and K. Meral, *RSC Adv.*, 2013, **3**, 11832–11838.

90 L. Sun, H. Yu and B. Fugetsu, *J. Hazard. Mater.*, 2012, **203–204**, 101–110.

91 S. Liu, W. Peng, H. Sun and S. Wang, *Nanoscale*, 2014, **6**, 766–771.

92 X. Yang, J. Li, T. Wen, X. Ren, Y. Huang and X. Wang, *Colloids Surfaces A Physicochem. Eng. Asp.*, 2013, **422**, 118–125.

93 Z. Pei, L. Li, L. Sun, S. Zhang, X. Shan, S. Yang and B. Wen, *Carbon*, 2013, **51**, 156–163.

94 F. Wang, J. J. H. Haftka, T. L. Sinnige, J. L. M. Hermens and W. Chen, *Environ. Pollut.*, 2014, **186**, 226–233.

95 J. Xu, L. Wang and Y. Zhu, *Langmuir*, 2012, **28**, 8418–8425.

96 Z. Qi, L. Hou, D. Zhu, R. Ji and W. Chen, *Environ. Sci. Technol.*, 2014, **48**, 10136–10144.

97 O. G. Apul, Q. Wang, Y. Zhou and T. Karanfil, *Water Res.*, 2013, **47**, 1648–1654.

98 B. Beless, H. S. Rifai and D. F. Rodrigues, *Environ. Sci. Technol.*, 2014, **48**, 10372–10379.

99 J. Wang, Z. Chen and B. Chen, *Environ. Sci. Technol.*, 2014, **48**, 4817–4825.

100 S. Solomon, G.-K. Plattner, R. Knutti and P. Friedlingstein, *Proc. Natl. Acad. Sci. U. S. A.*, 2009, **106**, 1704–9.

101 J. Yang, X. Yu, J. Yan and S. T. Tu, *Ind. Eng. Chem. Res.*, 2014, **53**, 2790–2799.

102 E. D. Bates, R. D. Mayton, I. Ntai and J. H. Davis, *J. Am. Chem. Soc.*, 2002, **124**, 926–927.

103 N. Dave, T. Do, G. Puxty, R. Rowland, P. H. M. Feron and M. I. Attalla, *Energy Procedia*, 2009, **1**, 949–954.

104 Z. H. Lee, K. T. Lee, S. Bhatia and A. R. Mohamed, *Renew. Sustain. Energy Rev.*, 2012, **16**, 2599–2609.

105 Y. Liu and J. Wilcox, *Environ. Sci. Technol.*, 2012, **47**, 95–101.

106 Y. Liu and J. Wilcox, *Environ. Sci. Technol.*, 2010, **45**, 809–814.

107 A. Ghosh, K. S. Subrahmanyam, K. S. Krishna, S. Datta, a. Govindaraj, S. K. Pati and C. N. R. Rao, *J. Phys. Chem. C*, 2008, **112**, 15704–15707.

108 G. Ning, C. Xu, L. Mu, G. Chen, G. Wang, J. Gao, Z. Fan, W. Qian and F. Wei, *Chem. Commun.*, 2012, **48**, 6815–6817.

109 D. Dutta, B. C. Wood, S. Y. Bhide, K. G. Ayappa and S. Narasimhan, *J. Phys. Chem. C*, 2014, **118**, 7741–7750.

110 P. Cabrera-Sanfelix, *J. Phys. Chem. A*, 2008, **113**, 493–498.

111 A. K. Mishra and S. Ramaprabhu, *J. Mater. Chem.*, 2012, **22**, 3708–3712.

112 Y. Zhao, H. Ding and Q. Zhong, *Appl. Surf. Sci.*, 2012, **258**, 4301–4307.

113 S.-M. Hong, S. H. Kim and K. B. Lee, *Energy & Fuels*, 2013, **27**, 3358–3363.

114 V. Chandra, S. U. Yu, S. H. Kim, Y. S. Yoon, D. Y. Kim, A. H. Kwon, M. Meyyappan and K. S. Kim, *Chem. Commun.*, 2012, **48**, 735–737.

115 A. Garcia-Gallastegui, D. Iruretagoyena, V. Gouvea, M. Mokhtar, A. M. Asiri, S. N. Basahel, S. A. Al-Thabaiti, A. O. Alyoubi, D. Chadwick and M. S. P. Shaffer, *Chem. Mater.*, 2012, **24**, 4531–4539.

116 I. Carrillo, E. Rangel and L. F. Magaña, *Carbon*, 2009, **47**, 2758–2760.

117 L. Wang, J. Zhao, L. Wang, T. Yan, Y.-Y. Sun and S. B. Zhang, *Phys. Chem. Chem. Phys.*, 2011, **13**, 21126–21131.

118 O. Leenaerts, B. Partoens and F. Peeters, *Phys. Rev. B*, 2008, **77**, 125416.

119 M. Seredych and T. J. Bandosz, *J. Phys. Chem. C*, 2010, **114**, 14552–14560.

120 C. Chen, K. Xu, X. Ji, L. Miao and J. Jiang, *Phys. Chem. Chem. Phys.*, 2014, **16**, 11031–11036.

121 S. Tang and Z. Cao, *J. Chem. Phys.*, 2011, **134**, 044710.

122 M. Seredych and T. J. Bandosz, *Langmuir*, 2009, **26**, 5491–5498.

123 C. Petit, B. Mendoza and T. J. Bandosz, *Langmuir*, 2010, **26**, 15302–9.

124 S. Tang and Z. Cao, *J. Phys. Chem. C*, 2012, **116**, 8778–8791.

125 M. Seredych, J. a. Rossin and T. J. Bandosz, *Carbon*, 2011, **49**, 4392–4402.

126 C. Petit and T. J. Bandosz, *Adv. Funct. Mater.*, 2011, **21**, 2108–2117.

127 M. Seredych and T. J. Bandosz, *J. Phys. Chem. C*, 2007, **111**, 15596–15604.

128 M. N. Chong, B. Jin, C. W. K. Chow and C. Saint, *Water Res.*, 2010, **44**, 2997–3027.

129 D. Ravelli, D. Dondi, M. Fagnoni and A. Albini, *Chem. Soc. Rev.*, 2009, **38**, 1999–2011.

130 X. An and J. C. Yu, *RSC Adv.*, 2011, **1**, 1426–1434.

131 A. Fujishima and K. Honda, *Nature*, 1972, **238**, 37–38.

132 R. Leary and A. Westwood, *Carbon*, 2011, **49**, 741–772.

133 A. L. Linsebigler, G. Lu and J. T. Yates, *Chem. Rev.*, 1995, **95**, 735–758.

134 Z. Khan, T. R. Chetia, A. K. Vardhaman, D. Barpuzary, C. V Sastri and M. Qureshi, *RSC Adv.*, 2012, **2**, 12122–12128.

135 B. Li and H. Cao, *J. Mater. Chem.*, 2011, **21**, 3346–3349.

136 Y. Wang, W. Wang, H. Mao, Y. Lu, J. Lu, J. Huang, Z. Ye and B. Lu, *ACS Appl. Mater. Interfaces*, 2014, **6**, 12698–12706.

137 J. Liu, H. Bai, Y. Wang, Z. Liu, X. Zhang and D. D. Sun, *Adv. Funct. Mater.*, 2010, **20**, 4175–4181.

138 Y. Zhang, Z.-R. Tang, X. Fu and Y.-J. Xu, *ACS Nano*, 2011, **5**, 7426–7435.

139 Y. Zhang, N. Zhang, Z.-R. Tang and Y.-J. Xu, *ACS Nano*, 2012, **6**, 9777–9789.

140 T. N. Lambert, C. A. Chavez, B. Hernandez-Sanchez, P. Lu, N. S. Bell, A. Ambrosini, T. Friedman, T. J. Boyle, D. R. Wheeler and D. L. Huber, *J. Phys. Chem. C*, 2009, **113**, 19812–19823.

141 Y. Liang, H. Wang, H. Sanchez Casalongue, Z. Chen and H. Dai, *Nano Res.*, 2010, **3**, 701–705.

142 M. Zhu, P. Chen and M. Liu, *ACS Nano*, 2011, **5**, 4529–4536.

143 X. Liu, L. Pan, T. Lv, T. Lu, G. Zhu, Z. Sun and C. Sun, *Catal. Sci. Technol.*, 2011, **1**, 1189–1193.

144 J. Zhang, Z. Xiong and X. S. Zhao, *J. Mater. Chem.*, 2011, **21**, 3634–3640.

145 G. Williams, B. Seger and P. V Kamat, *ACS Nano*, 2008, **2**, 1487–1491.

146 L. Zhang, H. Cheng, R. Zong and Y. Zhu, *J. Phys. Chem. C*, 2009, **113**, 2368–2374.

147 S. D. Perera, R. G. Mariano, K. Vu, N. Nour, O. Seitz, Y. Chabal and K. J. Balkus, *ACS Catal.*, 2012, **2**, 949–956.

148 Y. Zhang, Z.-R. Tang, X. Fu and Y.-J. Xu, *ACS Nano*, 2010, **4**, 7303–7314.

149 E. Gao, W. Wang, M. Shang and J. Xu, *Phys. Chem. Chem. Phys.*, 2011, **13**, 2887–2893.

150 H. Zhang, X. Lv, Y. Li, Y. Wang and J. Li, *ACS Nano*, 2009, **4**, 380–386.

151 M. S. Whittingham, J.-D. Guo, R. Chen, T. Chirayil, G. Janauer and P. Zavalij, *Solid State Ionics*, 1995, **75**, 257–268.

152 H. Zhang, P. Xu, G. Du, Z. Chen, K. Oh, D. Pan and Z. Jiao, *Nano Res.*, 2011, **4**, 274–283.

153 G. Jiang, Z. Lin, C. Chen, L. Zhu, Q. Chang, N. Wang, W. Wei and H. Tang, *Carbon*, 2011, **49**, 2693–2701.

154 C. Chen, W. Cai, M. Long, B. Zhou, Y. Wu, D. Wu and Y. Feng, *ACS Nano*, 2010, **4**, 6425–6432.

155 J. Du, X. Lai, N. Yang, J. Zhai, D. Kisailus, F. Su, D. Wang and L. Jiang, *ACS Nano*, 2010, **5**, 590–596.

156 X. Yang, H. Cui, Y. Li, J. Qin, R. Zhang and H. Tang, *ACS Catal.*, 2013, **3**, 363–369.

157 Z. Xiong, L. L. Zhang, J. Ma and X. S. Zhao, *Chem. Commun.*, 2010, **46**, 6099–6101.

158 Z. Chen, S. Liu, M.-Q. Yang and Y.-J. Xu, *ACS Appl. Mater. Interfaces*, 2013, **5**, 4309–4319.

159 S. Liu, Z. Chen, N. Zhang, Z.-R. Tang and Y.-J. Xu, *J. Phys. Chem. C*, 2013, **117**, 8251–8261.

160 Y. H. Ng, I. V Lightcap, K. Goodwin, M. Matsumura and P. V Kamat, *J. Phys. Chem. Lett.*, 2010, **1**, 2222–2227.

161 C. Zhai, M. Zhu, D. Bin, H. Wang, Y. Du, C. Wang and P. Yang, *ACS Appl. Mater. Interfaces*, 2014, **6**, 17753–17761.

162 S. K. Bhunia and N. R. Jana, *ACS Appl. Mater. Interfaces*, 2014.

163 X. Liu, L. Pan, T. Lv, G. Zhu, Z. Sun and C. Sun, *Chem. Commun.*, 2011, **47**, 11984–11986.

164 H. Ma, J. Shen, M. Shi, X. Lu, Z. Li, Y. Long, N. Li and M. Ye, *Appl. Catal. B Environ.*, 2012, **121–122**, 198–205.

165 O. Akhavan, M. Choobtashani and E. Ghaderi, *J. Phys. Chem. C*, 2012, **116**, 9653–9659.

166 O. Akhavan, E. Ghaderi and K. Rahimi, *J. Mater. Chem.*, 2012, **22**, 23260–23266.

167 O. Akhavan and E. Ghaderi, *J. Phys. Chem. C*, 2009, **113**, 20214–20220.

168 P. Gao, J. Liu, D. D. Sun and W. Ng, *J. Hazard. Mater.*, 2013, **250–251**, 412–420.

169 M. Q. Yang, N. Zhang and Y. J. Xu, *ACS Appl. Mater. Interfaces*, 2013, **5**, 1156–1164.

170 V. Berry, *Carbon*, 2013, **62**, 1–10.

171 F. Guo, G. Silverberg, S. Bowers, S.-P. Kim, D. Datta, V. Shenoy and R. H. Hurt, *Environ. Sci. Technol.*, 2012, **46**, 7717–24.

172 D. Prasai, J. C. Tuberquia, R. R. Harl, G. K. Jennings, B. R. Rogers and K. I. Bolotin, *ACS Nano*, 2012, **6**, 1102–8.

173 A. Alexiadis and S. Kassinos, *Chem. Rev.*, 2008, **108**, 5014–5034.

174 A. Striolo, *Nano Lett.*, 2006, **6**, 633–9.

175 Y. Liu and X. Chen, *J. Appl. Phys.*, 2014, **115**, 034303.

176 D. Cohen-Tanugi and J. C. Grossman, *Nano Lett.*, 2012, **12**, 3602–8.

177 M. Elimelech and W. A. Phillip, *Science*, 2011, **333**, 712–7.

178 D. Cohen-Tanugi, R. K. McGovern, S. H. Dave, J. H. Lienhard and J. C. Grossman, *Energy Environ. Sci.*, 2014, **7**, 1134.

179 K. Sint, B. Wang and P. Král, *J. Am. Chem. Soc.*, 2008, **130**, 16448–9.

180 D. Konatham, J. Yu, T. a Ho and A. Striolo, *Langmuir*, 2013, **29**, 11884–97.

181 J.-G. Gai and X.-L. Gong, *J. Mater. Chem. A*, 2014, **2**, 425.

182 J.-G. Gai, X.-L. Gong, W.-W. Wang, X. Zhang and W.-L. Kang, *J. Mater. Chem. A*, 2014, **2**, 4023.

183 M. A. Shannon, P. W. Bohn, M. Elimelech, J. G. Georgiadis, B. J. Mariñas, A. M. Mayes, B. J. Marinas, A. M. Mayes, B. J. Mariñas and A. M. Mayes, *Nature*, 2008, **452**, 301–10.

184 M. D. Fischbein and M. Drndic, *Appl. Phys. Lett.*, 2008, **93**, 113107.

185 B. Song, G. F. Schneider, Q. Xu, G. Pandraud, C. Dekker and H. Zandbergen, *Nano Lett.*, 2011, **11**, 2247–50.

186 S. Garaj, W. Hubbard, A. Reina, J. Kong, D. Branton and J. A. Golovchenko, *Nature*, 2010, **467**, 190–3.

187 C. J. Russo and J. a Golovchenko, *Proc. Natl. Acad. Sci. U. S. A.*, 2012, **109**, 5953–7.

188 D. Fox, a. O'Neill, D. Zhou, M. Boese, J. N. Coleman and H. Z. Zhang, *Appl. Phys. Lett.*, 2011, **98**, 243117.

189 J. Bai, X. Zhong, S. Jiang, Y. Huang and X. Duan, *Nat. Nanotechnol.*, 2010, **5**, 190–4.

190 S. P. Koenig, L. Wang, J. Pellegrino and J. S. Bunch, *Nat. Nanotechnol.*, 2012, **7**, 728–32.

191 L. Liu, S. Ryu, M. R. Tomasik, E. Stolyarova, N. Jung, M. S. Hybertsen, M. L. Steigerwald, L. E. Brus and G. W. Flynn, *Nano Lett.*, 2008, **8**, 1965–70.

192 S. C. O'Hern, C. a Stewart, M. S. H. Boutilier, J.-C. Idrobo, S. Bhaviripudi, S. K. Das, J. Kong, T. Laoui, M. Atieh and R. Karnik, *ACS Nano*, 2012, **6**, 10130–8.

193 S. C. O'Hern, M. S. H. Boutilier, J.-C. Idrobo, Y. Song, J. Kong, T. Laoui, M. Atieh and R. Karnik, *Nano Lett.*, 2014, **14**, 1234–41.

194 M. Peplow, *Nature*, 2013, **503**, 327–329.

195 R. R. Nair, H. a Wu, P. N. Jayaram, I. V Grigorieva and a K. Geim, *Science*, 2012, **335**, 442–4.

196 H. Huang, Y. Mao, Y. Ying, Y. Liu, L. Sun and X. Peng, *Chem. Commun.*, 2013, **49**, 5963–5.

197 R. K. Joshi, P. Carbone, F. C. Wang, V. G. Kravets, Y. Su, I. V Grigorieva, H. a Wu, a K. Geim and R. R. Nair, *Science*, 2014, **343**, 752–4.

198 M. Hu and B. Mi, *Environ. Sci. Technol.*, 2013, **47**, 3715–23.

199 Y. Han, Z. Xu and C. Gao, *Adv. Funct. Mater.*, 2013, **23**, 3693–3700.

200 P. Sun, F. Zheng, M. Zhu, Z. Song, K. Wang, M. Zhong, D. Wu, R. B. Little, Z. Xu and H. Zhu, *ACS Nano*, 2014, **8**, 850–859.

201 H. Huang, Z. Song, N. Wei, L. Shi, Y. Mao, Y. Ying, L. Sun, Z. Xu and X. Peng, *Nat. Commun.*, 2013, **4**, 2979.

202 N. Wang, S. Ji, G. Zhang, J. Li and L. Wang, *Chem. Eng. J.*, 2012, **213**, 318–329.

203 B. Mi, *Science*, 2014, **343**, 740–2.

204 X. Li, S. Zhang, F. Fu and T.-S. Chung, *J. Memb. Sci.*, 2013, **434**, 204–217.

205 A. P. Straub, N. Y. Yip and M. Elimelech, *Environ. Sci. Technol. Lett.*, 2014, **1**, 55–59.

206 M. Ionita, A. M. Pandele, L. Crica and L. Pilan, *Compos. Part B Eng.*, 2014, **59**, 133–139.

207 J. J. Lee, H.-R. Chae, Y. J. Won, K. Lee, C.-H. Lee, H. H. Lee, I.-C. Kim and J. J. Lee, *J. Memb. Sci.*, 2013, **448**, 223–230.

208 L. Yu, Y. Zhang, B. Zhang, J. Liu, H. Zhang and C. Song, *J. Memb. Sci.*, 2013, **447**, 452–462.

209 X. Chang, Z. Wang, S. Quan, Y. Xu, Z. Jiang and L. Shao, *Appl. Surf. Sci.*, 2014, **316**, 537–548.

210 F. Jin, W. Lv, C. Zhang, Z. Li, R. Su, W. Qi, Q.-H. Yang and Z. He, *RSC Adv.*, 2013, **3**, 21394.

211 C. Zhao, X. Xu, J. Chen and F. Yang, *J. Environ. Chem. Eng.*, 2013, **1**, 349–354.

212 S. Zinadini, A. A. Zinatizadeh, M. Rahimi, V. Vatanpour and H. Zangeneh, *J. Memb. Sci.*, 2014, **453**, 292–301.

213 Z. Xu, J. Zhang, M. Shan, Y. Li, B. Li, J. Niu, B. Zhou and X. Qian, *J. Memb. Sci.*, 2014, **458**, 1–13.

214 C. Zhao, X. Xu, J. Chen and F. Yang, *Desalination*, 2014, **334**, 17–22.

215 M. J. Eckelman, M. S. Mauter, J. a Isaacs and M. Elimelech, *Environ. Sci. Technol.*, 2012, **46**, 2902–10.

216 W. Choi, J. Choi, J. Bang and J.-H. Lee, *ACS Appl. Mater. Interfaces*, 2013, **5**, 12510–9.

217 K. Goh, L. Setiawan, L. Wei, R. Si, a G. Fane, R. Wang and Y. Chen, *J. Memb. Sci.*, 2015, **474**, 244–253.

218 F. Perreault, M. E. Tousley and M. Elimelech, *Environ. Sci. Technol. Lett.*, 2014, 71–76.

219 Y. L. F. Musico, C. M. Santos, M. L. P. Dalida and D. F. Rodrigues, *ACS Sustain. Chem. Eng.*, 2014, **2**, 1559–1565.

220 Y. Oren, *Desalination*, 2008, **228**, 10–29.

221 S. Porada, R. Zhao, a. van der Wal, V. Presser and P. M. Biesheuvel, *Prog. Mater. Sci.*, 2013, **58**, 1388–1442.

222 M. a. Anderson, A. L. Cudero and J. Palma, *Electrochim. Acta*, 2010, **55**, 3845–3856.

223 H. Li, T. Lu, L. Pan, Y. Zhang and Z. Sun, *J. Mater. Chem.*, 2009, **19**, 6773.

224 B. Jia and L. Zou, *Carbon*, 2012, **50**, 2315–2321.

225 H. Li, L. Pan, C. Nie, Y. Liu and Z. Sun, *J. Mater. Chem.*, 2012, **22**, 15556.

226 D. Zhang, X. Wen, L. Shi, T. Yan and J. Zhang, *Nanoscale*, 2012, **4**, 5440–6.

227 D. Zhang, T. Yan, L. Shi, Z. Peng, X. Wen and J. Zhang, *J. Mater. Chem.*, 2012, **22**, 14696.

228 Y. Wimalasiri and L. Zou, *Carbon*, 2013, **59**, 464–471.

229 H. Yin, S. Zhao, J. Wan, H. Tang, L. Chang, L. He, H. Zhao, Y. Gao and Z. Tang, *Adv. Mater.*, 2013, **25**, 6270–6.

230 X. Wen, D. Zhang, T. Yan, J. Zhang and L. Shi, *J. Mater. Chem. A*, 2013, **1**, 12334.

231 Q. Dong, G. Wang, B. Qian, C. Hu, Y. Wang and J. Qiu, *Electrochim. Acta*, 2014, **137**, 388–394.

232 Z. Wang, B. Dou, L. Zheng, G. Zhang, Z. Liu and Z. Hao, *Desalination*, 2012, **299**, 96–102.

233 H. Wang, D. Zhang, T. Yan, X. Wen, J. Zhang, L. Shi and Q. Zhong, *J. Mater. Chem. A*, 2013, **1**, 11778.

234 L. F. Melo and T. R. Bott, *Exp. Therm. Fluid Sci.*, 1997, **14**, 375–381.

235 M. P. Schultz, J. a Bendick, E. R. Holm and W. M. Hertel, *Biofouling*, 2011, **27**, 87–98.

236 B. J. Little, J. S. Lee and R. I. Ray, *Electrochim. Acta*, 2008, **54**, 2–7.

237 I. K. Konstantinou and T. a Albanis, *Environ. Int.*, 2004, **30**, 235–48.

238 K. Yang, Y. Li, X. Tan, R. Peng and Z. Liu, *Small*, 2013, **9**, 1492–503.

239 A. M. Jastrzębska, P. Kurtycz and A. R. Olszyna, *J. Nanopart. Res.*, 2012, **14**, 1320.

240 O. Akhavan and E. Ghaderi, *ACS Nano*, 2010, **4**, 5731–5736.

241 J. Chen, H. Peng, X. Wang, F. Shao, Z. Yuan and H. Han, *Nanoscale*, 2014, **6**, 1879–89.

242 W. Hu, C. Peng, W. Luo, M. Lv, X. Li, D. Li, Q. Huang and C. Fan, *ACS Nano*, 2010, **4**, 4317–23.

243 Y. Tu, M. Lv, P. Xiu, T. Huynh, M. Zhang, M. Castelli, Z. Liu, Q. Huang, C. Fan, H. Fang and R. Zhou, *Nat. Nanotechnol.*, 2013, **8**, 594–601.

244 J. Mao, R. Guo and L.-T. Yan, *Biomaterials*, 2014, **35**, 6069–77.

245 Y. Li, H. Yuan, A. von dem Bussche, M. Creighton, R. H. Hurt, A. B. Kane and H. Gao, *Proc. Natl. Acad. Sci. U. S. A.*, 2013, **110**, 12295–300.

246 H. Lei, X. Zhou, H. Wu, Y. Song, J. Hu, S. Guo and Y. Zhang, *Langmuir*, 2014, **30**, 4678–83.

247 K. L. Chen and G. D. Bothun, *Environ. Sci. Technol.*, 2014, **48**, 873–80.

248 J. Chen, X. Wang and H. Han, *J. Nanoparticle Res.*, 2013, **15**, 1658.

249 S. Gurunathan, J. W. Han, A. A. Dayem, V. Eppakayala and J.-H. Kim, *Int. J. Nanomedicine*, 2012, **7**, 5901–14.

250 S. Gurunathan, J. W. Han, A. A. Dayem, V. Eppakayala, M.-R. Park, D.-N. Kwon and J.-H. Kim, *J. Ind. Eng. Chem.*, 2013, **19**, 1280–1288.

251 S. Kang, M. S. Mauter and M. Elimelech, *Environ. Sci. Technol.*, 2008, **42**, 7528–34.

252 L. M. Pasquini, S. M. Hashmi, T. J. Sommer, M. Elimelech and J. B. Zimmerman, *Environ. Sci. Technol.*, 2012, **46**, 6297–305.

253 X. Liu, S. Sen, J. Liu, I. Kulaots, D. Geohegan, A. Kane, A. a Puretzky, C. M. Rouleau, K. L. More, G. T. R. Palmore and R. H. Hurt, *Small*, 2011, **7**, 2775–85.

254 M. Mols and T. Abee, *Environ. Microbiol.*, 2011, **13**, 1387–94.

255 S. Liu, M. Hu, T. H. Zeng, R. Wu, R. Jiang, J. Wei, L. Wang, J. Kong and Y. Chen, *Langmuir*, 2012, **28**, 12364–72.

256 O. Akhavan, E. Ghaderi and a Esfandiar, *J. Phys. Chem. B*, 2011, **115**, 6279–88.

257 X. Cai, S. Tan, M. Lin, A. Xie, W. Mai, X. Zhang, Z. Lin, T. Wu and Y. Liu, *Langmuir*, 2011, **27**, 7828–35.

258 B. Yuan, T. Zhu, Z. Zhang, Z. Jiang and Y. Ma, *J. Mater. Chem.*, 2011, **21**, 3471.

259 Y.-W. Wang, A. Cao, Y. Jiang, X. Zhang, J.-H. Liu, Y. Liu and H. Wang, *ACS Appl. Mater. Interfaces*, 2014, **6**, 2791–8.

260 J. Lalley, D. D. Dionysiou, R. S. Varma, S. Shankara, D. J. Yang and M. N. Nadagouda, *Curr. Opin. Chem. Eng.*, 2014, **3**, 25–29.

261 M. R. Das, R. K. Sarma, R. Saikia, V. S. Kale, M. V Shelke and P. Sengupta, *Colloids Surf. B. Biointerfaces*, 2011, **83**, 16–22.

262 T. He, H. Liu, Y. Zhou, J. Yang, X. Cheng and H. Shi, *Biometals*, 2014, **27**, 673–82.

263 Y. Zhou, J. Yang, T. He, H. Shi, X. Cheng and Y. Lu, *Small*, 2013, **9**, 3445–54.

264 Q. Bao, D. Zhang and P. Qi, *J. Colloid Interface Sci.*, 2011, **360**, 463–70.

265 A. F. de Faria, D. S. T. Martinez, S. M. M. Meira, A. C. M. de Moraes, A. Brandelli, A. G. S. Filho and O. L. Alves, *Colloids Surf. B. Biointerfaces*, 2014, **113**, 115–24.

266 J. Tang, Q. Chen, L. Xu, S. Zhang, L. Feng, L. Cheng, H. Xu, Z. Liu and R. Peng, *ACS Appl. Mater. Interfaces*, 2013, **5**, 3867–74.

267 S. Barua, S. Thakur, L. Aidew, A. K. Buragohain, P. Chattopadhyay and N. Karak, *RSC Adv.*, 2014, **4**, 9777.

268 A. F. de Faria, A. C. M. de Moraes, P. D. Marcato, D. S. T. Martinez, N. Durán, A. G. S. Filho, A. Brandelli and O. L. Alves, *J. Nanoparticle Res.*, 2014, **16**, 2110.

269 X.-Z. Tang, X. Li, Z. Cao, J. Yang, H. Wang, X. Pu and Z.-Z. Yu, *Carbon*, 2013, **59**, 93–99.

270 V. H. Nguyen, B.-K. Kim, Y.-L. Jo and J.-J. Shim, *J. Supercrit. Fluids*, 2012, **72**, 28–35.

271 X. Cai, M. Lin, S. Tan, W. Mai, Y. Zhang, Z. Liang, Z. Lin and X. Zhang, *Carbon*, 2012, **50**, 3407–3415.

272 Z. Tai, H. Ma, B. Liu, X. Yan and Q. Xue, *Colloids Surf. B. Biointerfaces*, 2012, **89**, 147–51.

273 Z. Zhu, M. Su, L. Ma, L. Ma, D. Liu and Z. Wang, *Talanta*, 2013, **117**, 449–55.

274 Y. Han, Z. Luo, L. Yuwen, J. Tian, X. Zhu and L. Wang, *Appl. Surf. Sci.*, 2013, **266**, 188–193.

275 I. Ocsoy, M. L. Paret, M. A. Ocsoy, S. Kunwar, T. Chen, M. You and W. Tan, *ACS Nano*, 2013, **7**, 8972–80.

276 M. R. Das, R. K. Sarma, S. C. Borah, R. Kumari, R. Saikia, A. B. Deshmukh, M. V Shelke, P. Sengupta, S. Szunerits and R. Boukherroub, *Colloids Surf. B. Biointerfaces*, 2013, **105**, 128–36.

277 J. Liu, D. a Sonshine, S. Shervani and R. H. Hurt, *ACS Nano*, 2010, **4**, 6903–13.

278 J. Dobias and R. Bernier-Latmani, *Environ. Sci. Technol.*, 2013, **47**, 4140–6.

279 L. Karimi, M. E. Yazdanshenas, R. Khajavi, A. Rashidi and M. Mirjalili, *Cellulose*, 2014, **21**, 3813–3827.

280 B. Z. Ristic, M. M. Milenkovic, I. R. Dakic, B. M. Todorovic-Markovic, M. S. Milosavljevic, M. D. Budimir, V. G. Paunovic, M. D. Dramicanin, Z. M. Markovic and V. S. Trajkovic, *Biomaterials*, 2014, **35**, 4428–35.

281 H. Sun, N. Gao, K. Dong, J. Ren and X. Qu, *ACS Nano*, 2014, **8**, 6202–6210.

282 T. S. Sreeprasad, S. M. Maliyekkal, K. P. Lisha and T. Pradeep, *J. Hazard. Mater.*, 2011, **186**, 921–931.

283 I. E. Mejias Carpio, J. D. Mangadlao, H. N. Nguyen, R. C. Advincula and D. F. Rodrigues, *Carbon*, 2014, **77**, 289–301.

284 W. He, H. Huang, J. Yan and J. Zhu, *J. Appl. Phys.*, 2013, **114**, 204701.

285 I. E. Mejías Carpio, C. M. Santos, X. Wei and D. F. Rodrigues, *Nanoscale*, 2012, **4**, 4746–56.

286 C. M. Santos, M. C. R. Tria, R. A. M. V Vergara, F. Ahmed, R. C. Advincula and D. F. Rodrigues, *Chem. Commun.*, 2011, **47**, 8892–4.

287 C. M. Santos, J. Mangadlao, F. Ahmed, A. Leon, R. C. Advincula and D. F. Rodrigues, *Nanotechnology*, 2012, **23**, 395101.

288 M. Pumera, *Chem. Soc. Rev.*, 2010, **39**, 4146–57.

289 F. Schedin, a K. Geim, S. V Morozov, E. W. Hill, P. Blake, M. I. Katsnelson and K. S. Novoselov, *Nat. Mater.*, 2007, **6**, 652–5.

290 W. Li, X. Geng, Y. Guo, J. Rong, Y. Gong, L. Wu, X. Zhang, P. Li, J. Xu, G. Cheng, M. Sun and L. Liu, *ACS Nano*, 2011, **5**, 6955–61.

291 S. Mao, S. Cui, G. Lu, K. Yu, Z. Wen and J. Chen, *J. Mater. Chem.*, 2012, **22**, 11009.

292 L. Al-Mashat, K. Shin, K. Kalantar-zadeh, J. D. Plessis, S. H. Han, R. W. Kojima, R. B. Kaner, D. Li, X. Gou, S. J. Ippolito and W. Wlodarski, *J. Phys. Chem. C*, 2010, **114**, 16168–16173.

293 Y. Si and E. T. Samulski, *Chem. Mater.*, 2008, **20**, 6792–6797.

294 S. Stankovich, D. A. Dikin, G. H. B. Dommett, K. M. Kohlhaas, E. J. Zimney, E. A. Stach, R. D. Piner, S. T. Nguyen and R. S. Ruoff, *Nature*, 2006, **442**, 282–286.

295 Y. Liu, X. Dong and P. Chen, *Chem. Soc. Rev.*, 2012, **41**, 2283–307.

296 M. Zhou, Y. Zhai and S. Dong, *Anal. Chem.*, 2009, **81**, 5603–13.

297 Y. Wang, Y. Li, L. Tang, J. Lu and J. Li, *Electrochem. commun.*, 2009, **11**, 889–892.

298 S. Eissa, A. Ng, M. Siaj, A. C. Tavares and M. Zourob, *Anal. Biochem.*, 2013, **85**, 11794–11801.

299 K. S. Novoselov, A. K. Geim, S. V Morozov, D. Jiang, Y. Zhang, S. V Dubonos, I. V Grigorieva and A. A. Firsov, *Science*, 2004, **306**, 666–669.

300 X. Li, Y. Zhu, W. Cai, M. Borysiak, B. Han, D. Chen, R. D. Piner, L. Colombo and R. S. Ruoff, *Nano Lett.*, 2009, **9**, 4359–63.

301 K. S. Novoselov, a K. Geim, S. V Morozov, D. Jiang, M. I. Katsnelson, I. V Grigorieva, S. V Dubonos and a a Firsov, *Nature*, 2005, **438**, 197–200.

302 L. Tang, Y. Wang, Y. Li, H. Feng, J. Lu and J. Li, *Adv. Funct. Mater.*, 2009, **19**, 2782–2789.

303 C. Gomez-Navarro, R. T. Weitz, A. M. Bittner, M. Scolari, A. Mews, M. Burghard, K. Kern and M. Festkoerperforschung, *Nano Lett.*, 2007, **7**, 3499–3503.

304 V. Dua, S. P. Surwade, S. Ammu, S. R. Agnihotra, S. Jain, K. E. Roberts, S. Park, R. S. Ruoff and S. K. Manohar, *Angew. Chem. Int. Ed. Engl.*, 2010, **49**, 2154–7.

305 J. D. Fowler, M. J. Allen, V. C. Tung, Y. Yang, R. B. Kaner and B. H. Weiller, *ACS Nano*, 2009, **3**, 301–6.

306 R. Ghosh, A. Midya, S. Santra, S. K. Ray and P. K. Guha, *ACS Appl. Mater. Interfaces*, 2013, **5**, 7599–603.

307 Q. Ji, I. Honma, S.-M. Paek, M. Akada, J. P. Hill, A. Vinu and K. Ariga, *Angew. Chem. Int. Ed. Engl.*, 2010, **49**, 9737–9.

308 G. Lu, L. E. Ocola and J. Chen, *Nanotechnology*, 2009, **20**, 445502.

309 S. Rumyantsev, G. Liu, M. S. Shur, R. a Potyrailo and A. a Balandin, *Nano Lett.*, 2012, **12**, 2294–8.

310 R. K. Joshi, H. Gomez, F. Alvi and A. Kumar, *J. Phys. Chem. C*, 2010, **114**, 6610–6613.

311 M. Gautam and A. H. Jayatissa, *Mater. Sci. Eng. C*, 2011, **31**, 1405–1411.

312 B. Huang, Z. Li, Z. Liu, G. Zhou, S. Hao, J. Wu, B.-L. Gu and W. Duan, *J. Phys. Chem. C*, 2008, **112**, 13442–13446.

313 H. J. Yoon, D. H. Jun, J. H. Yang, Z. Zhou, S. S. Yang and M. M.-C. Cheng, *Sensors Actuators B Chem.*, 2011, **157**, 310–313.

314 Y.-H. Zhang, Y.-B. Chen, K.-G. Zhou, C.-H. Liu, J. Zeng, H.-L. Zhang and Y. Peng, *Nanotechnology*, 2009, **20**, 185504.

315 K. Z. Milowska and J. a. Majewski, *J. Phys. Chem. C*, 2014, **118**, 17395–17401.

316 T. O. Wehling, K. S. Novoselov, S. V Morozov, E. E. Vdovin, M. I. Katsnelson, a K. Geim and a I. Lichtenstein, *Nano Lett.*, 2008, **8**, 173–7.

317 Y. Dan, Y. Lu, N. J. Kybert, Z. Luo and a T. C. Johnson, *Nano Lett.*, 2009, **9**, 1472–5.

318 R. Arsat, M. Breedon, M. Shafiei, P. G. Spizziri, S. Gilje, R. B. Kaner, K. Kalantar-zadeh and W. Wlodarski, *Chem. Phys. Lett.*, 2009, **467**, 344–347.

319 J. T. Robinson, F. K. Perkins, E. S. Snow, Z. Wei and P. E. Sheehan, *Nano Lett.*, 2008, **8**, 3137–40.

320 G. Lu, S. Park, K. Yu, R. S. Ruoff, L. E. Ocola, D. Rosenmann, J. Chen and L. U. E. T. Al, *ACS Nano*, 2011, 1154–1164.

321 X. Huang, N. Hu, R. Gao, Y. Yu, Y. Wang, Z. Yang, E. Siu-Wai Kong, H. Wei and Y. Zhang, *J. Mater. Chem.*, 2012, **22**, 22488.

322 P. a Russo, N. Donato, S. G. Leonardi, S. Baek, D. E. Conte, G. Neri and N. Pinna, *Angew. Chemie Int. Ed.*, 2012, **51**, 11053–7.

323 S. Liu, J. Tian, L. Wang, H. Li, Y. Zhang and X. Sun, *Macromolecules*, 2010, **43**, 10078–10083.

324 Y. Fang, S. Guo, C. Zhu, Y. Zhai and E. Wang, *Langmuir*, 2010, **26**, 11277–82.

325 K. Zhou, Y. Zhu, X. Yang, J. Luo, C. Li and S. Luan, *Electrochim. Acta*, 2010, **55**, 3055–3060.

326 Q. Zeng, J. Cheng, L. Tang, X. Liu, Y. Liu, J. Li and J. Jiang, *Adv. Funct. Mater.*, 2010, **20**, 3366–3372.

327 K. Chen, G. Lu, J. Chang, S. Mao, K. Yu, S. Cui and J. Chen, *Anal. Chem.*, 2012, **84**, 4057–62.

328 Y. Wen, F. Y. Li, X. Dong, J. Zhang, Q. Xiong and P. Chen, *Adv. Healthc. Mater.*, 2013, **2**, 271–4.

329 C. Yu, Y. Guo, H. Liu, N. Yan, Z. Xu, G. Yu, Y. Fang and Y. Liu, *Chem. Commun.*, 2013, **49**, 6492–4.

330 G. Zhou, J. Chang, S. Cui, H. Pu, Z. Wen and J. Chen, *ACS Appl. Mater. Interfaces*, 2014, **6**, 19235–19241.

331 S. Yang, J. Liang, S. Luo, C. Liu and Y. Tang, *Anal. Biochem.*, 2013, **85**, 7720–7725.

332 B. G. Choi, H. Park, T. J. Park, M. H. Yang, J. S. Kim, S. Jang, N. S. Heo, S. Y. Lee, J. Kong and W. H. Hong, *ACS Nano*, 2010, **4**, 2910–2918.

333 H. Fan, Y. Li, D. Wu, H. Ma, K. Mao, D. Fan, B. Du, H. Li and Q. Wei, *Anal. Chim. Acta*, 2012, **711**, 24–8.

334 C. Wu, D. Sun, Q. Li and K. Wu, *Sensors Actuators B Chem.*, 2012, **168**, 178–184.

335 L. Wang, K.-Y. Pu, J. Li, X. Qi, H. Li, H. Zhang, C. Fan and B. Liu, *Adv. Mater.*, 2011, **23**, 4386–91.

336 Y. Huang, X. Dong, Y. Liu, L.-J. Li and P. Chen, *J. Mater. Chem.*, 2011, **21**, 12358.

337 R. K. Srivastava, S. Srivastava, T. N. Narayanan, B. D. Mahlotra, R. Vajtai, P. M. Ajayan and A. Srivastava, *ACS Nano*, 2012, **6**, 168–75.

338 S. Alwarappan, A. Erdem, C. Liu and C.-Z. Li, *J. Phys. Chem. C*, 2009, **113**, 8853–8857.

339 L. Sheng, J. Ren, Y. Miao, J. Wang and E. Wang, *Biosens. Bioelectron.*, 2011, **26**, 3494–9.

340 K. R. Ratinac, W. Yang, S. P. Ringer and F. Braet, *Environ. Sci. Technol.*, 2010, **44**, 1167–76.

341 D. Chen, L. Tang and J. Li, *Chem. Soc. Rev.*, 2010, **39**, 3157–80.

342 A. Zurutuza and C. Marinelli, *Nat. Nanotechnol.*, 2014, **9**, 730–734.

343 W. Ren and H.-M. Cheng, *Nat. Nanotechnol.*, 2014, **9**, 726–730.

344 X. Hu and Q. Zhou, *Chem. Rev.*, 2013, **113**, 3815–35.

345 C. Bussy, H. Ali-Boucetta and K. Kostarelos, *Acc. Chem. Res.*, 2013, **46**, 692–701.

346 A. Bianco, *Angew. Chem. Int. Ed. Engl.*, 2013, **52**, 4986–97.

347 C. Gómez-navarro, M. Burghard and K. Kern, *Nano Lett.*, 2008, **8**, 2045–2049.

348 M. Lan, G. Fan, L. Yang and F. Li, *Ind. Eng. Chem. Res.*, 2014, **53**, 12943–12952.

349 M. Hu and B. Mi, *J. Memb. Sci.*, 2014, **469**, 80–87.

350 H. Li, L. Zou, L. Pan and Z. Sun, *Environ. Sci. Technol.*, 2010, **44**, 8692–7.

351 H. Li, S. Liang, J. Li and L. He, *J. Mater. Chem. A*, 2013, **1**, 6335.

352 Z. Li, F. Chen, L. Yuan, Y. Liu, Y. Zhao, Z. Chai and W. Shi, *Chem. Eng. J.*, 2012, **210**, 539–546.

353 X. Mi, G. Huang, W. Xie, W. Wang, Y. Liu and J. Gao, *Carbon*, 2012, **50**, 4856–4864.

354 V. Chandra and K. S. Kim, *Chem. Commun.*, 2011, **47**, 3942–3944.

355 X. Deng, L. Lü, H. Li and F. Luo, *J. Hazard. Mater.*, 2010, **183**, 923–930.

356 H.-L. Ma, Y. Zhang, Q.-H. Hu, D. Yan, Z.-Z. Yu and M. Zhai, *J. Mater. Chem.*, 2012, **22**, 5914–5916.

357 X. Hu, Y. Liu, H. Wang, A. Chen, G. Zeng, S. Liu, Y. Guo, X. Hu, T. Li, Y. Wang, L. Zhou and S. Liu, *Sep. Purif. Technol.*, 2013, **108**, 189–195.

358 D. Dinda, A. Gupta and S. K. Saha, *J. Mater. Chem. A*, 2013, **1**, 11221–11228.

359 S. W. Yan-Hui Li Jinquan Wei , Xianfeng Zhang , Cailu Xu ,Zhaokun Luan , Dehai Wu , Bingqing Wei, *Chem. Phys. Lett.*, 2002, **357**, 263–266.

360 Y.-H. Li, J. Ding, Z. Luan, Z. Di, Y. Zhu, C. Xu, D. Wu and B. Wei, *Carbon*, 2003, **41**, 2787–2792.

361 J. Goel, K. Kadirvelu, C. Rajagopal and V. Kumar Garg, *J. Hazard. Mater.*, 2005, **125**, 211–220.

362 M. Imamoglu and O. Tekir, *Desalination*, 2008, **228**, 108–113.

363 K. Selvi, S. Pattabhi and K. Kadirvelu, *Bioresour. Technol.*, 2001, **80**, 87–89.

364 L. Monser and N. Adhoum, *Sep. Purif. Technol.*, 2002, **26**, 137–146.

365 B. Pan, D. Lin, H. Mashayekhi and B. Xing, *Environ. Sci. Technol.*, 2008, **42**, 5480–5485.

366 K. Yang, L. Zhu and B. Xing, *Environ. Sci. Technol.*, 2006, **40**, 1855–1861.

367 Y. Li, Q. Du, T. Liu, X. Peng, J. Wang, J. Sun, Y. Wang, S. Wu, Z. Wang, Y. Xia and L. Xia, *Chem. Eng. Res. Des.*, 2013, **91**, 361–368.

368 P. Oleszczuk, B. Pan and B. Xing, *Environ. Sci. Technol.*, 2009, **43**, 9167–9173.

369 D. Lin and B. Xing, *Environ. Sci. Technol.*, 2008, **42**, 7254–7259.

370 J. Kong, N. R. Franklin, C. Zhou, M. G. Chapline, S. Peng, K. Cho and H. Dai, *Science*, 2000, **287**, 622–625.

371 A. Modi, N. Koratkar, E. Lass, B. Wei and P. M. Ajayan, *Nature*, 2003, **424**, 171–174.

372 R. J. Chen, S. Bangsaruntip, K. A. Drouvalakis, N. Wong Shi Kam, M. Shim, Y. Li, W. Kim, P. J. Utz and H. Dai, *Proc. Natl. Acad. Sci.*, 2003, **100**, 4984–4989.

373 P. Qi, O. Vermesh, M. Grecu, A. Javey, Q. Wang, H. Dai, S. Peng and K. J. Cho, *Nano Lett.*, 2003, **3**, 347–351.

374 E. Bekyarova, M. Davis, T. Burch, M. E. Itkis, B. Zhao, S. Sunshine and R. C. Haddon, *J. Phys. Chem. B*, 2004, **108**, 19717–19720.

375 J. Kong, M. G. Chapline and H. Dai, *Adv. Mater.*, 2001, **13**, 1384–1386.

2077

2078

2079

2080

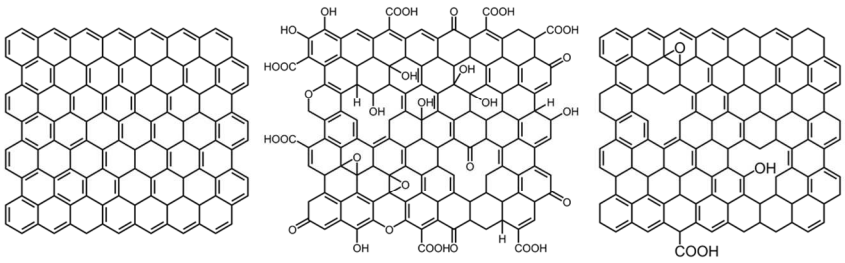

Properties	Graphene	Graphene Oxide	Reduced Graphene Oxide
Synthesis	-Chemical vapor deposition -Thermal decomposition of SiC -Graphite exfoliation	-Oxidation and exfoliation of graphite	-Reduction of graphene oxide
C:O ratio	No oxygen	2-4	8-246
Young's modulus (TPa)	1	0.2	0.25
Electron mobility ($cm^2 V^{-1} s^{-1}$)	10 000–50 000	insulator	0.05–200
Production cost	High	Low	Low

Fig. 1. Overview of structure and main properties of graphene-based nanomaterials relevant for environmental applications. [22,26,37,42,347]

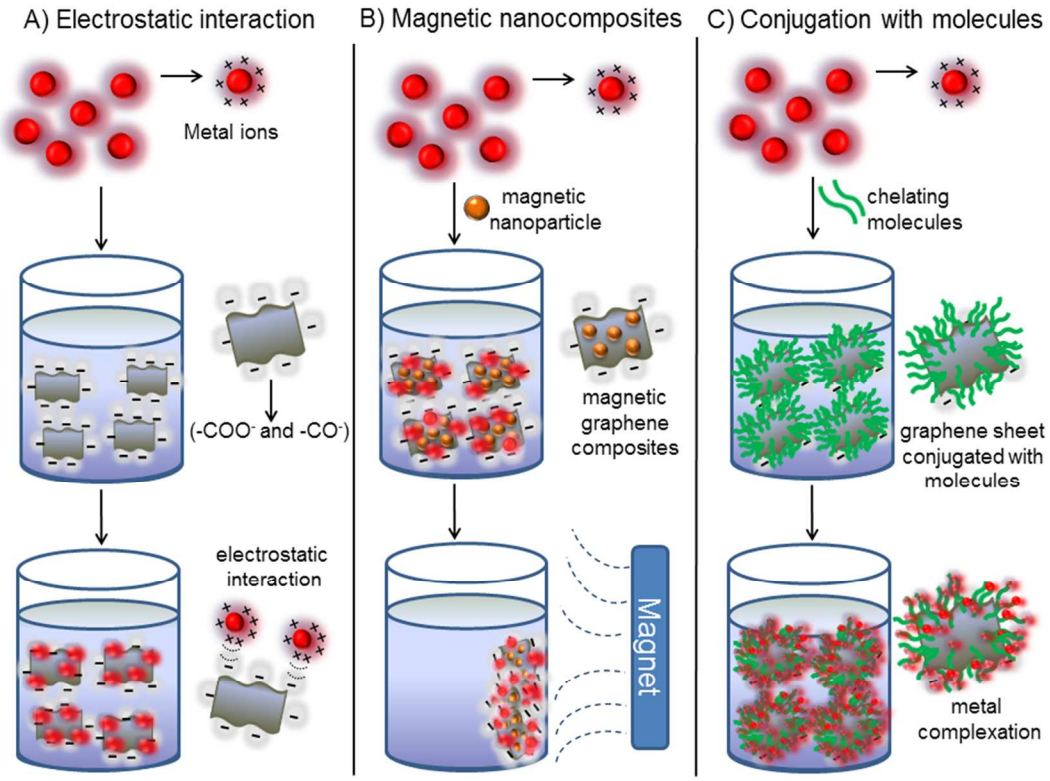

Fig. 2**.** Main strategies to apply graphene-based materials as adsorbents for the removal of metal ions from aqueous solutions. A) The sorption process can be performed using non-modified graphene oxide (GO), graphene, or reduced graphene oxide (rGO); the mechanism of adsorption is mostly due to electrostatic interaction between the negatively charged GO sheets and the positively charged metal ions. B) Graphene sheets can be functionalized with magnetic nanoparticles to improve adsorption capacity; since the GO nanocomposites possess magnetic properties, metal ions can be removed from water by magnetic attraction. C) Modification of graphene sheets with organic molecules can be used to prepare graphene-based adsorbents with improved effectiveness; the mechanism of adsorption is attributed to a synergetic effect between the chelating properties of the organic molecules and adsorption capacity of the graphene sheets.

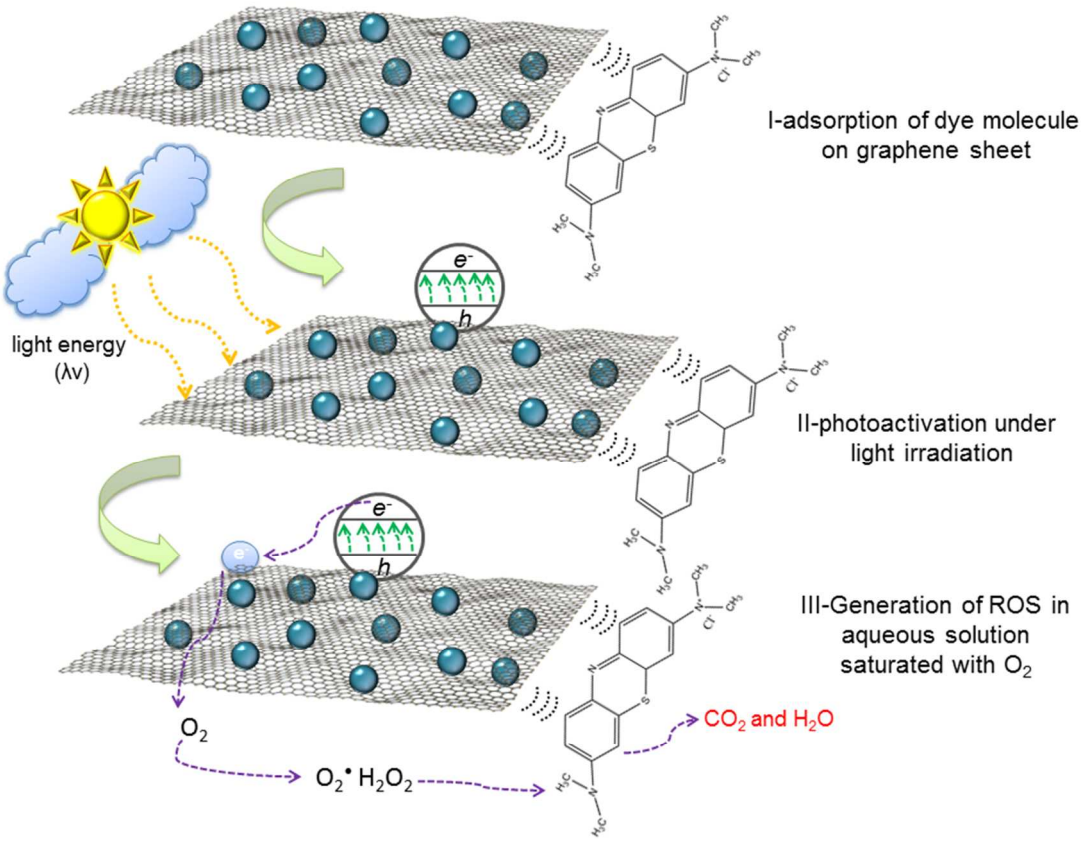

Fig. 3: Schematic illustration of the three-step mechanism proposed for the degradation of organic dye molecules[147,150] (e.g., methylene blue) by graphene hybrid composite photocatalysts. The first step corresponds to adsorption of dye molecules to the graphene surface through π-π stacking interactions. The second step is the photoexcitation of the graphene nanocomposite under UV or visible light. Upon light irradiation, electrons on valence band (VB) are excited to the conduction band (CB) of the semiconductor nanoparticles. These electrons can then travel through the sp^2-hybridized network of the graphene sheets. In the third step, the photoinduced electrons can be transferred to O_2 to generate reactive oxygen species (ROS) which are involved in the degradation of organic molecules. Similar schemes to illustrate the degradation mechanism of organic dyes by graphene-related photocatalysts were reported in previous publications.[136,137,141,145,147,150,156,348]

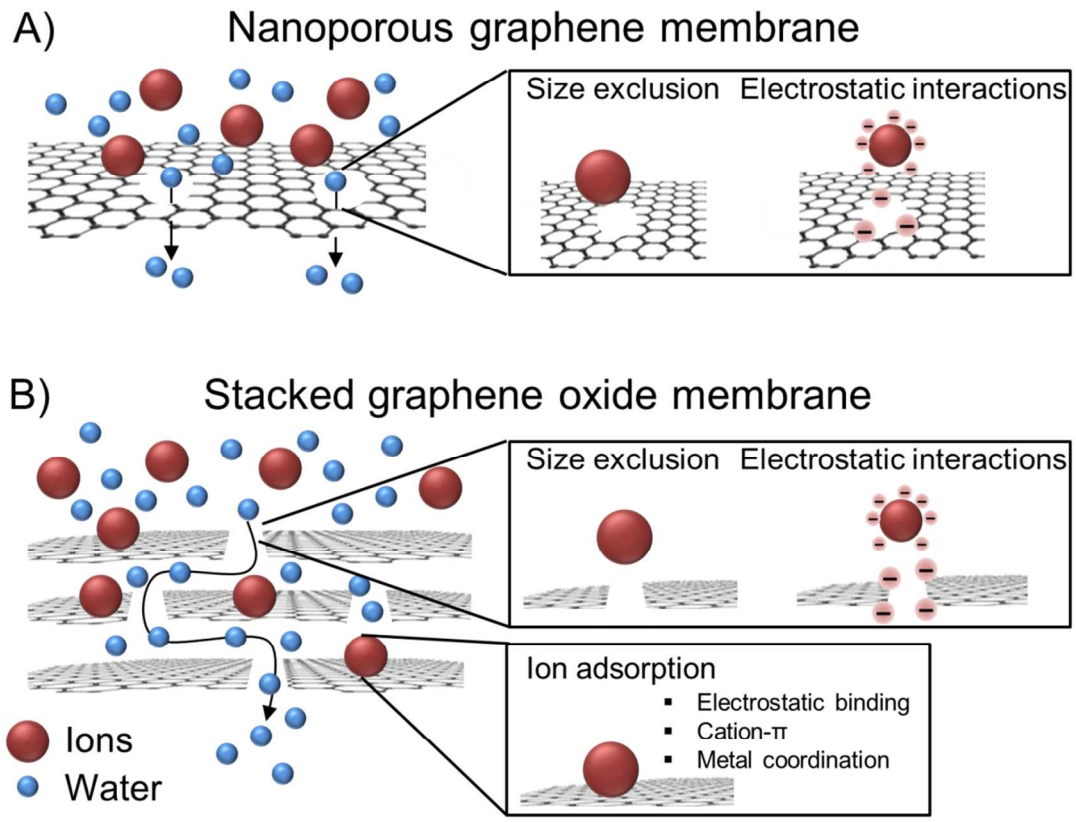

Fig. 4. Schematic representation of the two types of graphene-based membranes. (A) Nanoporous graphene membranes consist of a single layer of graphene with nanopores of defined pore size. Selectivity is achieved by size exclusion and electrostatic repulsion between charged species and the pores. (B) Membranes composed of stacked GO sheets. In stacked GO membranes, the size of the pores is determined by the interlayer distance between the sheets. In addition to size exclusion and electrostatic interaction, selectivity in stacked GO membranes also results from adsorption of ionic species to the GO sheets.

2081

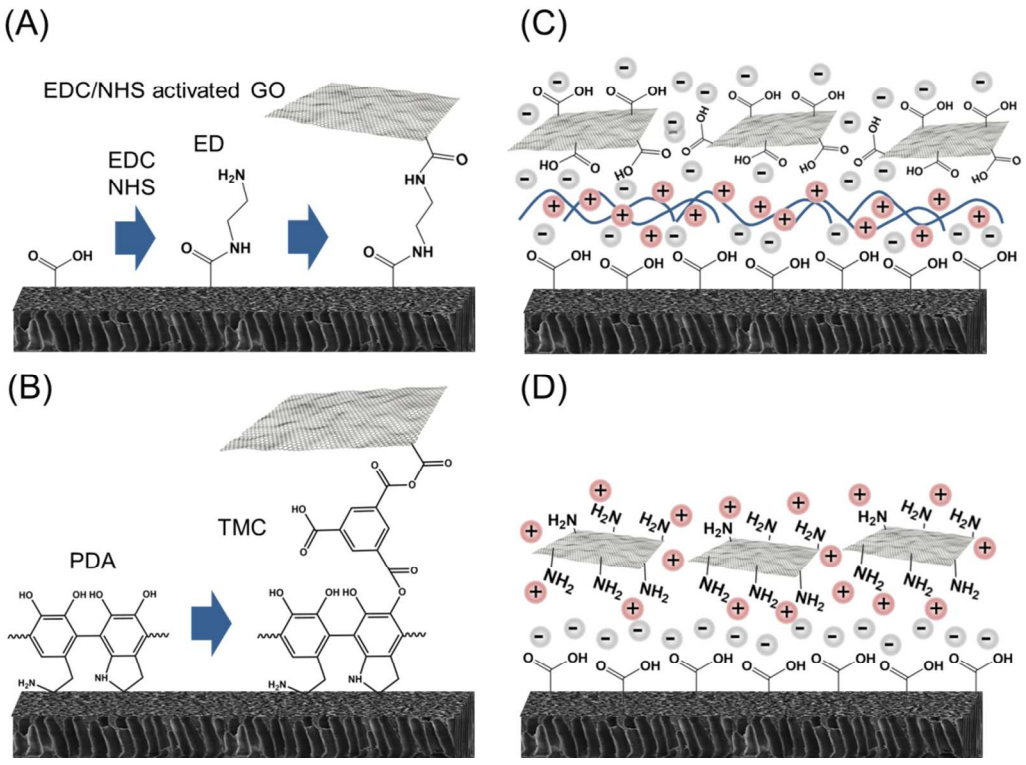

Fig. 5. Surface functionalization of membranes with graphene nanomaterials. (A) covalent binding of GO to the native functional groups of the membrane.[218] 1-ethyl-3-(3-dimethylaminopropyl) carbodiimide (EDC) and N-hydroxysuccinimide (NHS) are used to activate carboxyl groups and attach ethylenediamine (ED) to the membrane by amide coupling. Then, EDC/NHS activated GO sheets are covalently attached to the remaining amine group of ED. (B) Polydopamine (PDA) mediated binding of GO.[198] The membrane is first coated with PDA, which provides reactive sites for 1,3,5-benzenetricarbonyl trichloride (TMC) cross-linking between PDA and GO. (C) polymer-mediated adsorption of GO via electrostatic interactions.[217,349] Positively-charged polymers are applied on negatively-charged membrane. Then, GO sheets, which are negatively charged, are deposited on the positive polymer layer. (D) membrane coating using functionalized GO material.[216] GO sheets are aminated to provide positive charges, which can then be used to coat negatively-charged membranes via electrostatic interaction. Adapted from [198,216,218,349]; full details are given in the respective publications.

2082

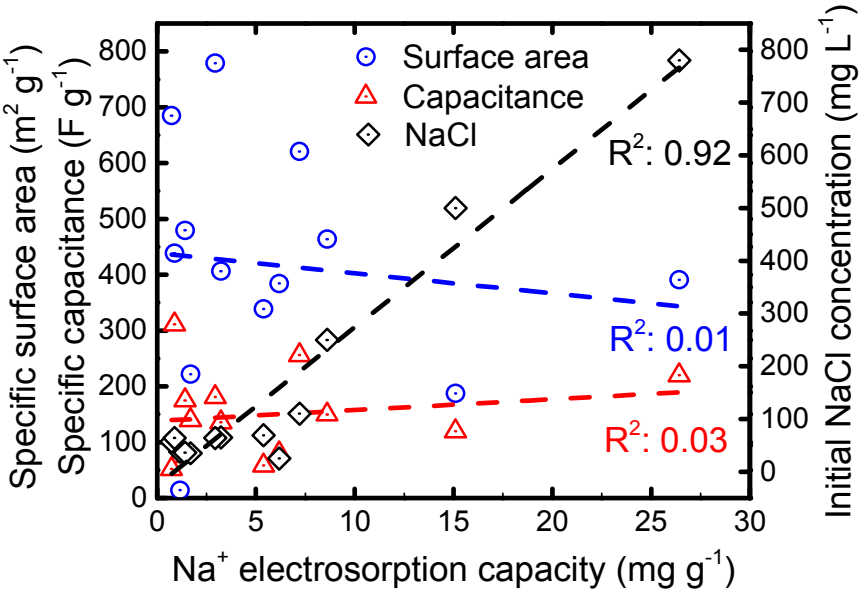

Fig 6. Effects of material specific surface area, specific capacitance, and initial feed water NaCl concentration in the electrosorption experiment on the measured electrosorption capacity of different graphene-based electrodes. Data cover the different types of graphene-based composite electrodes developed for CDI applications.[223–232,350,351]

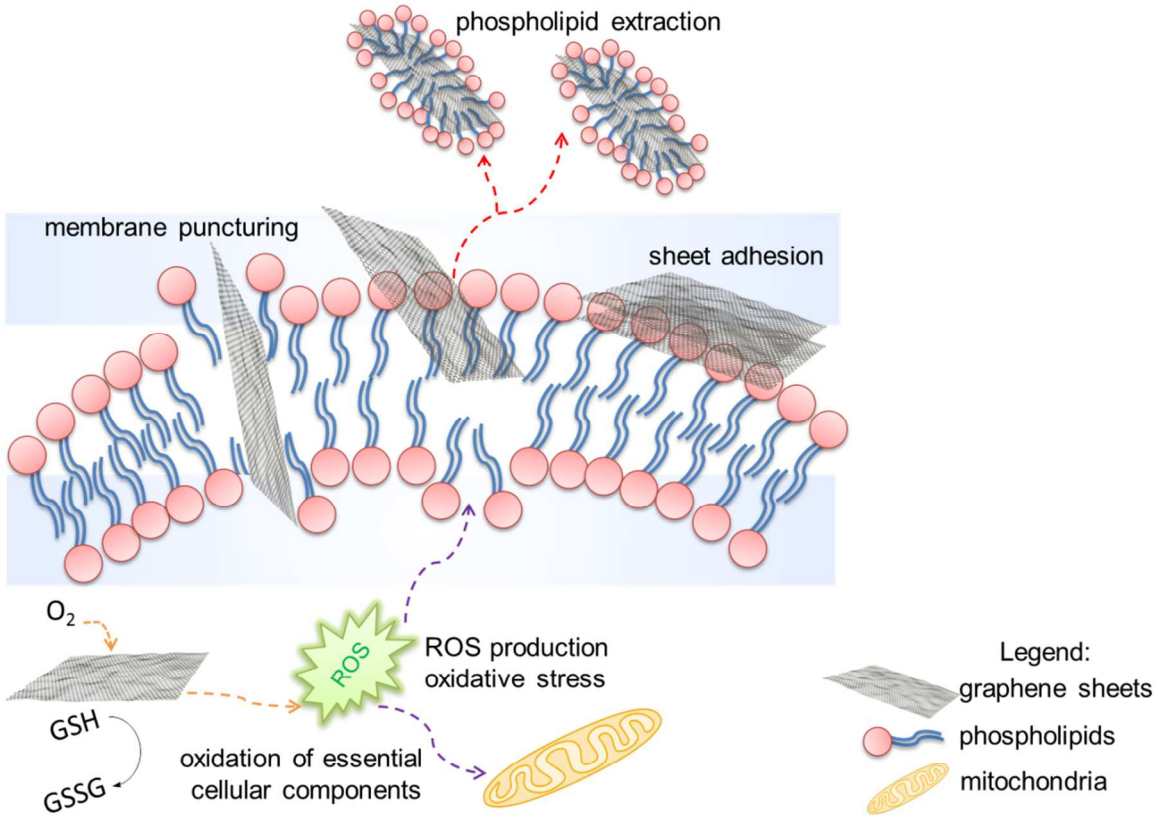

Fig. 7. Mechanisms of cellular interactions of graphene nanomaterials with bacteria. Bacterial inactivation by graphene nanomaterials may involve direct puncturing of the cell membrane, generation of reactive oxygen species (ROS), extraction of phospholipids from the lipid bilayer, and adhesion of graphene sheets on the cell surface.

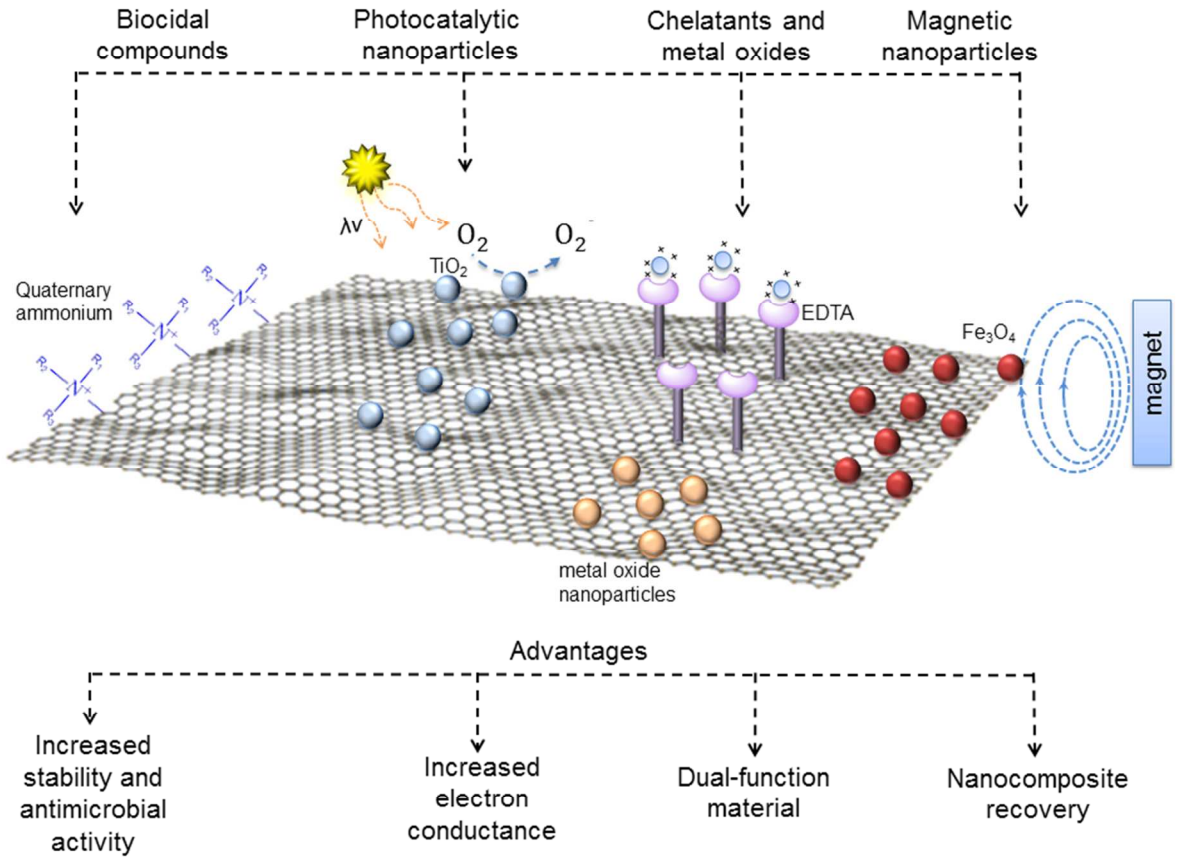

Fig. 8. Different types of graphene-based antimicrobial nanocomposites. Nanocomposites integrating biocidal compounds like quaternary ammonium salts allow for an increased antimicrobial activity. Additionally, dual-function antimicrobial nanocomposites may be developed using photocatalytic nanoparticles (e.g., TiO_2) or adsorbents (e.g. iron oxide nanoparticles, chelatants) for combined water disinfection and decontamination. Nanocomposites may also be imparted magnetic properties, using magnetic iron oxide nanoparticles, to facilitate the recycling of the antimicrobial nanocomposite.

2083

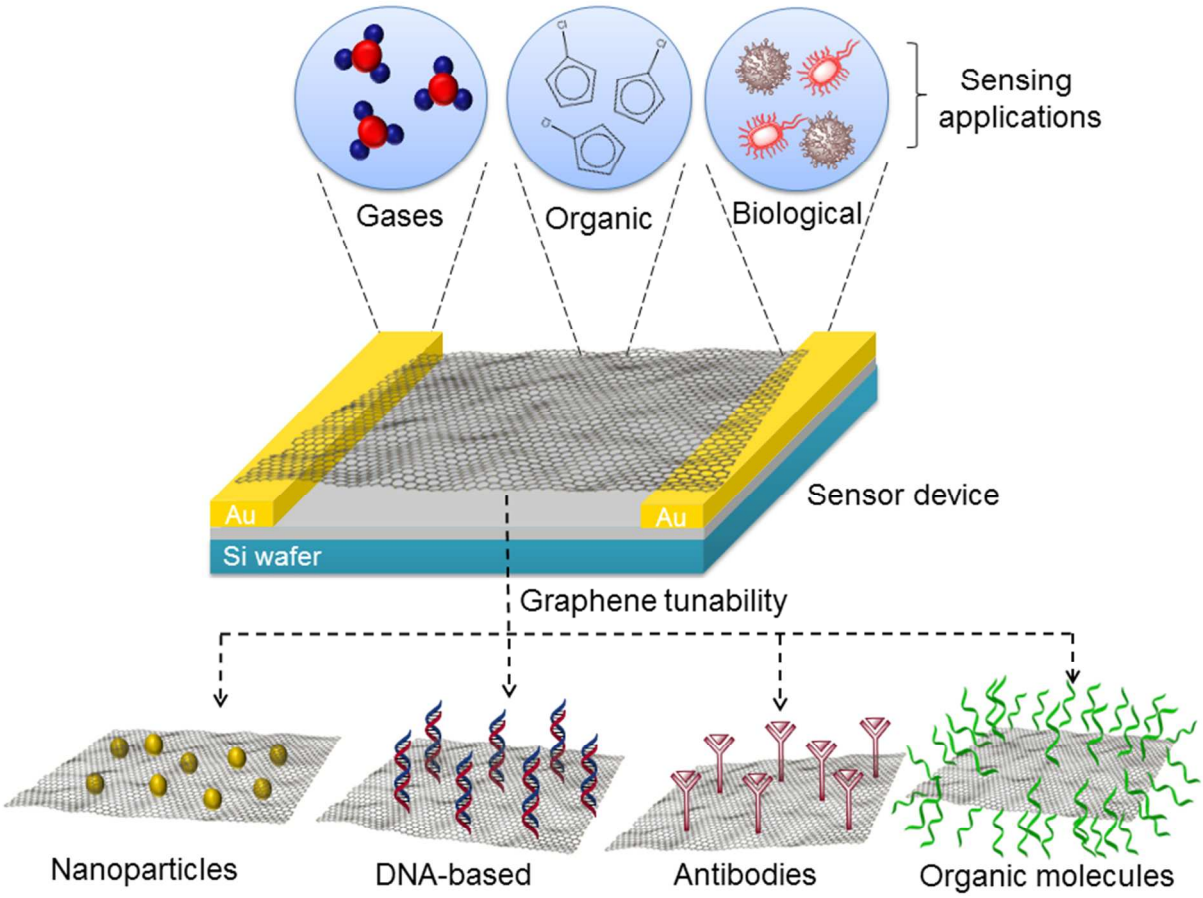

Fig. 9: A didactical scheme of a graphene-based sensor demonstrating its potential application as a platform for detection of gases, organic molecules, and microbial cells and biomolecules. The sensing capacity of graphene-based electrodes can be tuned by modifying the surface chemistry of the graphitic materials through immobilization of metallic nanoparticles, DNA, antibodies, and polymeric compounds.

Table 1. Specific mechanisms of interaction and possible advantages/disadvantages of using graphene materials as adsorbents to remove metal ions from aqueous solutions.

Graphene-based materials	**Mechanisms involved in the adsorption of metal ions**	**Advantages (A) and disadvantages (D)**	**References**
Graphene oxide (GO)	Electrostatic interactions Ion exchange	(A) High dispersibility in water; Good colloidal stability; Abundant presence of oxygenated functional groups (D) limited amount of sorption sites	52,58–60,62,352,353
Reduced GO (rGO) Pristine graphene	Electrostatic interactions Lewis-base-acid mechanism	(A) Reestablishment of sp^2 domains; Better electron-transport property; (D) Low density of oxygen-containing functional groups; Lower colloidal stability	61,73,282,354–356
Magnetic graphene nanocomposites	Electrostatic interactions with graphene Interactions with the surface of the particles Magnetic properties of the nanoparticles	(A) Larger surface area compared to the pristine forms; Increased amount of binding sites compared to pristine graphene; Easy recovery from aqueous solutions (D) Co-reduction of GO during the attachment of the particles reduces the colloidal stability	63–69,357
Graphene materials modified with organic molecules	Electrostatic interactions Complexation with organic molecules	(A) Larger surface area compared to pristine forms; Good colloidal stability; Improved amount of functional groups ($-NH_2$, -OH) (D) The stability of the loaded molecules vary according to the modification strategy (physical or chemical attachment)	71–73,76,355,358

Table 2. Summary of previous studies describing the adsorption of metal ions by graphene-based materials and different types of carbon-based materials. The type of material applied as adsorbent, metal ion used as model adsorbate, maximum adsorption capacity Qe (mg g^{-1}) (calculated using Langmuir isotherm model), and specific experimental conditions such as temperature and pH are listed.

Carbon Material	**Treatments**	**Metal**	**Qe (mg g^{-1})**	**Temp/pH**	**Reference**
Graphene (GNS)	Vacuum-promoted low temperature exfoliation	Pb(II)	22.42	303K/4	[61]
GNS 500	Heat treatment (500°C)	Pb(II)	35.21	303K/4	[61]
GNS 700	Heat treatment (700°C)	Pb(II)	35.46	303K/4	[61]
GO	Modified Hummers method; peroxidation step (H_2SO_4, $K_2S_2O_8$, P_2O_5) followed by an oxidation treatment (H_2SO_4 and $KMnO_4$)	Cu(II)	117.5	pH 5.3	[58]
GO	Modified Hummers method using $NaNO_3$, H_2SO_4, and $KMnO_4$	U(VI)	299	Room/4.0	[352]
Few-layer GO	Modified Hummers method; the oxidation step was performed in presence of H_2SO_4,	Co(II) and Cd (II)	68.2/106.3	303K/6.0	[52]

	and $KMnO_4$				
GO aerogel	Modified Hummers method was used to prepare GO; aerogels were obtained by freeze-drying process	Cu(II)	19.65	298K/6.3	[353]
Few layer GO	Modified Hummers; oxidation of graphite flakes by $NaNO_3$ and H_2SO_4	Pb(II)	842	293K/6.0	[60]
GO	Modified Hummers; oxidation of graphite in presence of $NaNO_3$, H_2SO_4, and $K_2Cr_2O_7$	Zn(II) and Pb(II)	345/1119	298K/5.0	[59]
GO	Modified Hummers method; oxidation of graphite by H_2SO_4 and $KMnO_4$	Zn(II)	246	293K/~7.0	[62]
rGO-Fe_3O_4 (M2-rGO)	GO reduced by Hydrazine at 90°C; Fe_3O_4 nanoparticles were prepared by reacting $FeCl_3$ and $FeCl_2$ with ammonia solution (30%)	As(III) and As(V)	13.10/5.273	293K/7.0	[67]
GO-Fe_3O_4	Hummers modified method ($NaNO_3$, H_2SO_4, and $KMnO_4$)	Co(II)	12.98	303K/6.8	[68]

	was used to prepare GO; magnetite particles were synthesized by exposure $FeCl_3$ and $FeCl_2$ to ammonia				
rGO-FeNPs	The simultaneous formation of rGO and iron nanoparticles was obtained exposing GO and $FeCl_3$ to a borohydrate solution at 90°C	Cr(VI)	162	293K/4.25	[69]
GO-Fe_3O_4	GO prepared from Hummers method and the Fe_3O_4 particles were precipitated by the contact of Fe^{+3}/Fe^{+2} ions with ammonia	Cu (II)	18.26	293K/5.3	[66]
rGO-FeNPs	Irradiation of GO in presence of ferrocene allowed the synthesis of ferromagnetic particles and consecutive reduction of GO	Pb(II)	6.0	Room/6.5	[64]

GO-chitosan ($CSGO_5$)	Physical incorporation of chitosan into an acetic acid GO dispersion and subsequent dropping of this solution in a base solution for formation of beads	Pd(II)	216.92	Room/3.0	[72]
GO-EDTA	GO prepared by modified Hummers method; GO-EDTA obtained by silanization reaction between GO and EDTA-silane in ethanol	Pb(II)	525	298K/6.8	[71]
rGO-PAM*	GO prepared from Staudenmaier method; rGO obtained from thermal reduction of GO; PAM attached to rGO sheets by free radical polymerization	Pb(II)	1000	298K/6.0	[73]
Sulfonated-Fe_3O_4-GO (SMGO)	Pre-oxidation with H_2SO_4, $K_2S_2O_8$, and P_2O_5 and a further oxidation under	Cu(II)	63.67	323K/5.0	[357]

	H_2SO_4 and $KMnO_4$; Fe_3O_4-GO was obtained by co-precipitation of Fe^{+3} and Fe^{+2} by adding ammonia solution; sulfonated groups were introduced by reacting Fe_3O_4-GO with aryl diazonium salt at low temperature				
Oxidized-CNTs	Oxidation of MWCNTs with HNO_3	Pb(II)	49.95	Room/7.0	[359]
Oxidized-CNTs	MWCNTs treated with HNO_3	Pb(II), Cu(II), and Cd(II)	97.08, 28.49, and 10.86	Room/5.0	[360]
Oxidized-MWCNTs	Exposure of MWCNTs to an HNO_3 solution	Cu(II), Co(II), and Pb(II)	3.49, 2.6, and 2.96	Room/9.0	[55]
HNO_3 and $KMnO_4$ Oxidized MWCNTs	Oxidation of MWCNTs in presence of HNO_3 or $KMnO_4$	Cd(II)	HNO_3-CNTs: 5.1 $KMnO_4$-CNTs:	pH=5.5	[51]

			11		
Coconut shell based granulated activated carbon (AC) from Active Carbon Ltd, India.	Exposed to an Na_2S aqueous solution for 24h	Pb(II)	21.88	310K/5.0	[361]
Hazelnut husks activated carbon	Treatment with zinc chloride at 973 K in N_2 atmosphere	Cu(II) and Pb(II)	6.645 and 13.05	291K/6.7	[362]
Coconut tree sawdust activated carbon	Exposure to concentrated H_2SO_4 and activation at 80°C for 12 h in air oven	Cr(VI)	3.46	pH=3.0	[363]
Commercial activated carbon (particle size 100-150 μm) (Fluka, Cedex, France)	Surface modification with tetrabutyl ammonium (TBA)	Cu(II), Zn(II), and Cr(VI)	38, 9.9, and 6.84	298K	[364]

* DAP:2,6-diamino pyridine; PAM: poly(acrylamide); EDTA: N-(trimethoxysilylpropyl) ethylenediamine triacetic acid; MWCNTs: Multi-walled carbon nanotubes

Table 3. Summary of organic compounds adsorption studies by carbon-based materials. The type of material used as adsorbent, the surface area of the material, the temperature and pH conditions used, and the maximum adsorption capacity (Qm or Qe) are listed.

Organic compounds	Material	Surface area ($g\ m^{-2}$)	Temperature /pH	Maximum Adsorption Capacities			Reference
				Polanyi-Mane Isotherm Qm ($mg\ g^{-1}$)	Langmuir Isotherm Qe ($mg\ g^{-1}$)	Freundlich Isotherm Qm [$(mg\ g^{-1})/(mg\ L^{-1})^{n}$]	
Naphthalene	GO-FeO-Fe_2O_3		283K/7.0		2.63	2.87	92
	MWCNTs-FeO-Fe_2O_3		283K/7.0		1.05	1.22	92
Phenanthrene	Graphene	624	293K			208.3	97
	GO	576	293K			174.6	97
	MWCNT	164	293K			61.5	97
	SWCNT	486	293K			293.3	97
Biphenyl	Graphene		293K			102.6	97
	GO		293K			59	97
	MWCNT		293K			29.8	97
	SWCNT		293K			126.1	97
Bisphenol A	rGO	327	302K/6.0		181.82	54.7 (KF)	95
	MWCNT	107		77	61.6		365,366
	SWCNT	541		591	455		365,366
Methylene Blue	GO		298K/6.0		714	469.6	86
	Activated carbon	1688	298K/6.0		270.27	263.23	367
	CNTs	177	298K/6.0		188.58	54.03	367
	GO	32	298K/6.0		243.9	114.86	367

Oxytretracycline	GO		298K/3.6		212.31	46.498	[79]
	MWCNT10 (<10 nm)	357	296K/7.0	190.2			[368,369]
	MWCNT100 (60-100 nm)	58	296K/7.0	30.4			[368,369]
PCB-52 (2,2',5,5'-tetrachlorobiphenyl)	Activated carbon	945	293K/neutral	18 ± 2.6	12 ± 0.71	15 ± 1.8	[98]
	CNTs	144	293K/neutral	3.9 ± 0.81	1.4 ± 0.12	0.74 ± 0.02	[98]
	Graphene	181	293K/neutral	12 ± 0.5	3.2 ± 0.19	2.5 ± 0.2	[98]
	GO	70.9	293K/neutral	0.79 ± 0.56	0.87 ± 0.83	0.81 ± 0.41	[98]

Table 4. Advantages and limitations of the different methods for nanopore formation in graphene

Method	Pore size	Advantages	Limitations	Reference
Focused electron beam irradiation	3.5 nm	-Controlled pore size	- Small area	[184]
Focused electron beam irradiation	0.7 nm	-Controlled pore size	-Small area	[185]
Focused electron beam irradiation	5-23 nm	-Controlled pore size	-Small area	[186]
Low-energy ion beam and unfocused electron beam irradiations	0.45-2.2 nm	-Controlled pore size	-Small area	[187]
Nitrogen-assisted electron beam irradiation	5.9 ± 0.4 nm	-Controlled pore size	-Small area	[188]
Block copolymer lithography and plasma etching	> 5 nm ± 2nm	-Large area and controlled pore size	-Pores too large for salt rejection	[189]
UV oxidative etching	0.4-10 nm	-Large area	- Wide pore size distribution	[190]
High temperature O_2 etching	20-250 nm	-Large area	-Wide pore size distribution	[191]
Low energy ion beam and chemical oxidation	0.4 ± 0.2 nm	-Large area -Controlled pore size	-Pore size range of <1 nm	[193]

Table 5. Summary of parameters, such as type of carbon nanomaterial, target compounds, and detection limit for the detection of gases, organic, and biological pollutants, for graphene-based and carbon-based sensors.

Carbon material	**Material preparation**	**Sensor fabrication**	**Target compound**	**Sensor response Detection limit**	**Sensor recovery**	**Reference**
Pristine graphene	Mechanical exfoliation of graphite	Electron-beam lithography	NO_2 gas	Single NO_2 molecules	Annealing at 150°C	[289]
Pristine graphene films and ribbons	CVD	Graphene deposited on sensor chips	CO, O_2, and NO_2	Sensor exhibited signal of 3 and 35 for 100 ppm of CO and NO_2, respectively	Sensors were regenerative	[310]
rGO	GO reduction obtained by annealing (100-300°C)	Casting graphene dispersion on gold interdigitated electrodes *via* lithography using Si wafers covered with a top-layer SiO_2 as a support	NO_2 gas	rGO prepared from annealing at 300°C showed sensitivity of 1.56 at 100 ppm NO_2	Exposure to a clean dry air flow	[308]
rGO	Reduction of rGO films by hydrazine	rGO films were anchored on interdigitated Ti/Au electrodes by photolithography	Warfare and explosive chemical such as DNT and	Minimal detectable level of 70 ppb and 0.1 ppb for HCN and DNT, respectively, at	------	[319]

			HCN	a detection time of 10 seconds		
rGO-SnO_2 nanocomposite	GO reduced by Hydroxylamine Hydrochloride ($H_3NO.HCl$)	Gold interdigitated electrodes prepared by electron-beam lithography	NH_3 and NO_2	Detection limit of 1 ppm for NO_2 and response time of 65 s	Clean-up through air flow	[291]
rGO-PANI	GO thermally reduced; rGO-MnO2 used as a template and oxidizing agent for aniline polymerization	Graphene deposited on an electrode device using a microsyringe	NH_3	59.2% change in resistance; 10.4 times improved response for NH3 compared to pristine rGO	Infrared illumination; 87% of the rGO-PANI resistance is recovered after 4 min exposure	[321]
rGO	GO reduced by hydrazine	Single-layered graphene films on gold interdigitated electrodes	NO_2, NH_3, and DNT	DNT: 28ppb	Room temperature over the 10 min purge time	[305]
rGO-AuNPs	Thermally reduced GO at 400°C	Self-assembly of rGO on amino-terminated Au electrode	Pb^{+2}	10 nM	Rinse in acidic buffer (pH=2.8)	[330]
Graphene-enzyme nanostructure	GO reduced by hydrazine	Immobilization of graphene-enzyme on glassy carbon electrodes	H_2O_2	1 x 10^{-7} M	------	[326]

Multi-layered graphene functionalized with urease and glutamate dehydrogenase	Produced using MWCNTs as precursors	Graphene films used as electrodes were prepared *via* deposition on indium tin oxide substrate	Urea	Detection limit of 3.9 mg dL^{-1} with a response time of 10s	------	[337]
Pristine graphene modified with anti-*E.coli* O and K antibodies	Graphene film obtained from CVD	Deposition of the graphene film on a quartz substrate	*E. coli* cells	Sensitivity at *E. coli* concentration of 10 CFU/mL	------	[336]
SWCNT	CNTs obtained by CVD	Sensor fabricated by growing SWCNTs on a catalyst-containing surface of SiO_2/Si	NO_2 and NH_3 gases	Response time of 2-10 s at 200 ppm NO_2 and 1-2 min at 1% NH_3	Recovery time of 12 h after replacement of NO_2 by air flow, reduced to 1 h at 200°C.	[370]
MWCNT	----	CVD growth of vertically aligned MWCNTs on a SiO2 substrate.	Detection and separation of gases in	Detection limit of 1% for NH_3 at room temperature in 20 µs	No hysteresis observed.	[371]

			mixtures (NH_3, Ar, CO_2, O_2, N_2)			
SWCNT and SWCNT-based nanocomposites	Non-covalent functionalization of SWCNTs with Tween 20. Conjugation of SWCNT-Tween with biotin, Staphylococcal protein A (SpA), and U1A antigen	Growth of SWCNTs on a quartz substrate by CVD using iron nanoparticles as catalysts. SWCNTs bridged by Ti/Au electrodes	Selective detection of proteins	sensors selective for detection at concentrations ≤ 1 nM	----	[372]
SWCNTs and polymer-functionalized SWCNTs	Immersion into a PEI/methanol solution for 2 h	SWCNTs were grown across pre-fabricated electrodes (Si/SiO_2 substrate) using CVD.	NO_2 and NH_3 gases	SWNCTs-PEI detect NO_2 at concentrations lower than 1 ppb but are insensitive to NO_3; Nafion-SWCNTs show sensitivity to NH_3 at 100 ppm but are insensitive to NO_2	SWNCTs-PEI sensors were recovered by UV illumination	[373]

SWCNTs and SWCNTs functionalized with PABS	SWCNTs and SWCNTs-PABS were obtained from Carbon Solutions Inc.	Nanomaterial dispersions were deposited on a gold interdigitated electrode	NH_3 gas	SWCNTs-PABS had improved sensitivity compared to pristine SWCNTs; SWCNTs-PABS showed response to NH_3 at 5 ppm	Recovery was performed by replacing NH_3 by N_2	[374]
SWNTs decorated with Pd nanoparticles.	Functionalization by electron-beam evaporation	SWCNTs were grown on a SiO_2 substrate by CVD	H_2 gas	Response time of 5-10 s at H_2 concentration of 400 ppm; Sensor presented high sensitivity at concentrations between 40-400 ppm	At low H_2 concentrations (<400 ppm), sensors exhibited an auto-recovery ability	[375]

* CVD: chemical vapor deposition; PANI: polyaniline; DNT: 2,4-dinitrotoluene; HCN: hydrogen cyanide; PABS: poly(m-aminobenzene sulfonic acid); PEI: polyethylenimine